

# **The Triassic of the Wandel Sea Basin – The Dunken-2 core data package report**

Contribution to Petroleum Geological Studies, Services  
and data in East and North-East Greenland

Morten Bjerager, Jørgen Bojesen-Koefoed, Claus Kjøller,  
Sofie Lindström & Jens Therkelsen



# **The Triassic of the Wandel Sea Basin – The Dunken-2 core data package report**

Contribution to petroleum geological studies, services and data in  
East and North-East Greenland

Morten Bjerager, Jørgen Bojesen-Koefoed, Claus Kjøller,  
Sofie Lindström & Jens Therkelsen

Confidential report

Copy No.

Released 01-07-2025

Preface:

© De Nationale Geologiske Undersøgelser for Danmark og Grønland (GEUS), 2016 (Geological Survey of Denmark and Greenland)

No part of this publication may be reproduced or utilised in any form or by any means, electronic or mechanical, including photocopying, recording or by any information storage and retrieval system, without prior written permission from the publisher, GEUS. Disputes on copyright and other intellectual property rights shall be governed by Danish law and subject to Danish jurisdiction.

# Contents

<b>Summary</b>	<b>4</b>
<b>1. Introduction</b>	<b>6</b>
1.1 Core hole data .....	7
1.2 Sampling programme at the drill site .....	8
1.3 Analytical program .....	9
1.4 References .....	9
<b>2. Stratigraphy</b>	<b>10</b>
2.1 Lithostratigraphy and sedimentology .....	10
2.1.1 Ugleungernes Dal Formation 141.84 to 40.75 m .....	10
2.1.2 Dunken Formation: 40.75 to 4.0 m .....	13
2.2 Biostratigraphy and bulk organic $\delta^{13}\text{C}$ -isotopes .....	16
2.3 Petrophysical logs .....	20
2.4 Sequence stratigraphy .....	22
2.5 References .....	23
<b>3. Petrography, Diagenesis and Reservoir properties</b>	<b>25</b>
<b>4. Cap-rock properties</b>	<b>29</b>
4.1 Methods .....	30
4.2 Core analysis – results .....	31
4.3 Mineralogy and grain size – results .....	33
4.4 Seal capacity .....	36
4.5 Discussion and conclusion .....	36
4.6 References .....	37
<b>5. Petroleum geology</b>	<b>38</b>
5.1 Introduction .....	38
5.2 Samples and Methods .....	38
5.3 Results and discussion .....	40
5.3.1 Petroleum potential and maturity .....	40
5.3.2 Biological markers .....	51
5.4 Summary .....	65
5.5 References .....	66
<b>Appendix</b>	<b>67</b>



## Summary

This report presents the core-data package of the Triassic Dunken-2 fully cored borehole drilled during the summer of 2012 in the Wandel Sea Basin in eastern Peary Land, North Greenland. The report is number four of five reports that are delivered to companies that have cosponsored the project: “The Triassic of the Wandel Sea Basin”. This project is described in appendix M1 in the collaboration agreement between GEUS and sponsoring Oil Companies regarding Petroleum Geological Studies, Services and Data in East and North-east Greenland.

The primary objective of the Dunken drilling was to test the presence of Triassic petroleum source rocks in the Spathian–Norian succession of the Wandel sea Basin. Additional objectives include high resolution biostratigraphy, sedimentology and sequence stratigraphy on the core. A caprock study is conducted on mudstone units and a combined diagenesis and reservoir properties study is conducted on the sandy units.

Dunken-2, GGU 517006, was drilled approximately 140 km NNW of Station Nord and 820 km from the North Pole. The name Dunken-2 is derived from the nearby mountain “Dunken”. The Dunken-2 core hole was drilled to a total depth of 141.84 m; the core diameter is 42 mm, and the core is well preserved with a recovery of 96%.

Except for 4m of Quaternary overburden the entire penetrated succession is Triassic in age. The Triassic succession consists of shallow marine biomottled sandstones and sand-dominated biomottled heteroliths and minor mudstone dominated heteroliths of the Dunken Formation from 4.0–40.9 m in the core. The Ugleungernes Dal Formation is represented from 40.9 to 141.84 m, and consist of laminated and biomottled offshore mudstones and minor biomottled heterolithic units and thin conglomeratic beds. The base of the Ugleungernes Dal Formation was not reached.

The biostratigraphic subdivision of the Dunken-2 core is based on 39 samples prepared for palynological studies. The samples have been assigned to biostratigraphic zones and correlated to chronostratigraphic zones. The recovered upper part of the Ugleungernes Dal Formation is represented by the Smithian (*N. striatus* Assemblage Zone) – Lower Spathian (*Pechorosporites disertus* Assemblage Zone). The interval represented by the lower parts of the Dunken Formation biostratigraphically spans the upper Spathian (*J. punctispora* Assemblage Zone).

Deposition of the Smithian – Spathian Ugleungernes Dal Formation occurred in oxic to dysoxic conditions in depositional environments that alternated between offshore, offshore transition and lower shoreface. The succession is overall shallowing upward with four stacked transgressive-regressive sequences.

The sandstones are mainly fine-grained and dominated by quartz and they are characterized as mature. The diagenesis of the sandstones shows that the dominating authigenic phase is quartz cementation, which is present in nearly all samples, except in a few sam-

ples where early concretionary calcite dominates. Both types of cement are pervasive and generally pore-occluding and thereby reducing the reservoir quality severely.

Reservoir quality of sandstone units is measured by conventional core analysis on 12 sandstone plugs of fine-grained sandstones. The Reservoir properties are generally poor in the recording porosities from 0.2–9.2% and permeabilities from <0.04–3.4 mD.

The cap-rock study is based on nine mudstone samples from the core. The mudstones comprises  $>\frac{2}{3}$  in the silt fraction. The clay fraction generally constitutes 7-10 % (w/w). A single sample records a clay fraction of c. 15% (w/w). The bulk mineralogical analysis shows (w/w) compositions of quartz with 42-57 %, Feldspar of 7-31% with a decreasing upward content, carbonates (calcite and dolomite) of 1-20% with lowest values in the lower part, highest values in the middle part and mediate values in the upper part. Illite is the main clay mineral with 8-20%, and chlorite amounts of 5-11%. The content of pyrite is 0.5–3%, and mica comprises up to 1%. The cap-rock study demonstrates reasonably good capillary sealing properties that will hold an oil column of at least 200 m. However, the best of the cap-rocks studied will presumably hold an oil column of at least 1,000 m, thus making these cap-rocks excellent capillary barriers.

Source rock evaluation of the Dunken-2 core is based on 122 samples covering the succession from approximately 20 metres to TD. The succession is generally poor in organic carbon (0 – 0.55%) shows low pyrolysis yields (0 – 0.79), and does not include petroleum source rocks. The cored interval is oil-window mature, and two narrow intervals show slightly enhanced organic matter contents and petroleum potentials. These intervals are stained by small quantities of oil, probably generated *in situ*. The presence of intervals with slightly enhanced petroleum potential and oil staining may hint at the presence of petroleum source rocks within the succession elsewhere, presumably in more distal parts of basins. The biological marker compositions of the oil stains include high proportions of tricyclic terpanes relative to pentacyclics, and high proportions of rearranged hopanes and steranes relative to regular hopanes and steranes. In general, the molecular composition complies with generation from a marine shale source rock of Triassic age, at a level of maturity well within the oil generative window.

# 1. Introduction

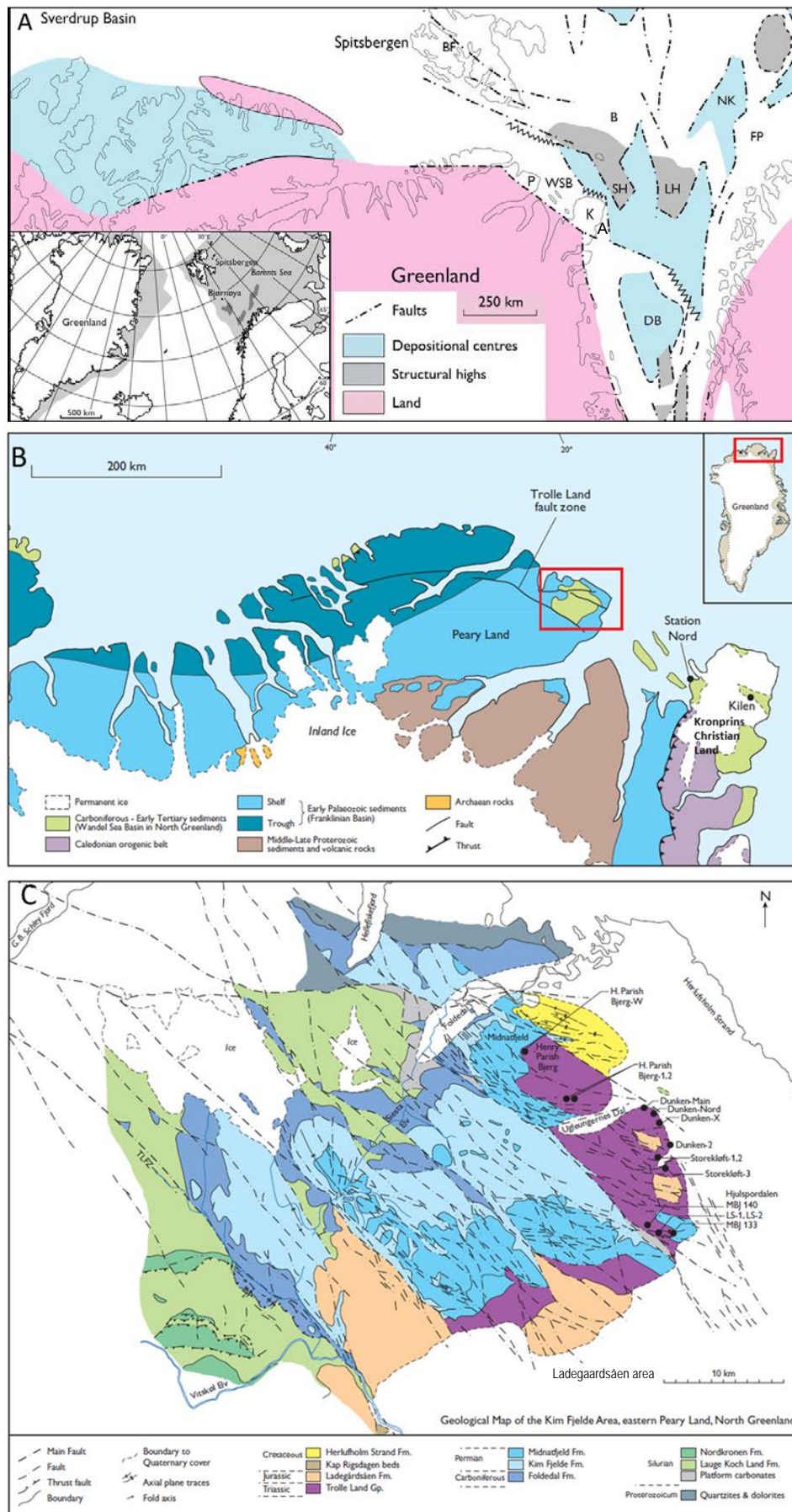
The Dunken-2 borehole is located in the northern part of Kim Fjelde, eastern Peary Land, North Greenland (Fig. 1.1), at the mouth of the canyon Storekløft. The south-eastern slope of the mountain Dunken rises just a few meters west of the drill site.

Dunken-2 is the sixth core hole in an onshore drilling program in East, North-East and North Greenland that began in 2008. The drilling program is part of collaboration between GEUS and a number of oil companies called *Petroleum Geological Studies, Services and Data in East, North-East Greenland*. The drilling programme includes following cores: Blokelyv in central Jameson Land (2008); Rødryggen-1 on Wollaston Forland (2009); Store Koldewey-1 on Store Koldewey and Brorson Halvø-1 on Wollaston Forland (2010); and Nanok-1 on Hold with Hope (2011). The results of the 2012 drilling season were Dunken-1, Dunken-2 and Kim Fjelde-1 in northern and eastern Kim Fjelde, and the cores are thus the first core data from the western continuation of the Barents Sea i.e. the Wandel Sea Basin. Approximately 1 m east of Dunken-2 another well, Dunken-1, were cored to 18.84 m but abandoned due to a frozen drill string. This core will not be referenced in this report as it is essentially the same. Initial results of the core drilling are presented in the completion report of Pilgaard (2013).

The primary objective of the Dunken drilling was to test the presence of petroleum source rocks in the Spathian to Norian interval of the Triassic succession of the Wandel sea Basin. Additional objectives were to have a high resolution biostratigraphy, sedimentology and sequence stratigraphy on the core. A cap rock study is conducted on mudstone units and a combined diagenesis and reservoir properties study is conducted on the sandy units.

A detailed description and interpretation of the Dunken-2 core together with a source rock analytical programme was planned and announced in Appendix B5 (not this report). But due to bad source rock indications in the preliminary results from the core (Pilgaard 2013), the appendix was redrawn on the 29<sup>th</sup> of November 2012. Instead a regional study of the Triassic succession was proposed in Appendix M1 including a detailed description and integration of the Dunken-2 corehole (this report). The results of the core study are integrated in the regional study (Bjerager et al. A, B; Lindstrøm and Alsen, Therkelsen et al.)

Fig. 1.1 (next page) A) Regional map of the Arctic from the Sverdrup Basin to the Finmark Platform showing the main Late Paleozoic tectonic elements (A Amdrup Land, B Bjørnøya, BF Billefjorden Trough, DB Danmarkshavn Basin, FP Finmark Platform, K Kronprins Christians Land (with Kilen), LH Loppa High, NK Nordkapp Basin, P Peary Land, SH Stappen High, WSB Wandel Sea Basin, Modified from Stemmerik & Worsley, 2005). B) Geological map of eastern part of North Greenland. C) Geological map of Peary Land with position of studied localities and the Dunken-2 corehole. The Triassic Formations are included in the Trolle Land Group (modified from Zinck-Jørgensen, unpublished geological map).



## 1.1 Core hole data

Country	Greenland / Denmark
Borehole number	GGU 517006
Borehole name	Dunken-2 (after nearby mountain Dunken) (Ca. 1 m west of Dunken-2 another well named Dunken-1 were drilled but abandoned at 18.84 m)
Area	Trolle Land, eastern Peary Land, North Greenland
Operator	GEUS
Drilling operator	GEUS

Borehole Location	
Altitude:	212 m above mean sea level.
Coordinates WGS 84:	Latitude: 82°40.204' N, Longitude: 21°04.850' W
UTM (wgs84):	9179629 N 498849 E (UTM Zone 27)

Drill rig	Sandvik DE 130
Drilling contractor	GEUS
Casing diameter	64/57 mm,
Casing depth	Casing 64/57 mm to 12.08 m
Borehole diameter	56 mm
Core diameter	42 mm
Total depth	141.84 m
Total core recovery	96%
Status	Top of casing closed with a steel cap.

Logistic history:	
First drilling crew members arrive on Station Nord	July 13 <sup>th</sup> 2012
Transportation of rig and crew from Station Nord to drill site	July 16 <sup>th</sup> –18 <sup>th</sup> 2012
Establishment of field camp and drilling rig	July 16 <sup>th</sup> –19 <sup>th</sup> 2012
Spud	July 21 <sup>st</sup> 2012
Drilling completed	July 30 <sup>th</sup> 2012
Demobilization and transportation to a new drill site	July 31 <sup>st</sup> - August 6 <sup>th</sup> 2012
Effective drilling	5 days
Total days on drill location	22 days

## 1.2 Sampling programme at the drill site

A total of 18 whole core samples from mudstone-intervals for potential gas analyses were collected immediately of the recovered core for every 6 m in average. Samples have lengths up to about 10 cm and they were stored in sealed metal cans. 122 samples from the core were collected for Rock-Eval/TOC screening and biostratigraphic age identification based on palynomorphs at GEUS.

A natural gamma ray (GR) log was run in the drill string after drilling completed from 134.5 m and upwards.

### 1.3 Analytical program

A comprehensive analytical programme is conducted on the core:

- Palynological biostratigraphy is based on 39 samples.
- Petrography, diagenesis and reservoir properties of sandstones are evaluated based on 12 samples.
- The cap-rock study is based on 9 mudstone samples from the core and a single sample from the Middle Triassic at Kilen.
- Petroleum geological studies are based on 122 samples including four selected samples analysed for biomarkers.
- A spectral gamma ray log and density log are measured on the entire core was measured.
- The core is sedimentologically logged in scale 1:50.
- Core photographs are produced in natural light in dry and wet conditions.

### 1.4 References

- Bjerager, M., Alsen, P., Keulen, N. Lindström, Piasecki, S. Rasmussen, M.B., Thomsen, T.B. & Therkelsen, J. 2016 A. The Triassic of the Wandel Sea Basin – Lithostratigraphy, Sedimentology, Sequence stratigraphy and Provenance. Danmarks og Grønlands Geologiske Undersøgelse Rapport 2016/6
- Bjerager, M., Alsen, P., Bojesen-Koefoed, J., Kjøller, C., Lindström, S. & Therkelsen, J. 2016 C. The Triassic of the Wandel Sea Basin and correlation to Svalbard and Western Barents Sea – A summary report. Danmarks og Grønlands Geologiske Undersøgelse Rapport 2016/10
- Lindström, S. & Alsen, P. 2016. The Triassic of the Wandel Sea Basin – Biostratigraphy and bulk organic  $\delta^{13}\text{C}$ -isotope stratigraphy. Danmarks og Grønlands Geologiske Undersøgelse Rapport 2016/7
- Pilgaard, A. 2013. Dunken-2 core hole GGU 517006, eastern Peary Land, North Greenland: Completion report. Danmarks og Grønlands Geologiske undersøgelse Rapport 2013/28, 21 pp.
- Therkelsen, J., Bojesen-Koefoed, J. & Kjøller, C. 2016. The Triassic of the Wandel Sea Basin: Petrography, Diagenesis, Cap-rock properties, Reservoir properties and Petroleum Geochemistry. Danmarks og Grønlands Geologiske Undersøgelse Rapport 2016/9

## 2. Stratigraphy

### 2.1 Lithostratigraphy and sedimentology

The new Triassic lithostratigraphy of the Wandel Sea Basin is described in Bjerager et al. A (this report package), and applied on the Dunken-2 core. The sandstone dominated Dunk-en Formation is represented from 4.0–40.75 m, and mudstone dominated Ugleungernes Dal Formation is represented from 40.75 to 141.84 m (Fig 2.4).

The core was sedimentologically logged in scale 1:50 (Appendix 1) and is in addition pre-sented in scale 1:1000 (Fig.2.5). The core was photographed in natural dry and wet condi-tions and in UV light (Appendices 2–3). Selected intervals were slabbbed and photographed for detailed sedimentological studies (Appendix 4).

#### 2.1.1 Ugleungernes Dal Formation 141.84 to 40.75 m

The formation consists of laminated and biomottled offshore mudstones and biomottled heterolithic units, minor homogenous sandstones and thin conglomeratic beds. The base of the Ugleungernes Dal Formation was not reached by the core.

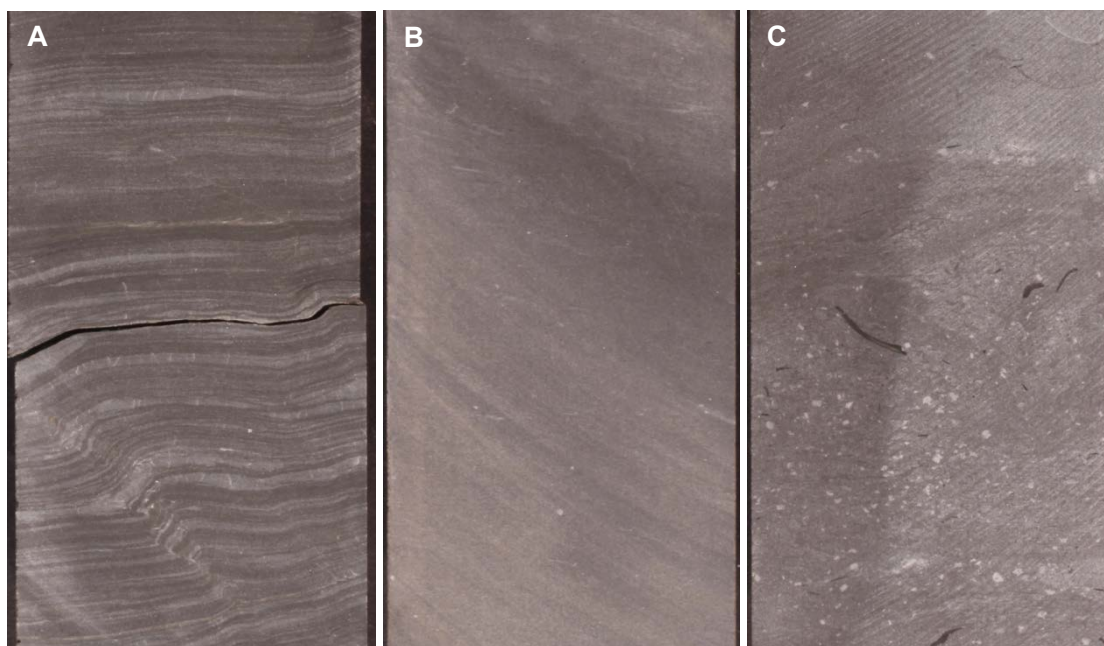


Figure 2.1 Dunken-2 core photos, core width 4.2 cm. A) Laminated mudstone with sand lami-nae, deformed bedding in the lower part (depth 140.2 m). B) Biomottled mudstone (depth 126. 8 m). C) Biomottled sandy mudstone with dispersed black and white bioclasts (depth 119.3 m).

#### 141.84 –128.9 m

Laminated dark grey mudstones, with minor bioturbation, and a few laminae are pyritized. Interlaminated light grey thin sandstones are common to abundant showing plane lami-nation and ripple lamination. The few trace fossils are observed in the lower part and they

become more frequent in the upper part; they include *Planolites* and spreite structures, which probably represent *Zoophycos*. The sand laminae and lenses have sharp boundaries to the mudstones and are increasing in abundance upwards and show many examples of slumped and contorted bedding or otherwise disturbed lamination, and one example with a small normal fault. An erosional pebble conglomerate, 2 cm thick occur at 140.0 m. Calcite filled fractures are common. The strata dip between 5° to 15°.

The mudstones are interpreted deposited in offshore environment with frequent deposition of thin storm sand laminae or distal turbidites. The common contorted bedding and slump structures suggest a gently sloping seafloor. The conglomerate is interpreted as a transgressive lag deposit.

#### **128.9–114.1 m**

The base of the interval is characterized by an intensely biomottled sandstone unit with common *Planolites* and *Rhizocorallium*, 1.4 m thick. It is overlain by bioturbated sandy mudstone, dark grey – grey; the degree of bioturbation is generally moderate. Fine-grained sandstone laminae and thin beds, up to 5 cm thick are common. A single muddy sandstone bed is up to 20 cm thick. Shell fragments may occur in common to abundant amounts in sandstones beds and are commonly associated with dispersed detrital grains in coarse sand fraction. The recorded trace fossil assemblage includes *Chondrites* and *Rhizocorallium* that are characteristic of the *Cruziana* Ichnofacies. The strata dip between 5° to 15°.

The basal sandstone is interpreted as deposited in a lower shoreface environment based on the bioturbated fabric and recorded trace fossil assemblage. The biomottled mudstones with associated *Cruziana* Ichnofacies trace fossil assemblages are interpreted as deposited in mainly offshore transition with frequent influx of storm-sand deposition.

#### **114.1–40.75 m**

The interval comprise alternating units of massive to faintly bedded sandstones, biomottled sandstones, biomottled muddy sandstones, biomottled sand-dominated heteroliths, biomottled mud-dominated heteroliths, biomottled sandy mudstones and mudstones. Strata dip 6°-12°. The interval represents depositional environments alternating between offshore transition and lower shoreface.

Massive to faintly bedded fine-grained sandstones occur as distinct beds 10 cm to about 1 m thick interbedded with mudstones. The sandstones commonly show plane bedding, wavy bedding or ripple lamination in the top part and occasionally show a weakly to moderately biomottled top draped by mudstone. The facies are distributed in the intervals 108.3– 96.6 m, 53.3–40.75 m. The facies is interpreted as deposited as mainly high density gravity flows, with occasional low density flows in the top part.

Biomottled sandstones, muddy sandstones, and sandstone dominated heteroliths comprise the main sandstone dominated facies types in the interval and are interbedded with mudstones. Beds vary between few cm and up to three m in thicknesses, with occasionally wavy bedding and ripple lamination visible, and individual beds are commonly draped by mudstones. Water escape structures and slumping are rarely observed. The degree of biomottling varies mainly between moderate and intense and diagnostic trace fossils include



*Thalassinoides*, *Planolites*, *Chondrites*, *Rhizocorallium*, and *Scolicia*. The sandstone distribution is dominant in the intervals 114.5-104.5 m, 102.5- 96.6 m, 94-85 m, 78.6-70.5 m, and 56.5-40.8 m. The sandstones are interpreted as deposited by gravity flows and storm beds in a lower shoreface to offshore transition settings with an intense burrowing activity in oxic seafloor conditions.

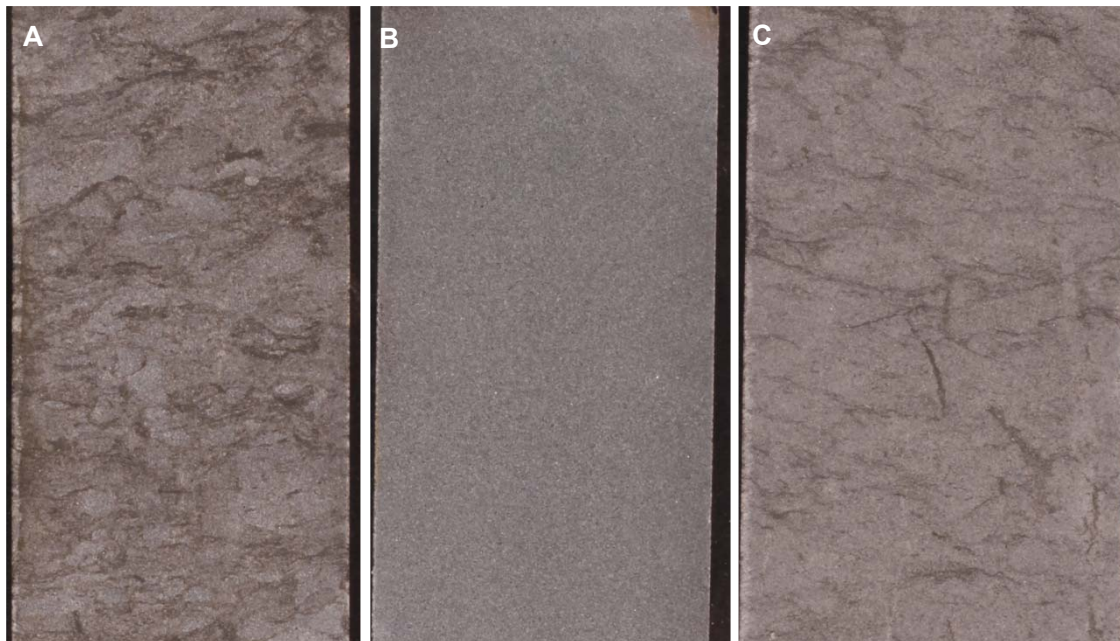


Figure 2.2 Dunken-2 core photos, core width 4.2 cm. A) Intensely biomottled heterolith, sandstone dominated (depth 89.55 m). B) Homogeneous sandstone (depth 102.1 m). C) Biomottled sandstone (depth 54.28 m).

Biomottled mudstone-dominated heteroliths and mudstones comprise units in cm scale to several metres. The muddy sediments are generally moderate to intense biomottled with visible trace fossils dominated by *Chondrites* and common to abundant *Rhizocorallium*, *Thalassinoides* and *Planolites*. Abundant thin sandstone beds, laminae and streaks are present showing faint plane bedding, wavy bedding, and occasionally ripple lamination. The facies are mainly distributed in the intervals 104.5–102.5 m, 96.6–94 m, 85–78.6 m, and 70.5–56.5 m. The muddy facies are interpreted deposited from suspension in an oxygenated offshore transition environment allowing a diverse and intense biomottling. The thin sandstone beds are interpreted as deposited during storms and as low density gravity flows.

Mudstones, plane and wavy bedded with thin sandstone laminae comprise minor parts of the interval. The facies may have a weak biomottled fabric of *Chondrites*, *Planolites* and *Thalassinoides*. The facies occur predominantly in the intervals 69.8-62.4 m, 49.7-49.5 m, and 44.5–42.2 m and it is additionally representing the mud draping units in the former described units in the interval. The mudstones are interpreted as deposited from suspension in a distal offshore transition environment.

An erosive pebble conglomerate, 2 cm thick, occurs at 94 m. It is clast-supported with rounded clasts and muddy sand matrix and common pyrite. It is interpreted as a transgressive lag of erosion.

### 2.1.2 Dunken Formation: 40.75 to 4.0 m

The cored interval of the Dunken Formation comprises the lower boundary interval of mainly sandstones, and minor conglomeratic and muddy units.

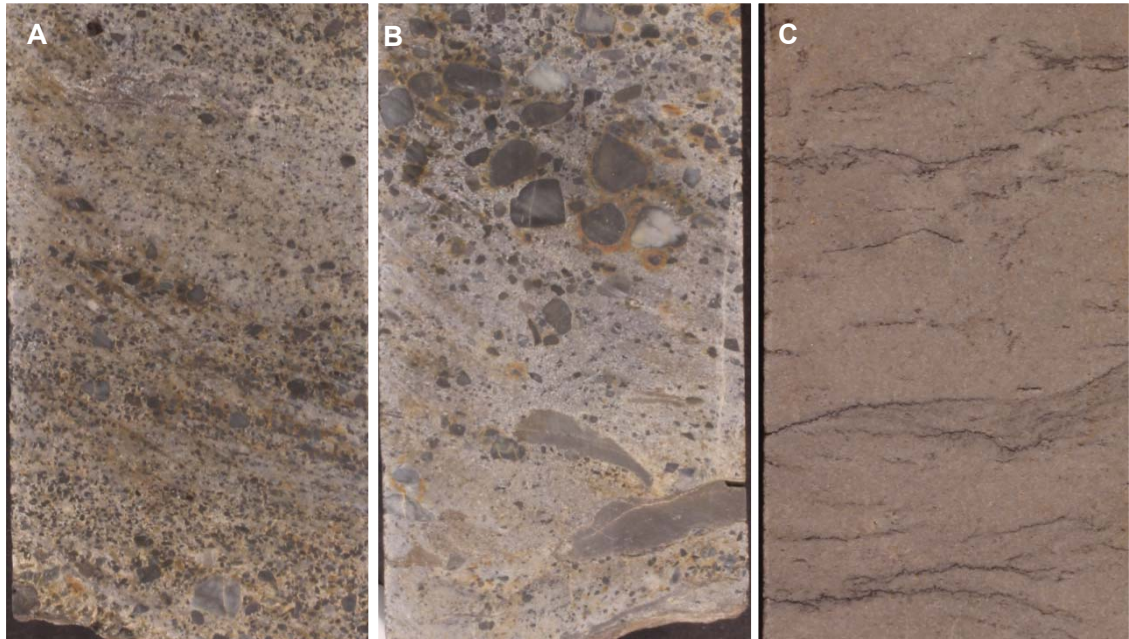


Figure 2.3 Dunken-2 core photos, core width 4.2 cm. A) Coarse-grained sandstone showing fining upward beds. Base of the Dunken Formation (depth 40.75 m). B) Pebbly sandstone overlain by pebble conglomerate, clasts comprise mainly quartzite and chert (depth 40.54 m). C) Homogeneous sandstone with common stylolites (depth 19.45 m).

#### 40.75 – 37.25 m

The base of the formation is marked by a pebble conglomerate, 20 cm thick, with common clasts of chert, mudstones and sandstones. It is overlain by a fining upward interval, 2.6 m thick, of coarse-grained to fine-grained sandstones with plane-, wavy- and low-angle ripple laminations and common mud drapes. The unit is succeeded by a prominent mudstone dominated heterolith, 0.7 m thick, with faint planar and wavy bedding. Strata dip 10°-12°. The lower part of the interval is interpreted as shallow marine with wave and current influenced deposition. The mudstone dominated heterolith are interpreted as deposited in an offshore transition environment.

#### 37.25 – 20.25 m

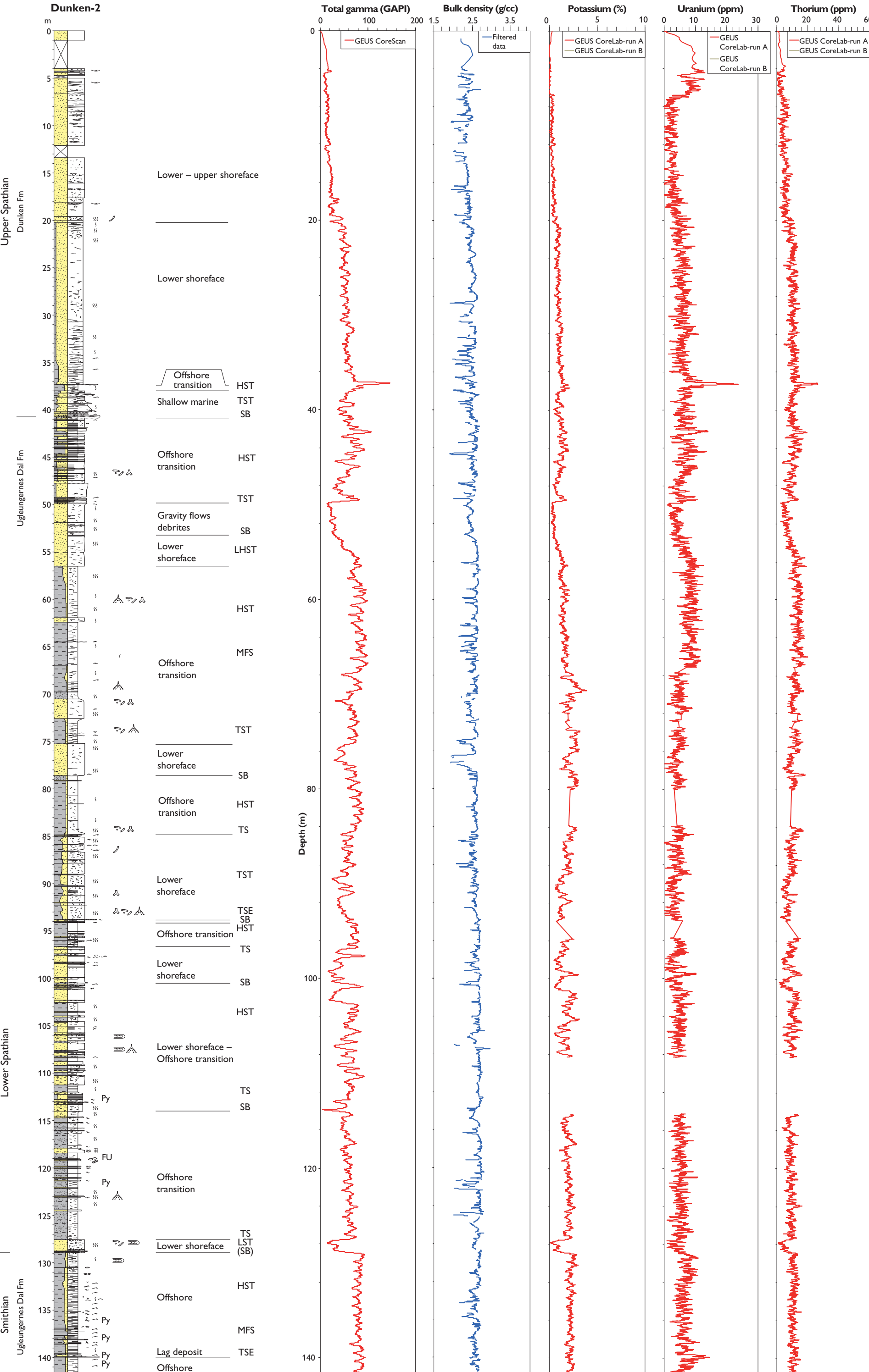
A pebbly lag marks the base over the overlying interval of sandstone dominated heteroliths. The interval shows wavy and indistinct bedding in the lower parts and an increasing degree of biomottling upwards. It is topped by a homogenous bed, 20 cm thick, which in turn is overlain by a burrowed horizon about 40 cm thick. The pebbly bed at the base probably

represents a regressive lag. The overlying biomottled sandstone-dominated heterolith is interpreted as deposited in a lower shoreface environment.

#### **19.54 to 5 m**

The interval is represented by relatively clean sandstones with common stylolites, and minor biomottled structures. Occasional planar bedding, low-angle cross-bedding are observed. Thin muddy beds are recorded in the upper part of the cored Dunken Formation. The interval is interpreted as deposited in lower – upper shoreface environments.

Figure 2.4 (next page) Sedimentological log of the Dunken-2 core, with lithostratigraphy, depositional environment and sequence stratigraphy. The total gamma ray curve, spectral gamma ray curves and filtered bulk density are based on core scanning. Legend in Appendix 1.



## 2.2 Biostratigraphy and bulk organic $\delta^{13}\text{C}$ -isotopes

The palynological study is based on 39 samples and reported in detail together with the biostratigraphic results in the regional study on the Triassic of the Wandel Sea Basin in Lindström & Alsen (this report package). The core was screened for age diagnostic macrofossil, but no ammonoids were recorded. The main palynological results from the core are presented here together with the bulk organic  $\delta^{13}\text{C}$ -isotopes in Table 2.1. The assemblages from the Dunken-2 core are generally very poorly preserved. No quantitative analyses have been carried out. The palynomorphs are dark brown to brownish black in colour.

### 141.40–131.74 m Smithian, *Naumovaspora striata* CAZ

**Palynology.** These assemblages are dominated by spores. The common occurrence of *Punctatisporites fungosus* (FAD latest Griesbachian, FCAD early Smithian; Vigran et al. 2014) indicates assignment to the Smithian *Naumovaspora striata* Composite Assemblage Zone.

**C-isotopes.** The interval 141.40–129.92m exhibit negative C-isotope values between -31.06‰ and 29.02‰. This is consistent with the Smithian negative excursion (Grasby et al. 2013, 2015).

**Remarks:** *P. fungosus* is a characteristic component of Dienerian to Smithian palynofloras. It is especially common in the *N. striata* CAZ. Vigran et al. (2014) have also registered *P. fungosus* in Spathian to middle Anisian strata.

### 127.07–122.37m Undetermined, but probably latest Smithian to earliest Spathian

**Palynology.** No age specific palynomorphs identified.

**C-isotopes.** The C-isotope values of this interval (127.07–118.74m) vary between -25.40‰ and -24.79‰. This is consistent with the positive excursion during the latest Smithian to earliest Spathian (Galfetti et al. 2007).

### 117.76m – 103.07m early Spathian, *Pechorosporites disertus* CAZ

**Palynology.** The assemblages of this interval are dominated by bisaccate pollen, which indicates that it is not older than early Spathian in age. It is tentatively correlated with the *P. disertus* CAZ of Vigran et al. (2014). The co-occurrence of *Rewanispora foveolata* (LADs early late Spathian; Vigran et al. 2014) and *Pechorosporites disertus* (LAD mid late Spathian; Vigran et al. 2014), and the apparent absence of typical late Spathian marker species allows correlation with the early Spathian *P. disertus* Composite Assemblage Zone of Vigran et al. (2014).

**C-isotopes.** In this interval the C-isotope values become more depleted upsection, from -24.70‰ at 114.78m to -26.41‰ at 107.13m, with a slight increase to -25.28‰ at 103.07m.

### 98.39–59.97m probably Spathian

**Palynology.** No age characteristic taxa were identified.

**C-isotopes.** During this interval (99.24m to 57.04‰) the C-isotope values become more depleted, from -26.40‰ to -29.56‰. This corresponds well with the early to mid Spathian C-isotope curves of Grasby et al. (2013, 2015) and Galfetti et al. (2007).

#### **49.53–25.09m late Spathian – *Jerseyaspora punctispinosa* CAZ**

**Palynology.** The presence in these assemblages of *Jerseyaspora punctispinosa* (FAD base *J. punctispinosa* CAZ of Vigran et al. 2014), *Cyclotriletes oligogranifer* (FAD late Spathian, *J. punctispinosa* Assemblage of Vigran et al. 2014) and *Striatoabieites balmei* (FAD late Spathian, *J. punctispinosa* Assemblage; Vigran et al. 2014) allows correlation with the late Spathian *Jerseyaspora punctispinosa* Composite Assemblage Zone of Vigran et al. (2014).

**C-isotopes.** The C-isotope values in this interval (47-49m to 24-26m) become more positive upwards in the succession, from a minimum of -29.90‰ to a maximum of -27.78‰.

#### **20.26–0.41m Undetermined**

**Palynology.** No age determination possible due to poor preservation.

**C-isotopes.** There is a change from values between -27.85‰ to -26.40‰ in the lower part of this interval to more negative values of -28.70‰ close to the top of the cored succession.

#### **Dunken-2B**

This outcrop section is located close to the drill site representing the interval above the Dunken-2 core.

#### **542742 and 542745 Early Anisian, *Anapiculatisporites spiniger* CAZ**

**Palynology.** The presence of *Eresinia spinellata* (FAD lower part of *Anapiculatisporites spiniger* CAZ; Vigran et al. 2014) in the uppermost assemblage allows correlation with the Early Anisian *Anapiculatisporites spiniger* Composite Assemblage Zone of Vigran et al. (2014).

**C-isotopes.** The C-isotope values within this interval lie between -26.57‰ (542745, low carbon content) and -25.95‰ (average value for 542742). This may reflect the more positive values registered in the earliest Anisian by Galfetti et al. (2007).



Table 2.1 Bulk organic  $\delta^{13}\text{C}$ -isotopes and palynostratigraphy in the Dunken-2 core.

Sample Code	height	Locality	Sample Description	Weight Before Acid Washing (g)	Weight After Acid Washing (g)	Measured Carbon Content (%)	Organic Carbon Content (TOC) (%)	$\delta^{13}\text{C}_{\text{V-PDB}}$ (‰)	Mean $\delta^{13}\text{C}_{\text{V-PDB}}$ (‰)	Age	Palynological zones (after Vigran et al. 2014)
517006-239	0,41	Dunken-2	Coarse	0,3184	0,2958	0,111	0,103	-28,70			
"	0,41	Dunken-2	"	"	"	0,120	0,111	-28,63	-28,66		
517006-240	17,63	Dunken-2	Coarse	0,3050	0,2985	0,117	0,115	-26,40			
517006-051	20,26	Dunken-2	Powder	0,3034	0,2905	0,061	0,058	-27,22			
517006-055	24,06	Dunken-2	Powder	0,3064	0,2804	0,186	0,170	-27,78			
"	24,06	Dunken-2	"	"	"	0,191	0,175	-27,85	-27,82		
517006-059	28,02	Dunken-2	Powder	0,3073	0,2409	0,180	0,141	-27,88		early late Spathian	<i>Jerseyaspora punctispinosa</i> CAZ
517006-063	32,05	Dunken-2	Powder	0,3033	0,2687	0,249	0,221	-27,92		early late Spathian	<i>Jerseyaspora punctispinosa</i> CAZ
517006-067	36,08	Dunken-2	Powder	0,3015	0,2410	0,368	0,294	-28,22		early late Spathian	<i>Jerseyaspora punctispinosa</i> CAZ
517006-071	39,89	Dunken-2	Powder	0,3090	0,2908	0,149	0,140	-29,70		early late Spathian	<i>Jerseyaspora punctispinosa</i> CAZ
517006-075	43,81	Dunken-2	Powder	0,3011	0,2847	0,390	0,369	-29,84		early late Spathian	<i>Jerseyaspora punctispinosa</i> CAZ
"	43,81	Dunken-2	"	"	"	0,390	0,369	-29,90	-29,87	early late Spathian	<i>Jerseyaspora punctispinosa</i> CAZ
517006-079	47,49	Dunken-2	Powder	0,3030	0,2706	0,143	0,128	-29,73		early late Spathian	<i>Jerseyaspora punctispinosa</i> CAZ
517006-083	57,04	Dunken-2	Powder	0,3074	0,2781	0,226	0,204	-29,56			
517006-087	60,95	Dunken-2	Powder	0,3003	0,2684	0,257	0,230	-29,28			
517006-091	64,75	Dunken-2	Powder	0,3238	0,2903	0,275	0,246	-29,69			
517006-095	68,33	Dunken-2	Powder	0,3066	0,2397	0,297	0,233	-29,61			
"	68,33	Dunken-2	"	"	"	0,287	0,224	-29,70	-29,65		
517006-099	71,94	Dunken-2	Powder	0,2947	0,2646	0,266	0,239	-29,11			
517006-103	75,82	Dunken-2	Powder	0,3166	0,2935	0,199	0,185	-28,64			
517006-107	79,71	Dunken-2	Powder	0,3087	0,2631	0,246	0,210	-28,57			
517006-111	83,61	Dunken-2	Powder	0,3002	0,2625	0,255	0,223	-27,82			
517006-115	87,59	Dunken-2	Powder	0,3133	0,2746	0,333	0,292	-27,96			
"	87,59	Dunken-2	"	"	"	0,322	0,282	-27,97	-27,97		
517006-119	91,41	Dunken-2	Powder	0,3095	0,2864	0,314	0,290	-28,36			
517006-123	95,45	Dunken-2	Powder	0,3008	0,2637	0,344	0,302	-26,93			
517006-127	99,24	Dunken-2	Powder	0,3064	0,1704	0,073	0,041	-26,40			
517006-131	103,07	Dunken-2	Powder	0,3211	0,2635	0,387	0,317	-25,28			<i>Pechorosporites disertus</i> CAZ
517006-135	107,13	Dunken-2	Powder	0,3087	0,1631	0,090	0,047	-26,41			<i>Pechorosporites disertus</i> CAZ
"	107,13	Dunken-2	"	"	"	0,082	0,043	-26,28	-26,35		<i>Pechorosporites disertus</i> CAZ
517006-139	111,08	Dunken-2	Powder	0,3082	0,2473	0,244	0,196	-24,70			<i>Pechorosporites disertus</i> CAZ
517006-143	114,78	Dunken-2	Powder	0,3169	0,2479	0,244	0,191	-24,74			<i>Pechorosporites disertus</i> CAZ
517006-147	118,74	Dunken-2	Powder	0,2986	0,2170	0,279	0,203	-24,93		early Spathian	<i>Pechorosporites disertus</i> CAZ
517006-151	122,37	Dunken-2	Powder	0,2999	0,2154	0,441	0,317	-24,79			
517006-155	126,04	Dunken-2	Powder	0,3060	0,2142	0,350	0,245	-25,28			
"	126,04	Dunken-2	"	"	"	0,351	0,246	-25,40	-25,34		
517006-159	129,92	Dunken-2	Powder	0,3024	0,2522	0,237	0,198	-29,02		Smithian	
517006-163	133,68	Dunken-2	Powder	0,3075	0,2787	0,230	0,209	-31,06		Smithian	<i>Naumovasporea striata</i> CAZ
517006-167	137,53	Dunken-2	Powder	0,3005	0,2765	0,235	0,216	-30,77		Smithian	<i>Naumovasporea striata</i> CAZ
517006-171	141,40	Dunken-2	Powder	0,3048	0,2810	0,335	0,309	-30,95		Smithian	<i>Naumovasporea striata</i> CAZ

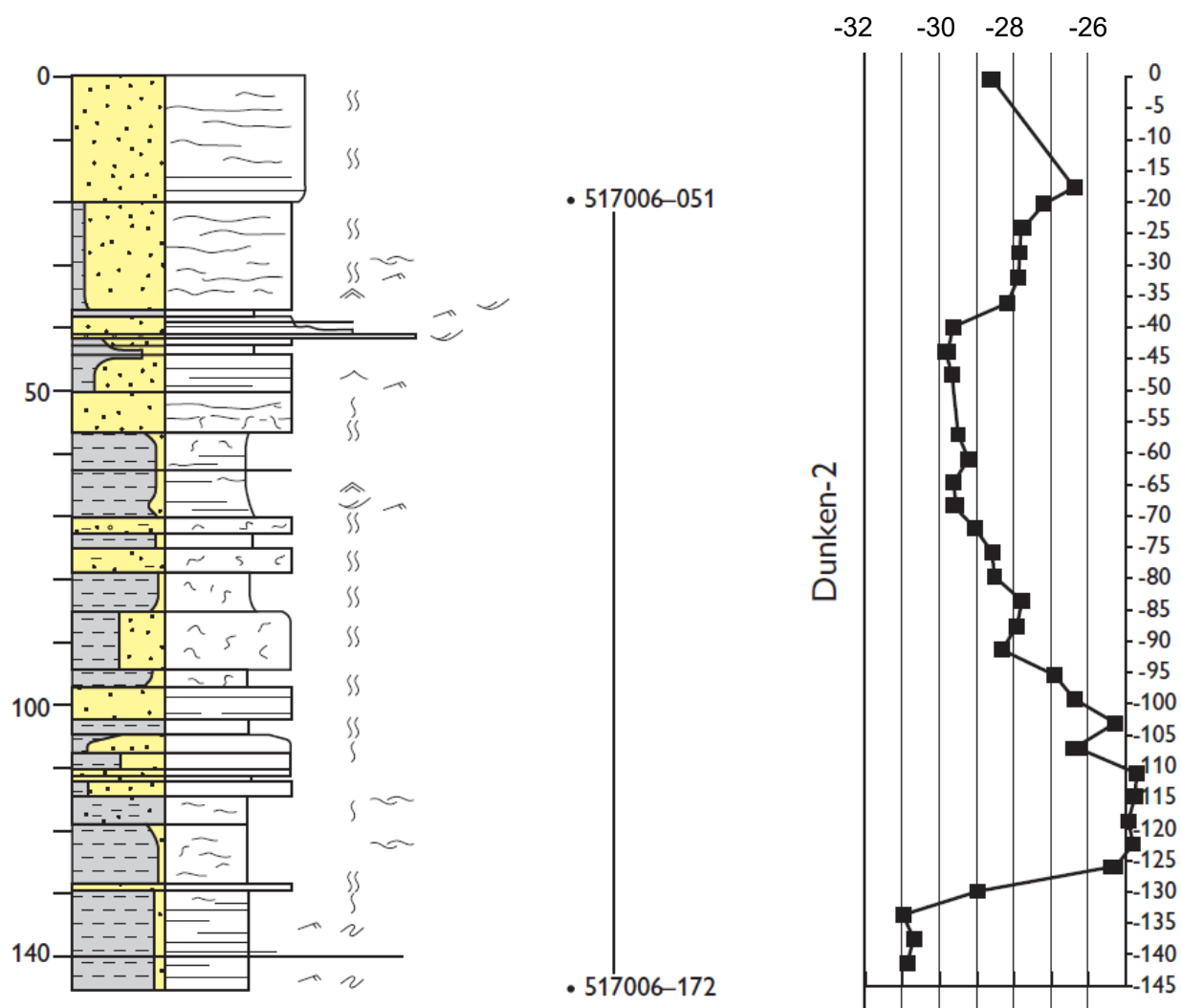


Figure 2.5. Dunken-2 core; lithological log in scale 1:1000 and bulk organic  $\delta^{13}\text{C}$ -isotope curve ( $\delta^{13}\text{C}_{\text{CV-PDB}}/\text{‰}$ ).



## 2.3 Petrophysical logs

This chapter presents the results of a spectral gamma and bulk density scanning of core sections from the Dunken-2. A total of 141.8 meters of core were scanned in two runs. The first run included the upper 113.8 m of the core while the second run included the remaining part of the core (Fig. 2.6). No repeat sections were scanned. The cores were generally in reasonable condition, with recovery close to 100%. A large part of the core length presented a full diameter, cylindrical core to the scanner. The fundamental requirement of the scanning procedure, that the scanned material is cylindrical, was therefore fulfilled for a large part of the cores. Disintegrated sections occurred occasionally, but were rare. The bulk density log trace gives a good indication of the quality of the core: core sections where significant parts of the core are missing have continuous bulk density traces with large amplitude variations and minimum bulk density readings below 1.85 g/ml. The core sections were scanned with the spectral gamma and bulk density scanner of GEUS Core Laboratory. The core sections were scanned sequentially with the core sections being fitted together to present the scanner to a continuous core slowly passing the detectors of the scanner. As part of the data processing, alignment with the wireline log recorded in the borehole was carried out (Fig.2.6). The detailed analytical procedures are presented in Appendix 8.

The main lithologies are reflected in the total gamma values that show several increasing and decreasing trends (Fig.2.4). The total gamma values in mudstones are generally between 50–90 API, The highest values (>60 API) are recorded in the intervals 141–129 m, 7–94, 85–78.5 m, 70.5–58 m, 45–42.5 and 38–37 m. In the mudstone dominated succession in the lower part (141- 114 m) a marked shift is recorded at 129 m showing high mean values of about 80 API below this level and mean values of about 60 API above this level. Relatively clean sandstones show gamma ray values <30 API; they are recorded in the interval 18.5–127.5 m, 102.5–101.5 m, 100–99 m, 52–50 m, and 19.5–5 m.

Heterolithic intervals and mixed mudstone-sandstone units record intermediate values between 40 and 60 API. A high gamma ray peak is recorded at 37 m which corresponds to a thin conglomeratic bed.

Potassium values are not directly reflecting the lithology. The mudstones from 141–114 m show a rather constant content with mean values of about 2 %. General high values up to about 5 % are recorded in the interval from 114–68 m that consists of interbedded sandstone, mudstone, and heteroliths. The potassium content shows a general upward decrease in values to about 1% from 68 to 7 m.

The uranium content is generally low with values below 5 ppm. A general increase in Uranium content to about 10 ppm is recorded in the mudstone dominated intervals 67–56.5 m and 48–37 m.

The thorium readings roughly reflect that of the total gamma ray values. The mudstones in the lower part of the core (141–114 m) show mean values of about 12 ppm. Above this interval there is an overall increasing trend culminating with mean values of about 22 ppm in the mudstone interval 70.5–56.5 m, and a following decrease to <10 ppm in the upper part of the core.

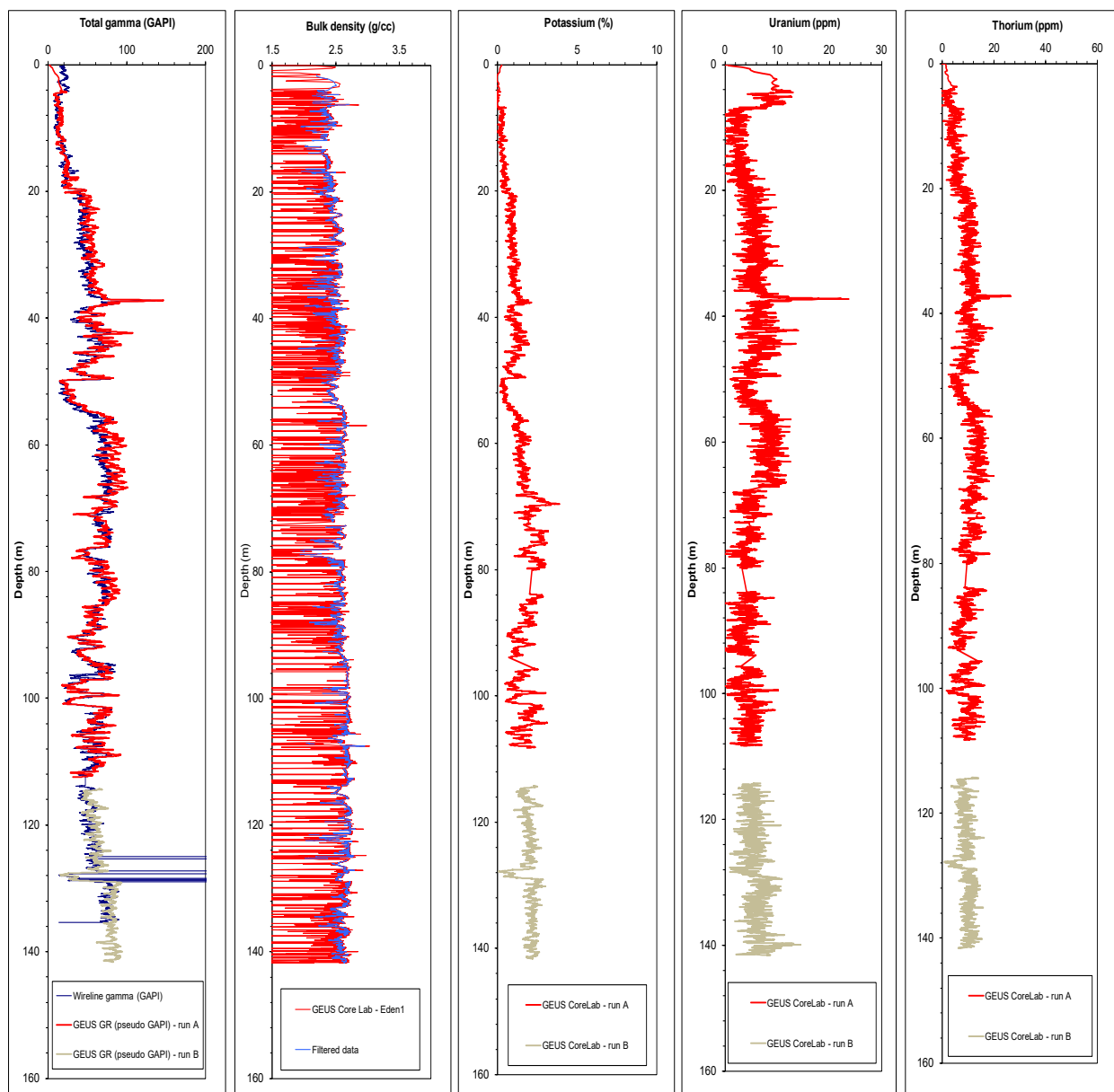


**Figure 2.6** Results of spectral and density logging of the Dunken-2 core.

## 2.4 Sequence stratigraphy

The cored Smithian – uppermost Spathian interval forms an overall shallowing upward succession in a probable 2<sup>nd</sup> order sequence (Fig. 2.4). The maximum flooding is recorded in offshore mudstones in the Smithian interval, and the uppermost Spathian are characterised by fine to medium-grained shallow marine sandstones and include a major sequence boundary at 40.75 m. Eight superimposed higher order sequences are recognised based on sedimentary facies distributions and combined with trends in the total gamma ray curve. They represent transgressive–regressive parasequences of 3<sup>rd</sup> order (Fig. 2.4).

### **Smithian, 141–128.9 m**

The interval represents the Smithian highstand systems tract including a maximum flooding surface in mainly offshore mudstones. A prominent transgressive surface of erosion is represented by a thin conglomerate bed at 140 m.

### **Uppermost Smithian – lower Spathian 128.9–114 m**

The sequence boundary is marked by the erosional biomottled sandstone bed about 1.2 m thick including a thin coarse-grained lag at the base. A transgressive surface is situated at 127.5 m at the base of the biomottled mudstone interval of offshore transition deposits. The succession shows a slightly upwards increase in the abundance of thin sandy beds.

### **Lower Spathian, 114–100.4 m**

The sequence boundary is placed at the base of the biomottled sandstone. The sequence consists of interbedded sandstones and mudstones of lower shoreface to offshore transition in an overall transgressive succession with the highstand represented in the mudstone from 104–102.5 m.

### **Lower Spathian, 100.4–93.8 m**

The sequence boundary is placed at the base of massive sandstone with post-depositional remobilization structures. The sequence consists of interbedded sandstones and mudstones of lower shoreface to offshore transition in an overall transgressive succession with the highstand represented in the mudstone from 96.8–94.2 m.

### **Upper? Spathian, 93.8–78.6 m**

The sequence boundary is represented by a few cm thick pebble conglomerate overlain by a transgressive lower shoreface succession of biomottled sandstone-dominated heterolithic units with cm thick mudstone drapes. The highstand systems tract is represented by offshore transition of biomottled sandy mudstones. The sequence is tentatively referred to upper Spathian but no age diagnostic palynomorphs have been recovered (see biostratigraphic section above).

#### **Upper? Spathian, 78.6–53.4 m**

The base of the sequence is represented by an intensely biomottled muddy sandstone 3.3 m thick. The transgressive succession comprises mainly biomottled sandy mudstones culminating in a highstand and maximum flooding surface in faintly laminated mudstones at 64 m. The late highstand systems tract is represented by few cm thick pebble conglomerate overlain by a transgressive succession of lower shoreface sandy deposits.

#### **Upper Spathian, 53.4–40.75 m**

The base of the sequence is represented by thin massive gravity flow sandstones followed by alternating biomottled sandstones and homogeneous sandstones. It is followed by a transgressive interval of interbedded mudstones and sandstones culminating with a highstand and maximum flooding at 42.7–42.25 m. The upper part is interpreted as a late highstand systems tracts characterized by an increasing sand- influx towards the top.

#### **Upper Spathian, 40.75–5 m**

The base of the sequence is marked by an erosional pebble conglomerate, about 20 cm thick. It is succeeded by a transgressive interval of fining upward units of sandstone with common mudrapes. Highstand offshore transition mudstones are recorded at 38–37.1 m and succeeded by late highstand biomottled sandstone-dominated heteroliths and which in turn is followed by biomottled clean sandstones.

#### **Anisian, 1.0–0 m**

Exposures adjacent to the corehole comprise lower to upper shoreface homogeneous biomottled sandstones that correlate to this interval.

## **2.5 References**

- Bjerager, M., Alsen, P., Keulen, N. Lindström, Piasecki, S. Rasmussen, M.B., Thomsen, T.B. & Therkelsen, J. 2016 A. The Triassic of the Wandel Sea Basin – Lithostratigraphy, Sedimentology, Sequence stratigraphy and Provenance. Danmarks og Grønlands Geologiske Undersøgelse Rapport 2016/6
- Håkansson, E., 1979, Carboniferous to Tertiary Development of the Wandel Sea Basin, eastern north Greenland: Rapport Grønlands Geologiske Undersøgelser 88, 73 pp.
- Kragh, K., Jensen, S. M., and Foug, H., 1997, Ore geological studies of the Citronen Fjord Zinc deposits, North Greenland: project 'Resources of the sedimentary basins of North and East Greenland': Geology of Greenland Survey Bulletin 176, 44-49.
- Kummel 1953. Middle Triassic ammonites from Peary Land. Meddelelser om Grønland 127, 1, 21 pp.
- Lindström, S. & Alsen, P. (this report package). The Triassic of the Wandel Sea Basin – Biostratigraphy and bulk organic  $\delta^{13}\text{C}$ -isotope stratigraphy. Danmarks og Grønlands Geologiske Undersøgelse Rapport 2016/7
- Mølgaard, S., Heinberg, C., Håkansson, E. & Piasecki, S. 1994. Triassic stratigraphy and depositional environment of eastern Peary Land. Scientific report #10 Wandel Sea Ba-

- sin: Basin Analysis. EFP-91 Project No. 0012 Completion report to the ministry of Energy, University of Copenhagen, 5pp, 8 Figures
- Peel, J. S, Daves, P.R. & Troelsen J.C. 1974. Notes on some Lower Palaeozoic to Tertiary faunas from eastern North Greenland Rapport Grønlands Geologiske Undersøgelse 65, 18-23.
- Stemmerik, L. & Håkansson, E. 1989. Stratigraphy and depositional history of Upper Palaeozoic and Triassic sediments in the Wandel Sea Basin, central and eastern north Greenland. Rapport Grønlands Geologiske Undersøgelse 143, 21–43.
- Stemmerik, L., Dalhoff, F., Larsen, B.D., Lyck, J., Mathiesen, A. & Nilsson, I 1998. Wandel Sea Basin, eastern North Greenland. Geology of Greenland Survey Bulletin **180**, 55–62.
- Stemmerik, L., Larsen, B.D. & Dalhoff, F. 2000. Tectono-stratigraphic history of northern Amdrup Land, eastern North Greenland: implications for the northernmost East Greenland shelf. Geology of Greenland Survey Bulletin **187**, 7–19
- Therkelsen, J., Bojesen-Koefoed, J. and Kjøller, C., 2016. The Triassic of the Wandel Sea Basin: Petrography, Diagenesis, Cap-rock properties, Reservoir properties and Petroleum Geochemistry. Contribution to Petroleum Geological Studies, Services, and Data in East and Northeast Greenland. Danmarks og Grønlands Geologiske Undersøgelse Rapport 2016/9
- Troelsen J.C. 1956. Geology In: Winther P.C. et al. A preliminary account of the Danish Peary Land Expedition, 1948–9, Artic 3, 6–8.
- Zinck-Jørgensen, K. & Håkansson, E., 1994, Geological Map of the Kim Fjelde Area, Eastern Peary Land, North Greenland

### 3. Petrography, Diagenesis and Reservoir properties

The evaluation of petrography and diagenesis has been performed on 12 sandstones from the Triassic succession encountered in the Dunken-2 core, which is located just northeast of Storekløft in Peary Land (Fig. 1.1). The samples belong to the Ugleungernes Dal Formation and Dunken Formation (Bjerager et al. 2016). Ten sandstone samples are fine-grained, whereas one is very fine to fine-grained and one is fine- to medium-grained.

Polished thin sections prepared from the plugs, which were used for the porosity and permeability measurements, has been examined by transmitted light microscopy and reflected light microscopy, SEM (Scanning Electron Microscopy) analyses, as well as rock chips from the samples has been used. Further has bulk rock analyses by X-ray diffractometry been performed (Table 3.1).

Framework grains in the sandstones are dominated by quartz with rare to abundant amounts of chert, K-feldspar occur generally in all samples in rare to minor amount, and plagioclase is absent in four samples and where it is present it occur in rare to minor amount (Table 3.2). Rock fragments are mainly metamorphic and are present in rare to common amount, but also rare sedimentary rock fragments (quartzite, carbonate clasts and apatite) occur. Biogenic rock fragments such as shell fragments (mainly apatitic) are present in rare amount. Mica are rare to minor but also absent from the samples. Heavy minerals occur only in traces and consist mainly of zircon, tourmaline and rutile. Detrital clay matrix and mud-clasts are rare except in one sample. Generally the sandstones can be characterized as mature.

The dominating authigenic phase in the sandstones is quartz cementation, which is present in nearly all samples, except in a few samples where early concretionary calcite dominates. Both types of cement are strong and generally pore-occluding and thereby affects the reservoir quality greatly. The high amount of quartz cement is related to a relatively high density of stylolites and dissolution contacts, which is a process commencing at relatively deep burial (cf. diagenetic sequence in Fig. 3.1). In a few samples the sandstones are strongly cemented by a burial related pore-occluding calcite cement, which like the quartz cemented sandstones harshly affects the reservoir quality. Encountered cements with minor influence on reservoir quality include pyrite, goethite and apatite, which probably all are related to early diagenesis (cf. Fig. 3.1). In a few samples burial related ferroan-dolomite/ankerite cement occur in rare to minor amount. The sandstones generally show high degree of mechanical compaction, with the exception of the samples containing early concretionary calcite cement.

The porosity and permeability reducing factors concerning diagenesis in the sandstones are the strong quartz cementation associated with stylolitisation and dissolution contacts and also strong calcite cementation. Porosity and permeability in the sandstones is generally low (<1–9% and <0.04–3.44 mD) (Fig 3.2). In four samples with primarily pore-occluding calcite cement the permeability is too low to be measured.

Experiments and simulations described in the literature suggest that quartz cementation is more pronounced in finer-grained than in coarser-grained sandstones (Heald and Renton, 1966; Walderhaug, 1996). This may be in good agreement with the present study, as the

majority of the samples are fine-grained and strongly quartz cemented. However, quartz cementation is a process which often commences at temperatures around 80°C and escalates with increasing temperature (Bjørlykke et al., 1992; Ehrenberg, 1990; Walderhaug, 1994; Walderhaug et al., 2001). This may indicate that the sandstones, due to the strong quartz cementation, may have experienced a very long burial residence time at this temperature or the burial temperatures may have been considerable higher in shorter time intervals (or a combination).

However a discrepancy occur in the amount of quartz cement and calculated maximum burial temperatures (from vitrinite reflectance data), which show maximum burial temperatures between 62–67°C in the Storekløft area (Therkelsen et al., 2016 this report package). These calculated temperatures are not high enough to create the high amount of quartz cement, which are present in the sandstones.

**Table 1.** Semi-quantitative XRD analysis related to porosity, cement type and grain size. Mineral quantities in wt%. Muscovite is most probably illite. Cement type: Q=Quartz. Cc=Carbonate (generally calcite); Estimated amount of cement (volume): \* 1-5%; \*\* 5-15%; \*\*\*15-50%.

Sample no.	Locality	Meter in log	Lithostratigraphy (Formations)	Quartz	Microcline	Albite	Illite/Muscovite	Chlorite	Calcite	Dolomite	Ankerite	Apatite	Crandallite	Pyrite	Gypsum	Porosity (%) Measured	Cement Type	Mean grain size (µm)
517006-201	Dunken-2	5.46	Dunken	98.6	0.6		0.4					0.3				5.00	Q***	200
517006-202	Dunken-2	8.17	Dunken	95.9	2.1		1.1		0.4			0.5				4.56	Q***	200
517006-204	Dunken-2	18.55	Dunken	96.5	1.7		0.7		0.7			0.3	0.2			4.41	Q***	150
517006-206	Dunken-2	32.75	Dunken	77.8	4.0	1.3	3.3	2.1	8.0	2.1		0.3		1.1		1.77	Q***+Cc**	125
517006-207	Dunken-2	40.27	Ugleungernes Dal	90.3	0.7	0.8	1.6	1.8	3.1			0.6	0.3	0.5	0.3	1.82	Q***+Cc*	250
517006-208	Dunken-2	48.17	Ugleungernes Dal	92.8	1.0	0.9	1.7	2.2	traces			1.1	0.3			8.13	Q***	225
517006-209	Dunken-2	50.38	Ugleungernes Dal	90.6	1.1	1.6	1.8	1.2	0.6		2.2	0.3		0.4		3.05	Q***	175
517006-210	Dunken-2	52.65	Ugleungernes Dal	90.8	0.9	1.5	1.8	1.7	0.1	0.4	2.2	0.3		0.2		3.71	Q***+Cc*	175
517006-213	Dunken-2	77.93	Ugleungernes Dal	61.0	4.3	5.1	14.2	12.5	2.6					0.3		9.22	Cc*	175
517006-215	Dunken-2	98.25	Ugleungernes Dal	55.9	0.8	3.0	1.6	1.6	34.4	1.9				0.7		0.34	Cc***	150
517006-217	Dunken-2	110.98	Ugleungernes Dal	49.6	1.4	2.9	3.7	2.9	35.9	2.9				0.7		0.21	Cc***	150
517006-218	Dunken-2	127.96	Ugleungernes Dal	70.7	0.5	0.5	0.6	0.6	26.4					0.7		0.2	Cc***	200

**Table 2.** Semi-quantitative petrographic evaluation. Abundance is given as: Rare (R): <1%; Minor (M): 1-5%; Common (C): 5-15%; Abundant (A): 15-50%; Dominating (D): >50%.

Sample ID	Locality	Lithostrat. (formation)	Framework grains										Diagenetic changes								Porosity (%)	Permeability (mD)	Mean grain size (µm)	
			Quartz	Chert	K-feldspar	Plagioclase	Rock fragments	Biogenic rock fragments	Mica	Heavy minerals	Mud-clasts	Detrital clay	Quartz	calcite (concretionary)	Calcite	Fractured ankerite	Apatite	Goethite	Pyrite	Grain dissolution (secondary porosity)				
517006-201	Dunken-2	Dunken	D	M	R		R	R		R	R	R	A							R-M	5.00	0.07	200	
517006-202	Dunken-2	Dunken	D	R-M	R-M		R-M	R	R	R	R-M	R-M	A		R				R	M	4.56	0.06	200	
517006-204	Dunken-2	Dunken	D	R-M	R-M		R-M	R	R	R	R-M	R	A		R					R	M	4.41	0.04	150
517006-206	Dunken-2	Dunken	D	M	M	R-M	M	R	R	R		M	M-C		C	R-M				R-M	R	1.77	<0.04	125
517006-207	Dunken-2	Ugleungernes Dal	D	C	R		R	R		R	R	R	A		M		R			R		1.82	0.04	250
517006-208	Dunken-2	Ugleungernes Dal	D	C	R		R	R-M	R	R	R	R-M	A		R		R	R		R	M	8.13	3.44	225
517006-209	Dunken-2	Ugleungernes Dal	D	M	R-M	R-M	M	R	R	R	R	R	A		R	R-M	R			R		3.05	0.07	175
517006-210	Dunken-2	Ugleungernes Dal	D	R-M	R-M	R-M	R-M			R		R	A			M	R			R	R	3.71	0.04	175
517006-213	Dunken-2	Ugleungernes Dal	D	M	M	M	R-M	R	M	R		A			R-M			R		R	R	9.22	0.08	175
517006-215	Dunken-2	Ugleungernes Dal	A-D	C	R-M	R-M	C		R-M	R	R	R		A	R					R		0.34	<0.04	150
517006-217	Dunken-2	Ugleungernes Dal	A-D	C	R-M	R-M	C		M	R	R	R		A	R					R		0.21	<0.04	150
517006-218	Dunken-2	Ugleungernes Dal	D	A	R	R	R	R	R	R	R				A					R		0.20	<0.04	200

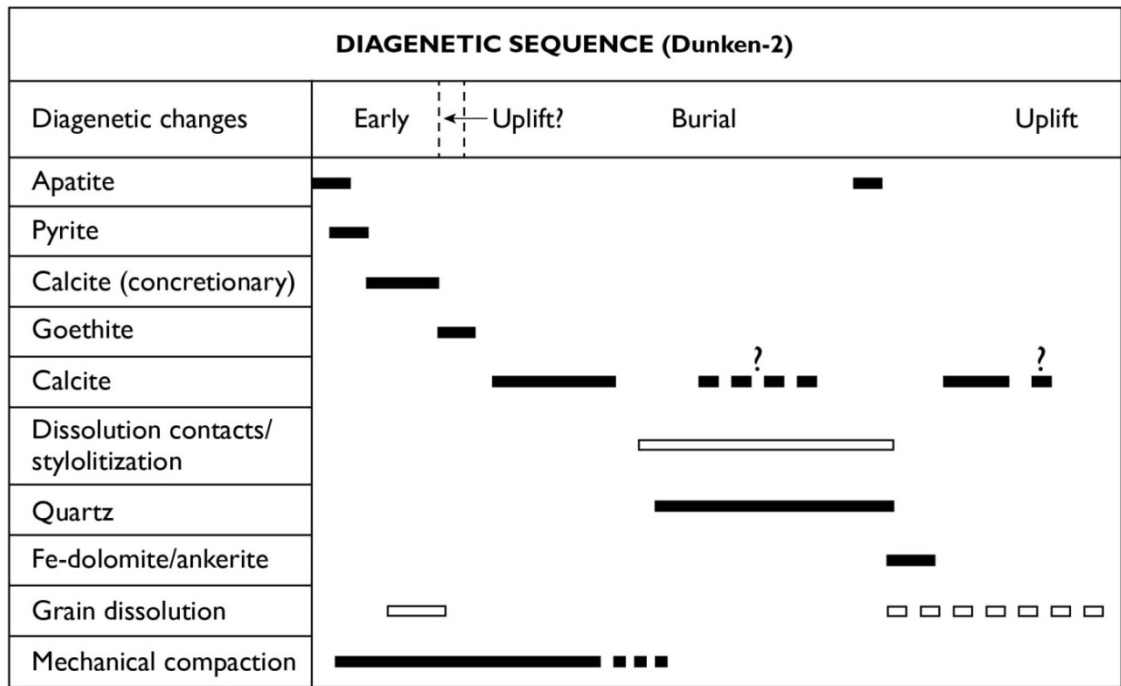


Figure 3.1. Diagenetic sequence for the Dunken-2 core samples.

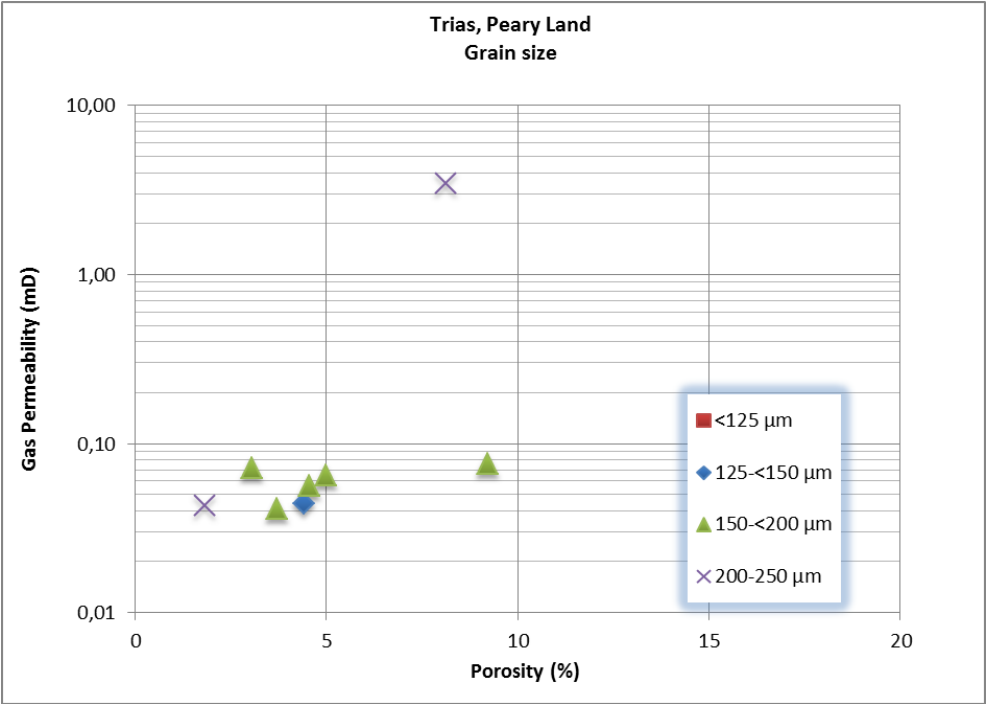


Figure 3.2. Plug porosity and permeability related to grain size. Note that four samples are not shown due to too low permeability (<0.04 mD).

References



- Bjerager, M., Alsen, P., Keulen, N. Lindström, Piasecki, S. & Therkelsen, J., this report package. A. The Triassic of the Wandel Sea Basin – Lithostratigraphy, Sedimentology, Sequence stratigraphy and Provenance. Contribution to Petroleum Geological Studies, Services, and Data in East and Northeast Greenland Danmarks og Grønlands Geologiske Undersøgelse Rapport. 2016/6
- Bjørlykke, K., Nedkvitne, T., Ramm, M., and Saigal, G.C., 1992. Diagenetic processes in the Brent Group (Middle Jurassic) reservoirs of the North Sea; an overview, in Morton, A.C., Haszeldine, R.S., Giles, M.R., and Brown, S., eds., *Geology of the Brent Group*: London, Geological Society Special Publications, 61, p. 263–287.
- Ehrenberg, S. N., 1990. Relationship between diagenesis and reservoir quality in sandstones of the Garn Formation, Haltenbanken, mid-Norwegian continental shelf. *American Association of Petroleum Geologists Bulletin* 74, 1538–1558.
- Heald, M.T. and Renton, J.J., 1966. Experimental study of sandstone cementation. *Journal of Sedimentary Petrology*, v. 36, p. 977–991.
- Therkelsen, J., Bojesen-Koefoed, J. and Kjøller, C., 2016. The Triassic of the Wandel Sea Basin: Petrography, Diagenesis, Caprock-/Reservoir-properties and Petroleum Geochemistry.
- Walderhaug, O., 1994. Temperatures of quartz cementation in Jurassic sandstones from the Norwegian Continental Shelf - evidence from fluid inclusions: *Journal of Sedimentary Research*, v. 64A, p. 311–323.
- Walderhaug, O., 1996. Modelling of quartz cementation and porosity loss in deeply buried sandstone reservoirs. *American Association of Petroleum Geologists Bulletin* 74, 731–745.
- Walderhaug, O., Bjørkum, P.A., Nadeau, P. H. and Langnes, O., 2001. Quantitative modelling of basin subsidence caused by temperature-driven silica dissolution and reprecipitation. *Petroleum Geoscience*, Vol. 7, p. 107–113.

## 4. Cap-rock properties

To evaluate the potential sealing capacity of the mudstones in the Triassic of the Wandel Sea Basin, a limited cap-rock investigation was carried out. The cap-rock investigation was based on analysis of nine (9) mudstone samples from the Dunken-2 well (samples 517006-230 to 517006-238; Fig. 4.1), and one (1) selected outcrop mudstone (sample 545514). The samples were selected in order to represent the variation in potential cap-rocks occurring in the Basin.

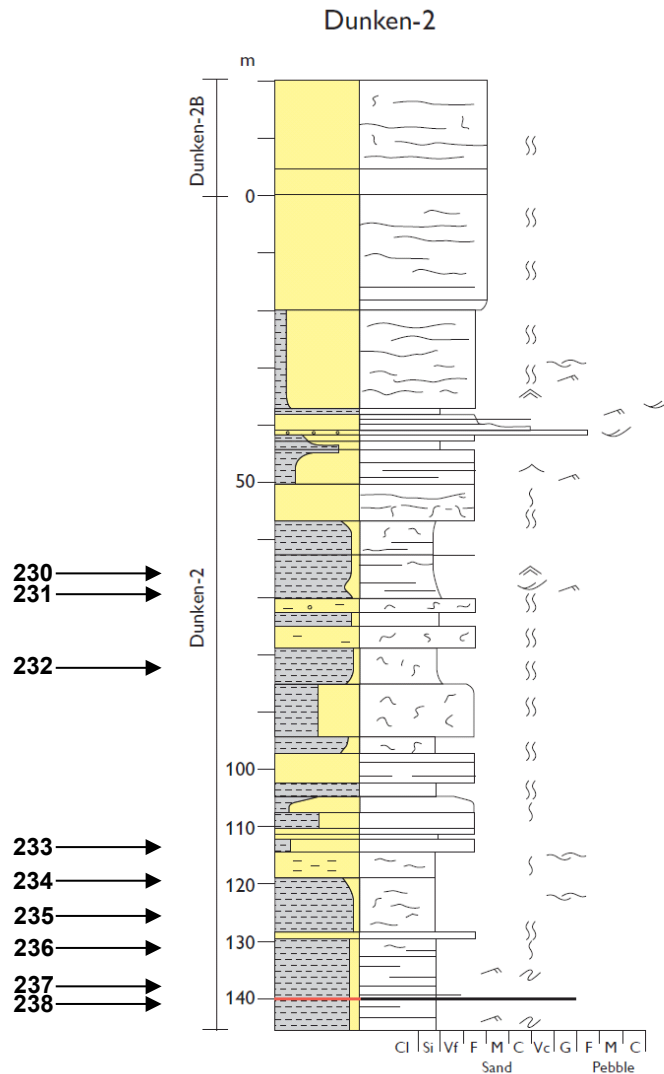


**Figure 4.1:** Lithological log showing the depths of cap-rocks from the Dunken-2 well (Well ID: 517006) studied in the limited cap-rock study presented in this report. Depths are also provided in Table 4.2.

## 4.1 Methods

The cap-rock characterization is based on a variety of analyses, including conventional core analyses (CCAL) such as He-porosity, grain density, and gas permeability. Other methods applied are grain size analysis, mineralogical compositional analysis by X-ray diffractometry (XRD), specific surface area (SSA) measurement, and mercury-injection capillary pressure (MICP) measurements. This section provides a short description of the methods used.

Core analyses (CCAL) were carried out on small plug samples of 1" diameter drilled from the core and left to dry at 60°C in an oven until constant weight. No cleaning was attempted because the core derives from the vadose/groundwater zone. The samples were analyzed in a dried condition according to "API recommended practice for core analysis procedure" (API, 1998). Porosity and grain density were measured by the He-expansion technique. The uncorrected permeability to N<sub>2</sub>-gas was measured at a confining pressure of 400 psi. The lower limit for permeability measurements is 0.05 mD.

Porosity, capillary pressure and pore throat sizes were measured on sub-samples/trims from the CCAL plug samples using a Micromeritics Autopore-IV porosimeter located at SKM Services in Aberdeen. Hg-drainage capillary pressure is measured in an injection sweep from vacuum to 60.000 psia (400 MPa). Pore throat sizes can be measured from 200 µm down to ~ 3 nm, covering pore size distributions in the micro-, meso- and macropore range. He-porosity was also measured on the sub-samples/trims prior to Hg-injection. These measurements were performed by COREX in Aberdeen.

For the mineralogical characterization, a sub-sample from the CCAL plug was hand-ground to pass a 0.25 mm sieve. Samples used for grain size analysis were further dispersed by ultrasonic treatment. Chemical pretreatment involved extraction with NaAc at pH 5.5 to remove calcite, followed by NaOCl at pH 9.0 to remove organic matter (Anderson, 1963), and then Na-dithionite, bicarbonate, and citrate at pH 7 to remove Fe- and Al-oxides (Mehra & Jackson, 1958). The mild dissolution of calcite is carried out in order to avoid dissolution of non-calcite minerals. The grain size distribution was then obtained from a particle size centrifuge (Slater and Cohen, 1962).

Bulk mineralogical composition was evaluated from XRD analysis of randomly oriented powder of the bulk sample. Clay mineralogy was evaluated from XRD on oriented specimens prepared from the clay fraction (<2 µm fraction). The oriented specimens were prepared by the pipette method as follows:

1. Mg-saturated air dry
2. Mg-saturated and glycolated (exposed to glycol vapour for three days at 60°C)
3. K-saturated air dry
4. K-saturated, air-dry and after heating for 1 hour at 300°C
5. K-saturated, air-dry and after heating for 1 hour at 550°C

Comparison of XRD results from (2) with (1) helps distinguishing smectite from chlorite and vermiculite; comparison of (4) with (3) helps distinguishing vermiculite from chlorite; comparison of (5) and (3) helps distinguishing kaolinite from chlorite. Details regarding the analytical equipment are listed in Table 4.1 below. Preparation of specimens was carried out by GEUS Core Laboratory while XRD analysis and interpretation was performed by the XRD Laboratory at the Natural History Museum of Denmark. Rietveld method (Topas 4

program, Bruker-AXS product) was used for the determination of crystalline mineral proportions.

**Table 4.1:** Details regarding analytical equipment and instrument set-up for the XRD analyses on 9 samples from the Dunken-2 well and 1 sample from Kilen, NE Greenland.

<b>Instrument</b>	<b>Bruker-AXS powder diffractometer D8 Advance</b>
<b>Radiation</b>	<b>Cu X-ray tube</b>
<b>Monochromator</b>	<b>Primary beam Ge111</b>
<b>Wavelength</b>	<b>1.54059 Å</b>
<b>Geometry</b>	<b>Bragg-Brentano</b>
<b>Detector</b>	<b>LynxEye, linear PSD, 3.3° opening</b>
<b>Divergence slit</b>	<b>Fixed, 0.45°</b>
<b>Measuring range (clay fraction)</b>	<b>2 – 30° 2<math>\theta</math></b>
<b>Measuring range (bulk samples)</b>	<b>5 – 90° 2<math>\theta</math></b>
<b>Step</b>	<b>0.02°</b>

Specific surface area was determined from a multipoint adsorption isotherm measured on a Surface Area and Pore Size Analyzer (Beckman Coulter) using N<sub>2</sub>. The samples were out-gassed 1020 minutes at 80°C. The specific surface area was calculated according to the BET model (Brunauer et al., 1938).

Total Organic Carbon (TOC, wt%) was determined by combustion using a LECO CS-200 induction furnace. TOC was determined after elimination of carbonate-bonded carbon by prolonged HCl-treatment at elevated temperature.

## 4.2 Core analysis – results

Data for Helium (He-) porosity and Mercury (Hg-) porosity are listed in table 4.2 below. Except for the Hg-porosity of sample 230, all measured porosities are relatively low and below 6 %. In general, there is a reasonable correlation between He-porosity and Hg-porosity measurements although the measured Hg-porosity in some cases is up to 2-3 % (p.u.) higher than the measured He-porosity. The exact reason for this remains unexplained, although it is likely that the variation in porosity is related to the small trim sample size used for Hg-injection and He-porosimetry at COREX (Table 4.1). As the porosity is relatively low and the bulk volume is also low, the uncertainty on the measured porosity becomes higher. Grain density is elevated compared to normal clastic rocks having “quartz-feldspar” grain density of 2.65 g/cc (Table 4.1). This is most likely due to carbonate cementation and possibly also small amounts of pyrite (Table 4.4).

**Table 4.2:** Conventional core analysis data measured for cap-rock samples from the Dunken-2 well and Kilen. Three different measures of the sample porosity is given by Helium (GEUS = large plug sample; COREX = sub-sample/trim) and Mercury (SKM = sub-sample/trim) injection, respectively. For an explanation refer to the text above. Gas permeability was measured on large plug samples with a detection limit of 0.05 mD. Sample ID refers to sub-sample ID from well 517006 (Dunken-2). n.a. = not analysed.

			GEUS - plug	COREX - trim	SKM - trim		
Sample ID	Type Outcrop/Well	Depth [m]	Porosity <sub>(He)</sub> [%]	Porosity <sub>(He)</sub> [%]	Porosity <sub>(Hg)</sub> [%]	Grain density [g/cc]	Gas perm. [mD]
230	W	66.2	4.2	4.8	7.2	2.736	0.05
231	W	68.9	3.7	4.3	3.9	2.727	0.07
232	W	82.1	2.9	1.8	4.5	2.724	<0.05
233	W	112.7	1.0	0.7	1.7	2.691	<0.05
234	W	118.6	1.8	2.0	3.2	2.714	0.05
235	W	125.9	1.8	2.0	1.7	2.713	<0.05
236	W	130.2	2.3	3.0	5.5	2.734	0.05
237	W	137.8	0.6	2.4	2.5	2.682	<0.05
238	W	140.7	1.0	0.7	3.0	2.706	<0.05
545514	O	n.a.	n.a.	3.6	3.1	n.a.	n.a.

Mercury injection data listed in Table 4.3 are extracted from the diagrams in Appendix 1. Most samples have capillary threshold pressures between c. 1,000 psia and c. 4,000 psia suggesting a reasonable cap-rock quality. In some of the samples, the entry of mercury in the 10-15% largest pore throats occur gradually (samples 230, 234, 236, 238, 545514). For these samples, the estimated threshold pressure is based on a qualitative assessment (Table 4.3). Samples with the highest capillary entry pressures (samples 233, 234, 235, 237) also have the most narrow pore throat size distributions (Appendix 7). As a consequence, the pore throat radius of 50% mercury saturation ( $r_{50}$ , Table 4.3) is similar in all samples while the pore throat radius of 10% mercury saturation ( $r_{10}$ , Table 4.3) varies considerably between samples. The general trend for all samples is a bi-, tri- or multimodal pore throat size distribution rather than a uni-modal distribution which is sometimes preferred for good cap-rocks (cf. Appendix 7). However, the vast majority of pore throat sizes are in the sub-micro and nano range (0.01-0.25  $\mu\text{m}$ ) which is in good agreement with the low permeability of all samples (Table 4.2).

**Table 4.3:** Seal capacity data in an air-mercury fluid system read from high-pressure mercury injection measurements on 10 cap-rock samples from the Dunken-2 well and Kilen;  $r_{10}$  and  $r_{50}$  denotes the pore throat radius in nm (nano-meter) where 10% and 50%, respectively, of the sample pore volume has been filled by injected mercury. A small distance (tens of nm) between  $r_{10}$  and  $r_{50}$  identifies a narrow pore throat size distribution and vice-versa. The threshold pressure is estimated by the tangent method.

Sample ID	Porosity <sub>(Hg)</sub> [%]	Threshold P <sub>(Air-Hg)</sub> [psia]	Pore radius	
			r <sub>50</sub> [nm]	r <sub>10</sub>
230	7.2	~1,100	9	70
231	3.9	950	25	88
232	4.5	1,900	9	37
233	1.7	3,700	8	19
234	3.2	~3,000	7	19
235	1.7	3,200	10	24
236	5.5	~2,000	6	30
237	2.5	3,200	7	20
238	3.0	~1,500	5	80
545514	3.1	~2,500	8	42

Cross-plotting of porosity and threshold pressures suggests a general increase in threshold pressure with decreasing porosity (Figure 4.2)

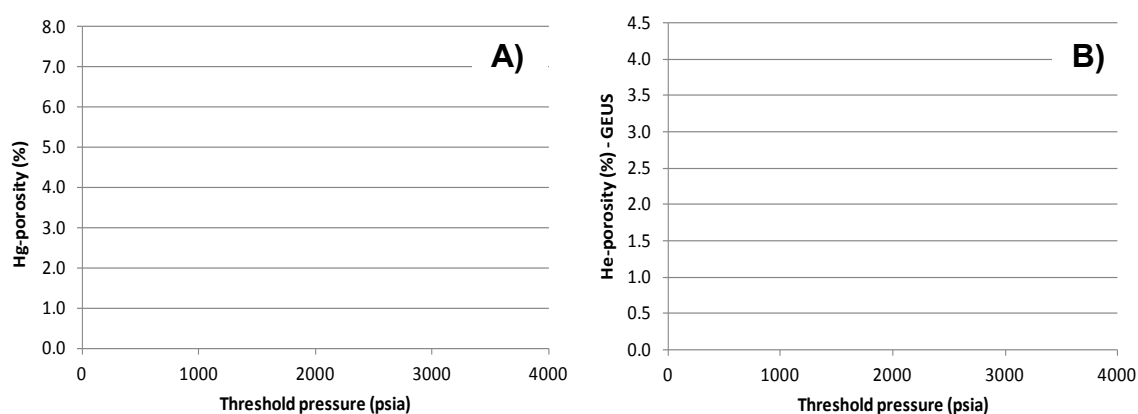


**Figure 4.2:** Cross-plot of porosity and Hg threshold pressure for 9 cap-rock samples from the Dunken-2 well and 1 cap-rock sample from Kilen. A) Porosity derived from MICP on sub-samples from the sampled specimens. B) Porosity measured by He-porosimetry on 1" plug specimens.

### 4.3 Mineralogy and grain size – results

The grain size distribution and mineralogy are listed in Tables 4.4 and 4.5. It appears that all samples should be classified as laminated siltstones because more than  $\frac{2}{3}$  of the fraction below 63  $\mu\text{m}$  comprise silt-size grains (63-2  $\mu\text{m}$ ) (Lundegard & Samuels, 1980). The highest clay contents are observed in the uppermost samples from the Dunken-2 well (samples 230-232) as well as the outcrop sample from Kilen (sample 545514). In these samples, the clay fraction comprise c. 15% (w/w) of the grains while in the remaining samples, the clay fraction comprises 7-10 % (w/w) of the sample. Samples taken from the Dunken-2 well all have a low TOC below 0.4 % (w/w) while the TOC content of the Kilen sample is slightly higher (Table 4.4). The N<sub>2</sub>-BET specific surface area increases with increasing clay content (Figure 4.3). Although the sample from Kilen deviates from this general trend, the relationship shown in Figure 4.3 suggests that the N<sub>2</sub>-BET specific surface area is mainly controlled by the clay fraction of the samples.

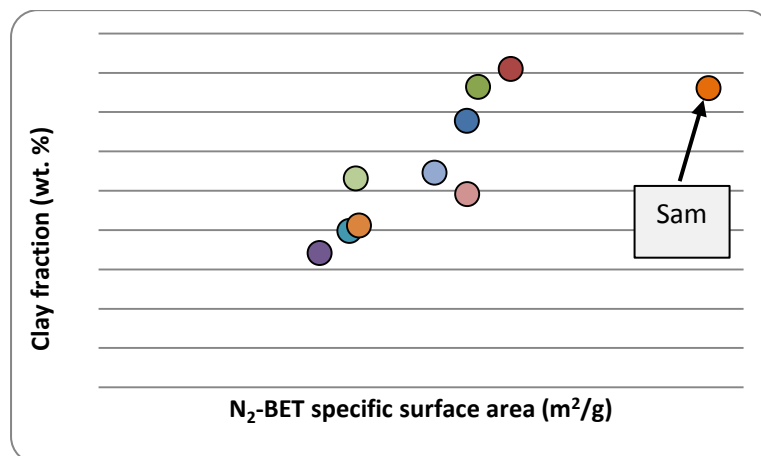


**Figure 4.3:** Cross-plot of clays fraction and specific surface area for 9 cap-rock samples from the Dunken-2 well and 1 cap-rock sample from Kilen.

The amount of clay and the Hg threshold pressure of the samples do not correlate well (compare Tables 2.3 and 2.4). Rather, it seems that the threshold pressure is highest for the least sorted samples (e.g. samples 233 and 237). A pictorial representation of the grain size distribution can be seen from the histogram in Figure 4.4.

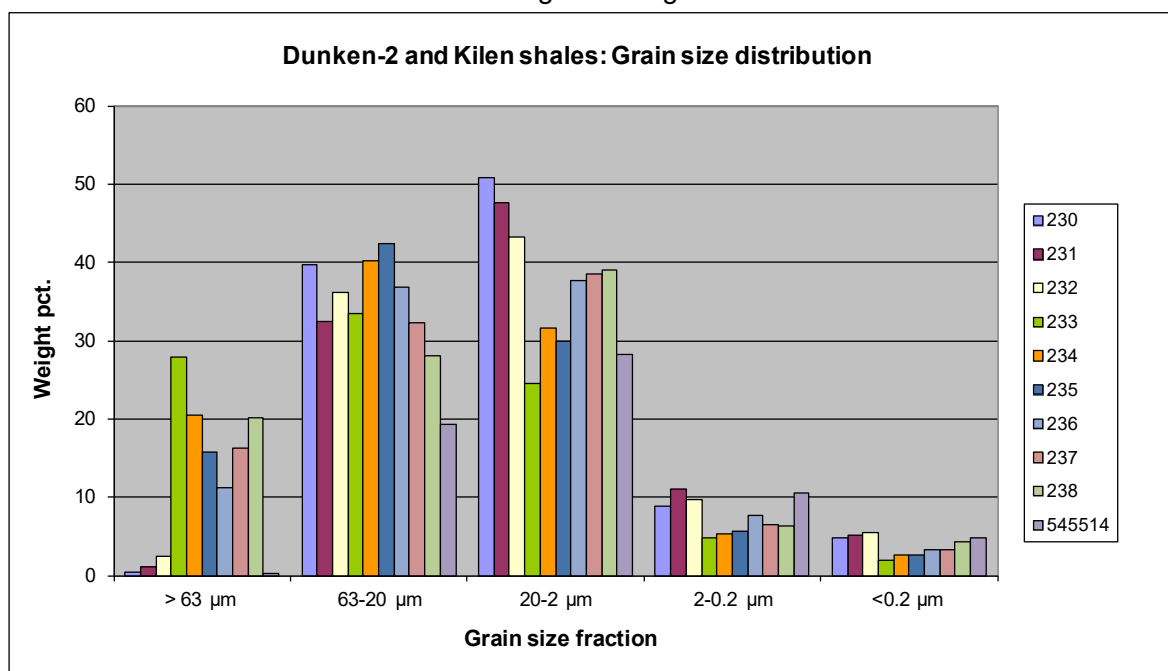


**Figure 4.4:** Grain size distribution data measured on nine (9) siltstone samples from the Dunken-2 well (samples 230-238) and one (1) outcrop sample from Kilen (sample 545514). The silt and clay size fractions have been split into coarse and fine sub-fractions to help interpret other experimental data.

The mineralogical analysis shows quartz contents of c. 45-55 % (w/w) in all samples from the Dunken-2 well (Table 4.5). The carbonate content is highest in the middle part of the cored section (samples 233-235) with a total carbonate content of c. 20 % (w/w). For comparison, the carbonate content in the upper part of the cored section is c. 10 % (w/w) (samples 230-232) while in the lower part of the cored section, the carbonate content is only 1-2 % (w/w). The high carbonate contents in samples 233-235 indicate

that carbonate cementation is one reason for the higher threshold pressures obtained in these samples (cf. Table 4.3).

With regard to the clay mineral assemblage of samples from the Dunken-2 well, samples 230-238 contain illite as the main clay mineral plus chlorite as the secondary clay mineral. Small quantities of kaolinite might be present as well (estimated amount is around 5 % (w/w) of the clay minerals). The diffraction diagram of illite (not shown) suggests that it also contains a mixed-layer fraction dominated by illite, and containing chlorite or smectite layers in addition. The low content of the latter two did not allow more accurate determination of the mixed clay mineral nature and content, which also is estimated to be 5% or less.

The outcrop sample from Kilen (sample 545514) is distinct in having relatively low quartz content (26 % (w/w)) and a high content of pyrite (36 % (w/w)). Oxidation of the pyrite in this sample during grain size analysis is probably the reason for the bad mass balance obtained during grain size analysis (Table 4.4). With regard to the clay mineral composition of the Kilen sample, illite and kaolinite are the main components. Mixed-layer illite-chlorite (or smectite) is also present in equally small quantities and a very small amount of chlorite could also be identified.

In general, the relatively low content of swelling clays, such as smectite and mixed-layer clays, in all samples is favorable for the cap-rock properties of the rocks.

**Table 4.4:** Grain size distribution, N<sub>2</sub>-BET, and TOC data for 1 outcrop cap-rock sample from Kilen (sample 545514) and 9 cap-rock samples taken at different depths along the core from the Dunken-2 well. Observe that summation of fractions making up less than 95 wt-% is due to other components eg. calcite and organic material removed during the initial sample preparation.

nr.	wt - %					Σ clay size [% - w/w]		Σ silt size [% - w/w]		N <sub>2</sub> BET [m <sup>2</sup> /g]	TOC [% - w/w]
	> 63 μm	63-20 μm	20-2 μm	2-0.2 μm	<0.2 μm	Σ grains	<2 μm	63-2 μm			
# 230	0.4	39.7	50.9	8.8	4.8	100	14	91		4.57	0.20
# 231	1.1	32.4	47.6	11.1	5.2	97	16	80		5.11	0.28
# 232	2.5	36.1	43.2	9.7	5.5	97	15	79		4.71	0.34
# 233	28.0	33.5	24.4	4.8	2.0	93	7	58		2.74	0.09
# 234	20.5	40.3	31.6	5.3	2.7	100	8	72		3.11	0.19
# 235	15.8	42.3	29.9	5.7	2.6	96	8	72		3.23	0.23
# 236	11.1	36.9	37.7	7.7	3.2	97	11	75		4.16	0.20
# 237	16.2	32.3	38.6	6.5	3.3	97	10	71		4.57	0.15
# 238	20.1	28.1	39.1	6.3	4.3	98	11	67		3.19	0.22
# 545514*	0.2	19.2	28.2	10.5	4.7	63	15	47		7.56	1.02

\* Organic material as well as Fe- and Al-oxides removed from sample by oxidation prior to grain size analysis. Wt-% is related to total sample weight.

**Table 4.5:** Mineralogical data for 1 outcrop cap-rock sample from Kilen (sample 545514) and 9 cap-rock samples taken at different depths along the core from the Dunken-2 well. Data are obtained from XRD analysis.

nr.	wt - %											Σ minerals
	quartz	microcline	albite	mica	illite	chlorite	kaolinite	calcite	dolomite	pyrite	apatite	
# 230	49	4	7	1	19	8	2	4	4	3	0	101
# 231	49	4	6	1	18	8	2	5	4	3	0	100
# 232	51	5	6	1	18	10	2	4	3	2	0	102
# 233	57	2	5	1	8	5	1	14	6	0.5	0	99.5
# 234	48	2	8	1	13	6	1	15	5	2	0	101
# 235	46	2	9	1	14	6	2	12	5	2	0	99
# 236	45	4	11	1	20	10	1	2	2	3	0	99
# 237	46	5	16	1	18	10	1	0	1	2	0	100
# 238	42	5	15	1	21	11	1	0	1	2	0	99
# 545514	26	0	6	3	14	3	2	2	5	36	2	99

Chlorite is intermediate clinocllore-chamosite with Fe:(Mg+Al) around 1:1



## 4.4 Seal capacity

The fundamental sealing capacity of a cap-rock is mainly defined by the grain size distribution and mineralogy, as well as the physical properties of the fluid to be contained below the seal. Based on data from Table 4.3, the maximum height of an oil column that may be capped by each cap-rock can be estimated. In this report, the estimate is calculated by assuming generalized figures for oil and brine density as well as for the interfacial tension for an oil-brine fluid system. Furthermore, it is assumed that the fluid-rock system is completely water-wet. The failure strength as well as an evaluation of faults and fractures in the region from seismic mapping and/or core description is outside the scope of this preliminary study.

Table 4.6 lists the results for a hypothetical oil reservoir at a depth of 2,000-3,000 m overlain by one of the cap-rocks investigated in this study. Pore throat size has been set at the  $r_{50}$  level and the  $r_{10}$  level (Table 4.3) to test a very conservative estimate. The generalized data for oil and brine are held constant with depth. Although this is not strictly correct, minor variations in these properties with depth cannot compromise the general conclusion that any of the cap-rocks investigated in the present study is likely to hold an oil column of more than 200 m. For the best suited cap-rocks (sample 233, 234, and 237) this figure is between 1,040-1,100 m.

**Table 4.6.** Evaluation of the capillary seal capacity for a hypothetical oil reservoir capped by each of the cap-rocks from the Dunken-2 well and Kilen. Pore radius data have been adopted from Table 4.3. It is assumed that the fluid-rock system is water-wet. Data in the table is given in SI units. The hypothetical oil reservoir is estimated to be located within a depth of 2,000-3,000 m.

Sample ID	$\rho_w$ (brine) [kg/m <sup>3</sup> ]	$\rho_{nw}$ (oil) [kg/m <sup>3</sup> ]	IFTxcos $\Theta$ [mN/m]	Pore radius		$P_{ce, r50}$ [MPa]	$P_{ce, r10}$ [Mpa]	$H_{max, r50}$ [m]	$H_{max, r10}$ [m]
				$r_{50}$ [nm]	$r_{10}$				
230	1015	761	26	9	70	6	1	2319	298
231	1015	761	26	25	88	2	1	835	237
232	1015	761	26	9	37	6	1	2319	564
233	1015	761	26	8	19	7	3	2609	1098
234	1015	761	26	7	19	7	3	2981	1098
235	1015	761	26	10	24	5	2	2087	870
236	1015	761	26	6	30	9	2	3478	696
237	1015	761	26	7	20	7	3	2981	1043
238	1015	761	26	5	80	10	1	4174	261
545514	1015	761	26	8	42	7	1	2609	497

Legend:  $\rho_w$  = density of wetting phase (brine); a brine density gradient of 0.44 psi/foot is assumed  
 $\rho_{nw}$  = density of non-wetting phase (oil); an oil density gradient of 0.33 psi/foot is assumed  
 $P_{ce}$  = capillary entry pressure/threshold pressure  
 $r$  = pore radius  
IFT = interfacial tension  
 $\Theta$  = contact angle

## 4.5 Discussion and conclusion

From the data presented in this limited study of cap-rock properties it can be concluded that most of the fine-grained lithologies analyzed are siltstones with medium quartz content and a low amount of organic matter (< 0.4% TOC) for the Dunken-2 core samples. The Kilen sample (sample 545514) has slightly higher organic matter content of c. 1% TOC.

The Dunken-2 and Kilen siltstones are reasonably good cap-rocks having a large proportion of very small pore throats and capillary threshold pressures which in most cases are higher than 1,000 psia (6.9 MPa) in an air-mercury system. In general the cap-rocks studied here are generally reasonably good cap-rocks that in most cases can cap an oil column

of 500 m in thickness or more. The best suited cap-rocks occur in the central part of the Dunken-2 core (samples 233-235). Their better cap-rock properties are mainly due to a more narrow pore throat distribution, a higher threshold pressure, and secondary cementation with carbonate.

However, the sealing properties of a potential cap-rock is not only a matter of having an effective capillary seal, but also depends on faults and fractures and the thickness of the cap-rock section. Faults and fractures may be evaluated from core description and or seismic interpretation, the thickness from regional mapping and other qualifiers indicating the burial of the geological section.

To conclude, the present limited cap-rock study with samples from the Dunken-2 well and Kilen demonstrates reasonably good capillary sealing properties that will hold an oil column of at least 200 m. However, the best of the cap-rocks studied will presumably hold an oil column of at least 1,000 m, thus making these cap-rocks excellent capillary barriers. A regional evaluation of cap-rock properties should preferably include more boreholes, more extensive sampling and evaluation of regional geological phenomena such as occurrence of fractures, faults, etc.

## 4.6 References

- Anderson, J.U., 1963: An improved pretreatment for mineralogical analyses of samples containing organic matter. *Clays Clay Mineral*, 10, 380–388.
- API RP 40, Recommended Practice for Core Analysis, second edition, 1998. Washington DC: American Petroleum Institute.
- Brunauer, S., Emmett, P.H. and Teller, E. 1938: Adsorption of gases in multimolecular layers. *J. Am. Chem. Soc.*, 60, 309.
- Lundegard, P.D. and Samuels, N.O. 1980: Field classification of fine-grained sedimentary rocks. *J. Sedimentary Petrol.*, 50, 781-786.
- Mehra, O.P and Jackson, M.L. 1960: Iron oxide removal from soils and clays by a dithionite-citrate system buffered with sodium bicarbonate. *Clays Clay Miner.*, 7, 317-327.
- Slater, C. and Cohen, L., 1962: A centrifugal particle size analyzer. *J. Sci. Instruments*, 39, 614-617.

## 5. Petroleum geology

### 5.1 Introduction

The Dunken-2 fully cored borehole was drilled to test the presence of petroleum source rocks in the Triassic succession of the Wandel Sea Basin. The background was the existence of data on a few outcrop samples from the Dunken Mountain area, collected around 1990, which seemed to show slightly enhanced petroleum potential. Hence, it was decided that a borehole should be drilled to test the presence of petroleum source rocks equivalent to the Anisian-Ladinian Bravaisbjerget/Botneheia Formations (Spitzbergen) and/or the slightly older (Spathian-Anisian) Steinkobbe Formation of the Svalis Dome, southern Barents Sea, or perhaps younger deposits equivalent of the Shublik Formation of Alaska, which extends into the Norian (Leith *et al.* 1993, Peters *et al.* 2006, Lundschieen *et al.* 2014 and references therein).

### 5.2 Samples and Methods

The Dunken-2 borehole terminated at 141.84m below reference level (212m above sealevel) with a core recovery of 96%. A total of 122 samples were collected for petroleum geochemical analysis, covering the succession from approximately 20 metres to TD. The upper approximately 20 metres are sand-dominated and have not been sampled for petroleum potential analysis.

Total Carbon (TC, wt%), Total Organic Carbon (TOC, wt%) and Total Sulphur (TS, wt%) were determined by combustion using a LECO CS-200 induction furnace. TOC was determined after elimination of carbonate-bonded carbon by prolonged HCl-treatment at elevated temperature. Details of the protocol are available on request.

Petroleum potential was determined by Rock-Eval-type pyrolysis using a Source Rock Analyzer (SRA) instrument, manufactured by Humble Instruments and Services (presently Weatherford Ltd.). The instrument was calibrated using the IFP-160000 standard and produces data identical to those obtained by using the Rock-Eval 6 instrument. Sets of one blank and one in-house control standard were run for every 10 samples to ensure instrument stability.

Vitrinite reflectance measurements were considered futile in light of the very low organic matter contents recorded. Hence, no vitrinite reflectance data are available. However, based on correlation of Tmax-data and R<sub>o</sub>-data from a large number of samples of different ages in the Wandel Sea Basin (Fig. 5.1), equivalent R<sub>o</sub>-data have been calculated from available Tmax data.

Solvent extraction was carried out using a Soxtec™ apparatus, dichloromethane/methanol (93+3 vol./vol.) as solvent, keeping the samples in boiling solvent for 1h, followed by 3h rinsing.

Asphaltenes were precipitated by addition of 40-fold excess n-pentane. Maltenes were separated into saturated, aromatic and polar fractions by MPLC.

Gas chromatography was carried out using a Shimadzu GC-2010 instrument equipped with a splitless injector and a ZB-1 capillary column (25 m x 0.25 mm i.d., film thickness 0.10

µm). The temperature program was 5°C/min from 80 to 300°C, followed by 15 min at 300°C. The concentration for GC analyses was ~5 mg / ml isooctane.

Gas chromatography – mass spectrometry (GC-MS and GC-MS-MS) was carried out using an Agilent 6890 N gas chromatograph connected to a Waters Quattro Micro GC tandem quadrupole mass spectrometer. The GC-column used was an Agilent HP-5, 30m x 0.25 mm i.d., film thickness 0.10 µm. The instrument was run in both “Selected Ion Monitoring” mode (GC-MS<sub>SIM</sub>) and parent–daughter mode (GC-MSMS). To enhance the signal, hopanes and steranes were analysed using two different methods, including 10 and 5 different parent–daughter transitions, respectively.

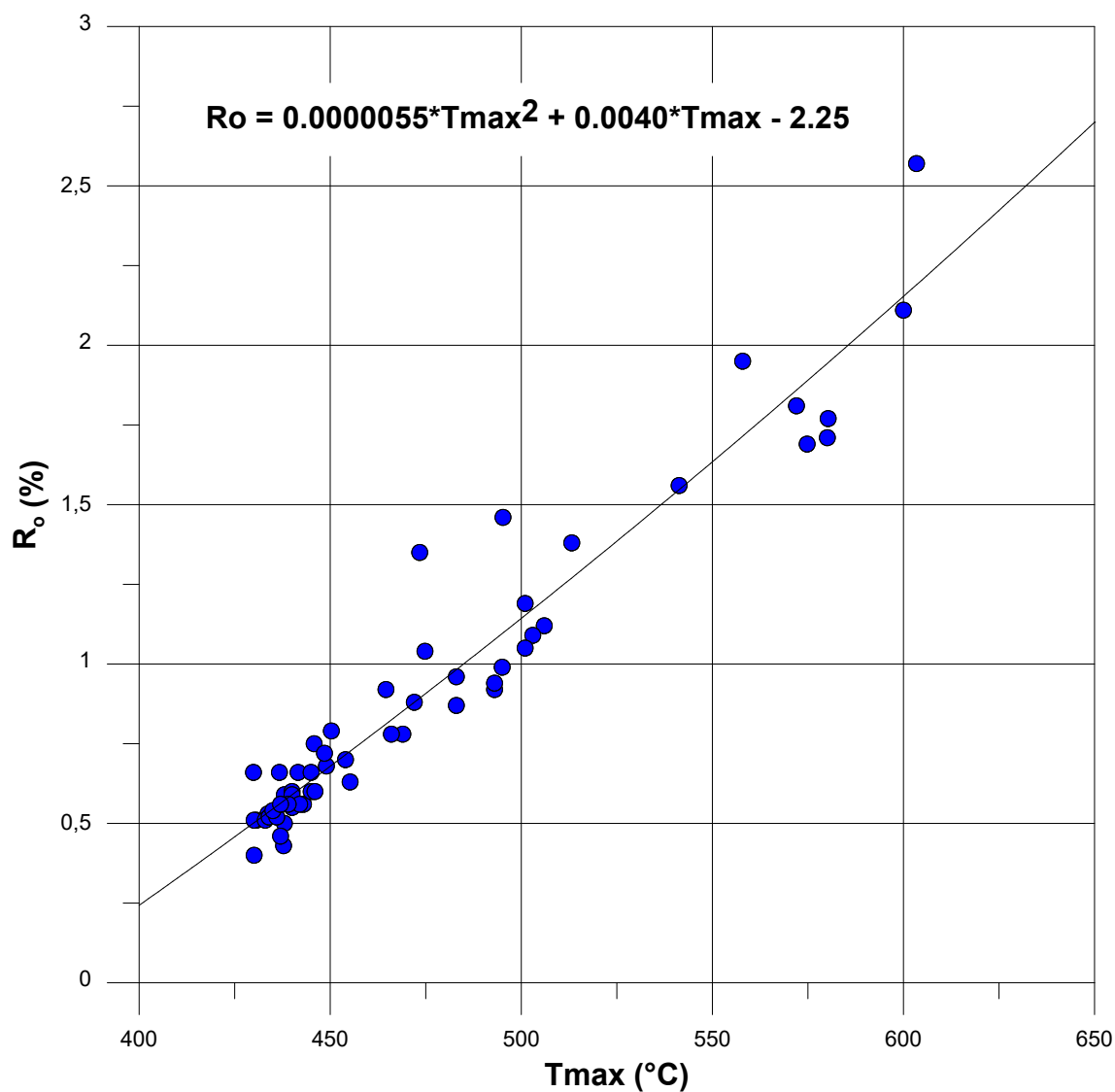


Fig. 5.1 Tmax and vitrinite reflectance (Ro) data for a large number of samples of different formations in the Wandel Sea Basin. The constructed trend-line has been used to calculate Ro-values from Tmax-data in the following. Note that for Tmax greater than approximately 500 the trend-line is very poorly constrained and the predictive power accordingly low.

## 5.3 Results and discussion

Before drilling, the succession exposed at the Dunken Mountain was poorly dated and the well-site was chosen from a best age-assessment available at the time. The exposed succession seems to be overall coarsening-upwards and drilling into the underlying unexposed part could reasonably be assumed to yield a higher proportion of fine-grained rocks. However, later biostratigraphic datings of the core have shown that the penetrated succession is slightly older than the target interval. The succession penetrated by the Dunken-2 borehole is dated to the early to late Spathian, *i.e.* slightly older than the oldest expected source rock interval.

### 5.3.1 Petroleum potential and maturity

TC/TOC/TS/Rock-Eval type screening pyrolysis data are listed in Table 5.1a,b,c. Plots of the dataset versus depth are shown in Fig. 5.2.

The Total Carbon (TC) content varies from 0.02% to 5.34% with an average of 1.42%, pointing to a notable proportion of minerogenic Carbon, particularly in the lower half of the succession (Fig. 5.2), since the level of Total Organic Carbon is generally very low, 0–0.55% with an average of only 0.16% (Fig 5.2). A narrow interval centered at approximately 37m, which shows slight enhancement of organic content and petroleum potential, is recorded as a notable spike in the Uranium-trace of the spectral Gamma-log (Fig. 5.3).

The Total Sulphur content (TS) is ranges from 0.02% to 1.59% with an average of 0.59%, which is surprisingly high considering the low contents of organic Carbon recorded (Fig. 5.4).

S1 is generally close to zero (0.0–0.22 mg/g; avg.: 0.03 mg/g).

Likewise S2 is low, 0.0–0.79 mg/g with an average of only 0.03 mg/g. A few samples in the interval 33–40 metres and a single sample at 86.58 m stand out by showing slightly higher values of S2, but still in absolute terms the level is far too low for the deposits to qualify as petroleum source rocks (Figs 5.2 and 5.5).

Consequently, the calculated Hydrogen Index (HI) is very low, 0–144, with an average of only 10 (Figs 5.2 and 5.6).

Despite the absence of any notable petroleum generation potential, slight hydrocarbon staining is observed in two intervals, *viz.* around approximately 36m and 87m (see table 5.1 and Fig. 5.2 for details). These stains seem clearly indigenous, *i.e.* generated *in situ* and not migrated from elsewhere. Biological marker analysis of the stains is reported below.

The presence of staining agrees well with the level of thermal maturity provided by Tmax (after nonsense values caused by poor pyrolysis-yields have been weeded out) and the Production Index (PI), see Figs 5.2 and 5.7. Tmax falls mainly within the interval 445°C – 450°C, suggesting a level of thermal maturity well within the oil-generative window. Calculating vitrinite reflectance values based on Tmax as described above yields R<sub>o</sub> in the interval 0.64% – 0.70%.

It is clear from the above that the succession penetrated by the Dunken-2 borehole is essentially without petroleum source potential, and that such potential never existed, since the level of TOC is far below the accepted threshold for petroleum source rocks, even allowing for depletion in consequence of thermal maturation. However, the presence of slight organic enrichment and enhanced petroleum potential allowing staining to occur in two

narrow intervals of the succession may be taken to indicate the presence of petroleum source potential further basinwards. The upper interval with oil stains and slightly enhanced petroleum potential (33–37m) may be age-equivalent to the Steinkobbe Formation of the Svalis Dome (Barents Sea) where petroleum source rocks occur (Lundschien *et al.* 2014 and references therein). The succession is thermally mature and well within the oil-generative window.

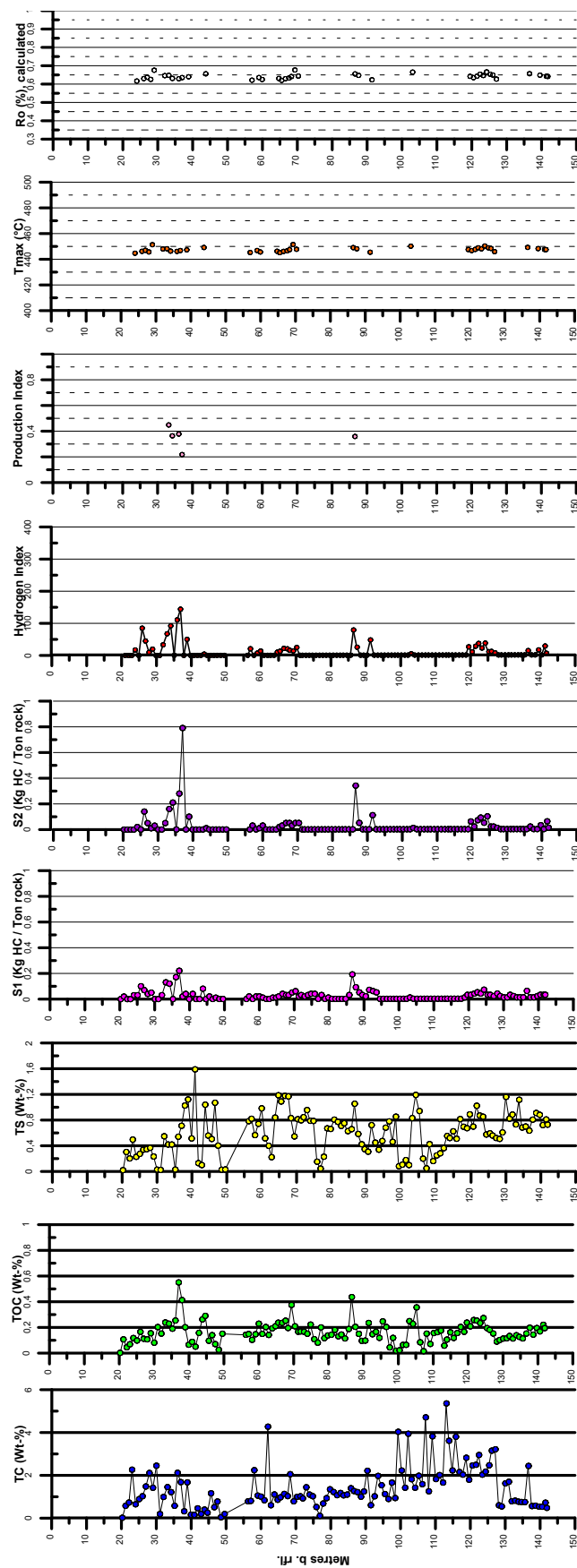


Fig. 5.2. Dunken-2 core: Petroleum geochemistry data versus depth

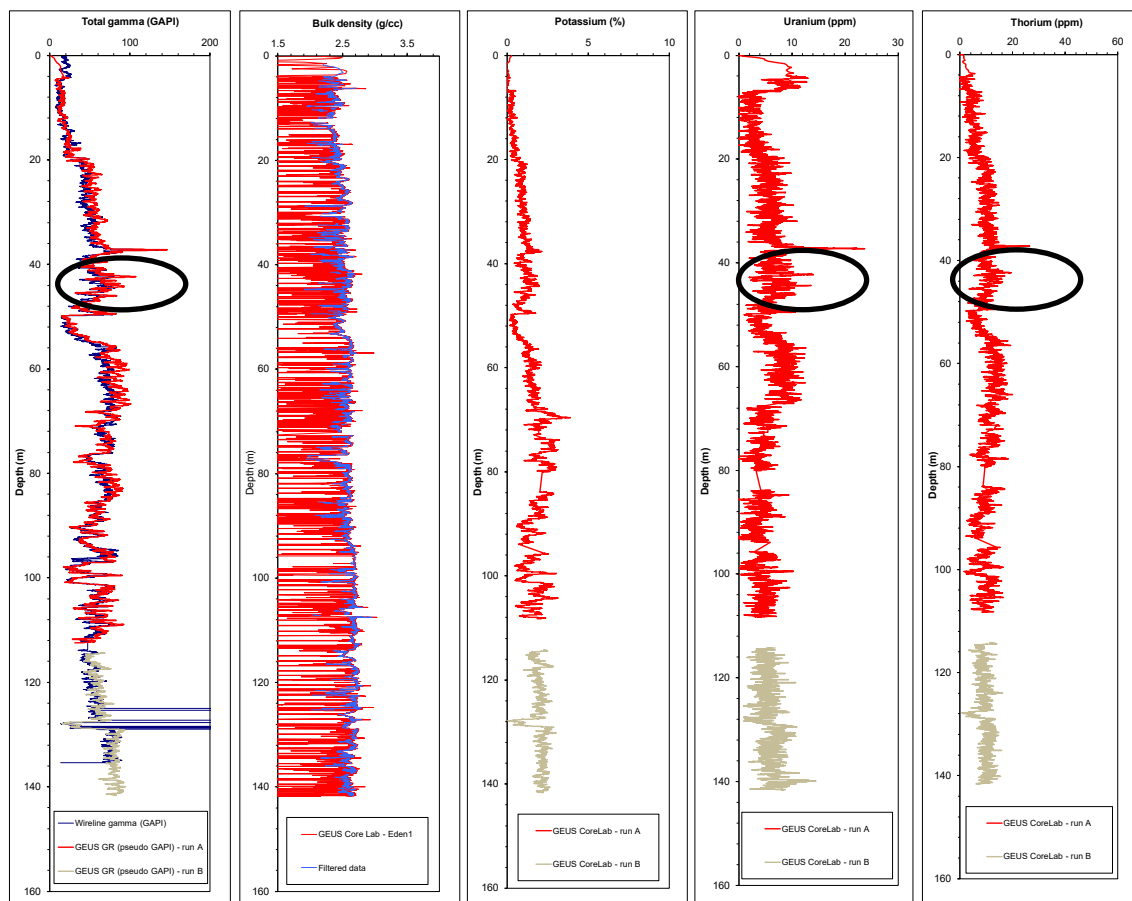


Fig. 5.3. Spectral GR-log of the Dunken-2 core and wireline GR-log of the Dunken-2 borehole. Spike indicating organic enrichment at a narrow interval centered at 36-37 m is encircled.



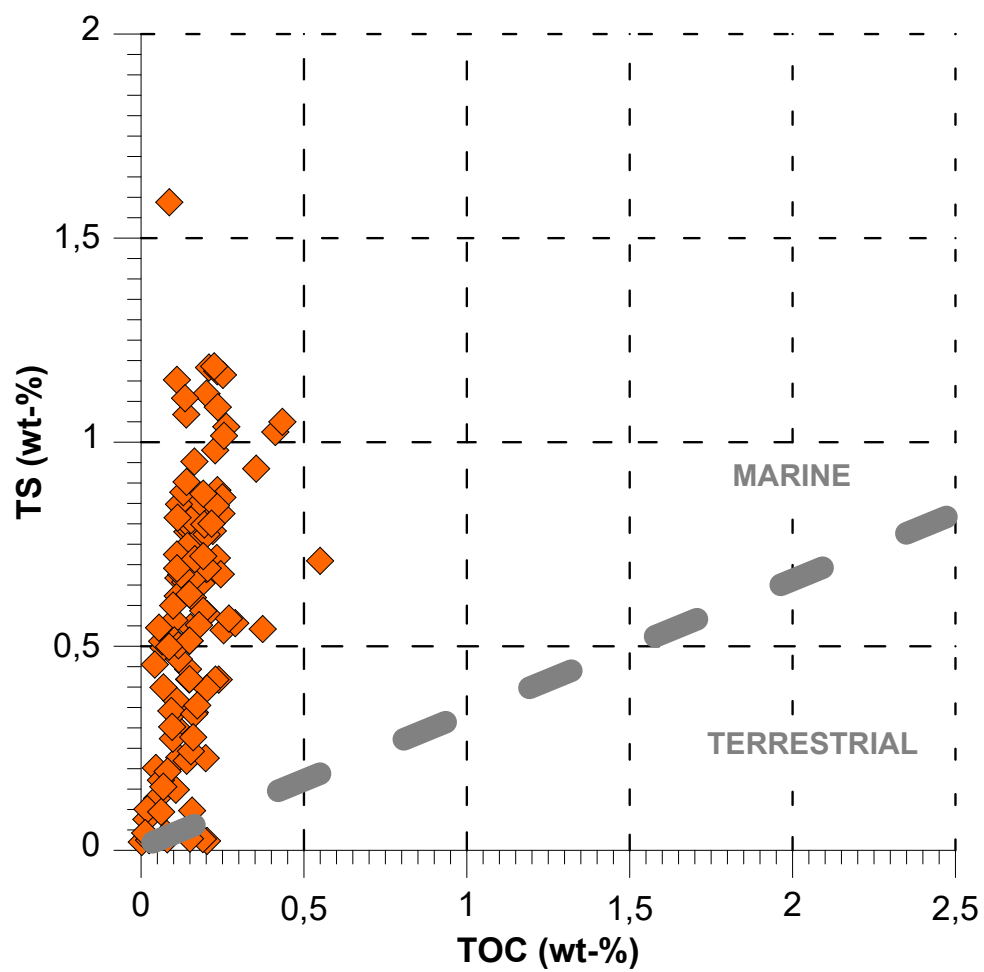


Fig. 5.4. Total Organic Carbon (TOC, wt-%) versus Total Sulphur (TS, wt-%) for samples from the Dunken-2 core.

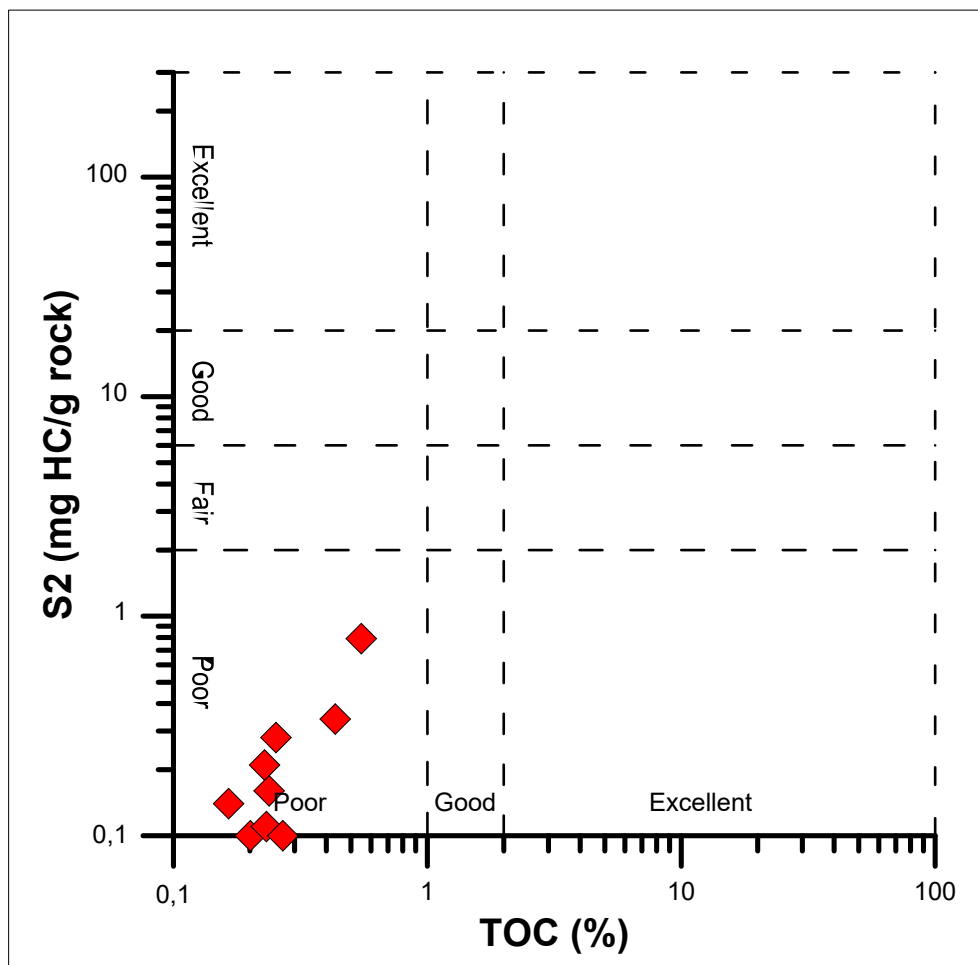


Fig. 5.5. TOC versus S2 for samples of the Dunke-2 core. Note absence of petroleum source potential

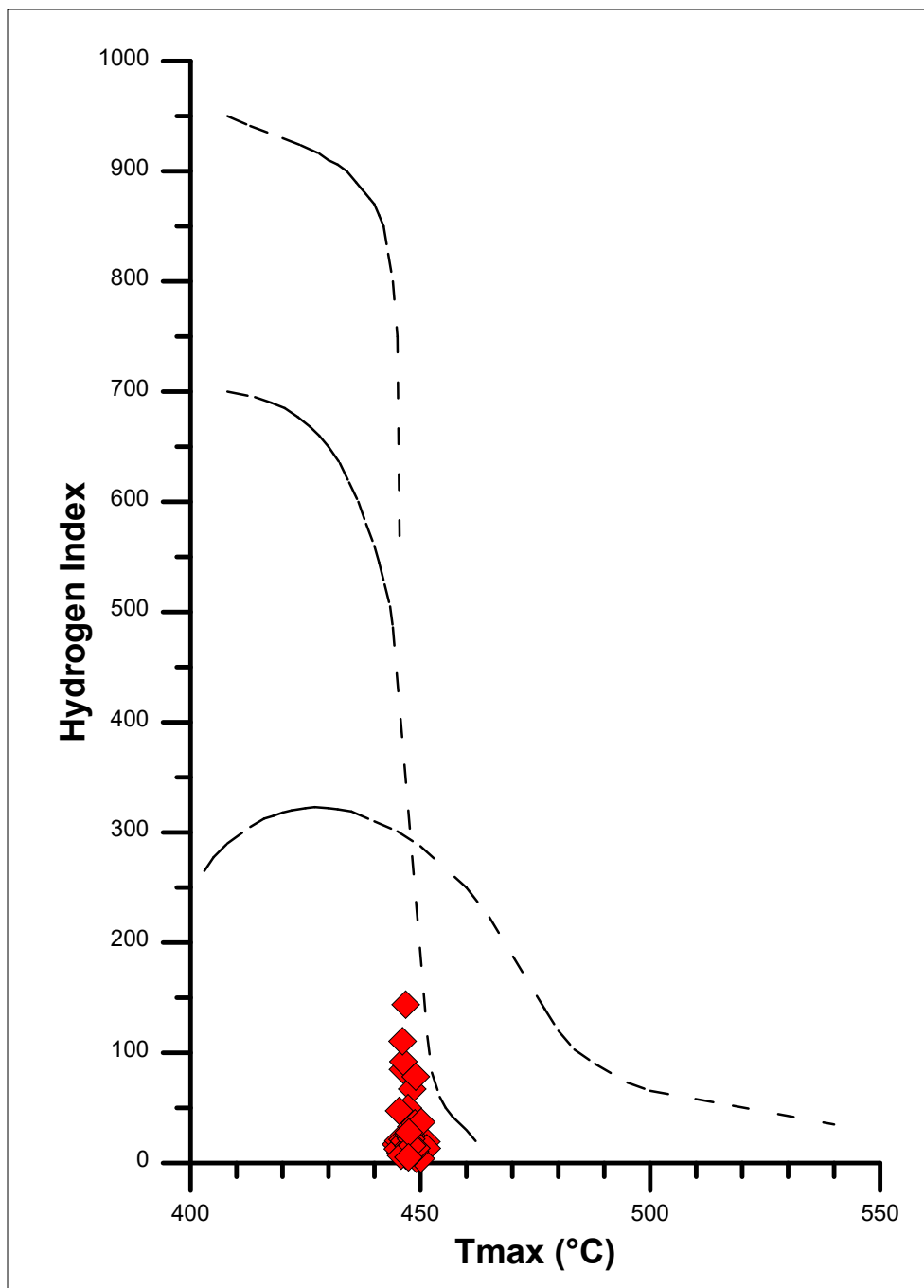


Fig. 5.6. Tmax versus Hydrogen Index for samples from the Dunken-2 core. Note near-absence of petroleum source potential.

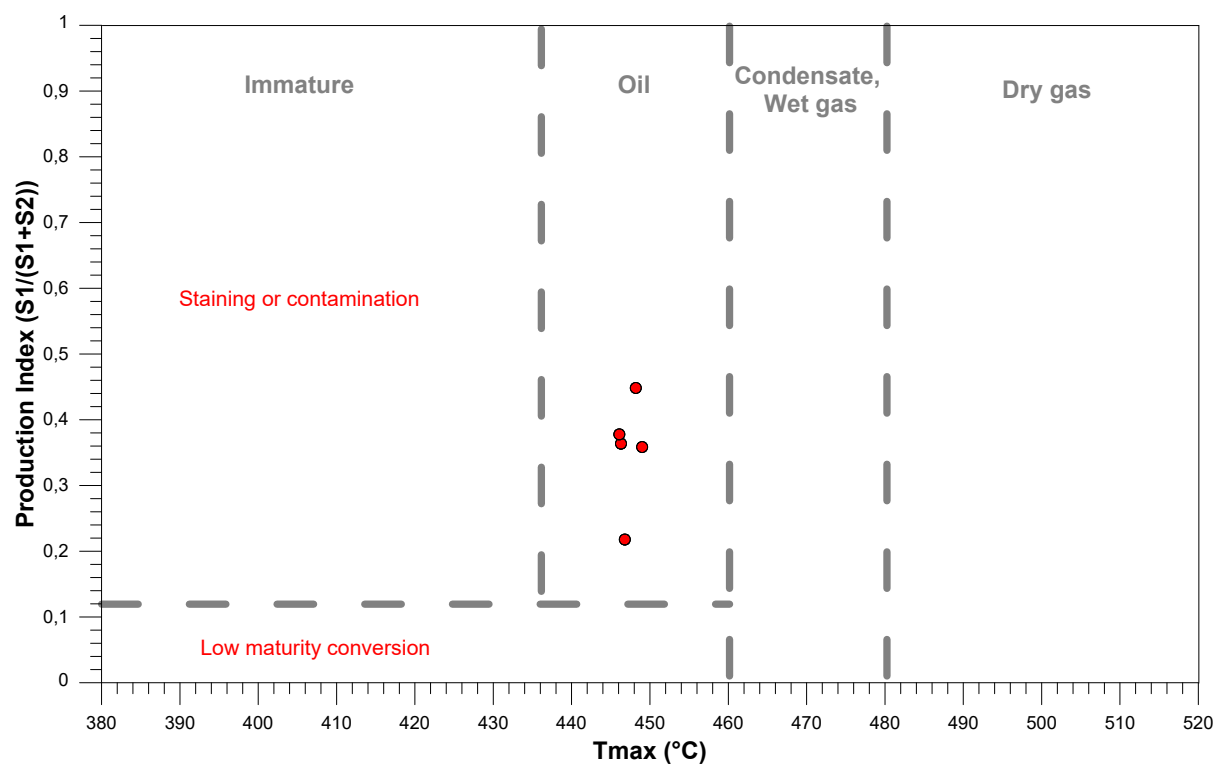


Fig. 5.7. Tmax versus PI for samples of the Dunken-2 core.

Lab.no.	Sample	Depth (m)	TOC (w/w%)	TC (w/w%)	TS (w/w%)	Tmax (°C)	S1 (mg/g)	S2 (mg/g)	HI	PI	PC	Ro (%), calculat.
22671	517006-051	20,26	0,00	0,02	0,02		0,00	0,00			0,00	n.a.
22672	517006-052	21,19	0,11	0,58	0,30		0,02	0,00	0		0,00	n.a.
22673	517006-053	22,17	0,05	0,73	0,20		0,00	0,00	0		0,00	n.a.
22674	517006-054	23,06	0,07	2,26	0,50		0,00	0,00	0		0,00	n.a.
22675	517006-055	24,06	0,12	0,65	0,23	445	0,03	0,02	17		0,00	0,62
22676	517006-056	25,09	0,10	0,89	0,27		0,03	0,00	0		0,00	n.a.
22677	517006-057	26,06	0,16	1,02	0,34	446	0,10	0,14	85		0,02	0,63
22678	517006-058	27,01	0,11	1,48	0,35	447	0,07	0,05	45		0,01	0,64
22679	517006-059	28,02	0,11	2,11	0,37	446	0,04	0,01	9		0,00	0,63
22680	517006-060	29,02	0,15	1,42	0,23	451	0,05	0,03	19		0,01	0,68
22681	517006-061	30,02	0,08	2,45	0,03		0,00	0,00	0		0,00	n.a.
22682	517006-062	31,04	0,20	0,19	0,02		0,00	0,00	0		0,00	n.a.
22683	517006-063	32,05	0,15	0,99	0,55	448	0,03	0,05	33		0,01	0,65
22684	517006-064	33,19	0,24	1,45	0,42	448	0,13	0,16	67	0,45	0,02	0,65
22685	517006-065	34,23	0,23	1,22	0,42	446	0,12	0,21	92	0,36	0,03	0,63
22686	517006-066	35,23	0,19	0,58	0,03		0,00	0,00	0		0,00	n.a.
22687	517006-067	36,08	0,25	2,12	0,54	446	0,17	0,28	111	0,38	0,04	0,63
22688	517006-068	37,03	0,55	1,68	0,71	447	0,22	0,79	144	0,22	0,08	0,64
22689	517006-069	37,98	0,41	0,32	1,03		0,02	0,00	0		0,00	n.a.
22690	517006-070	38,88	0,20	1,67	1,12	447	0,04	0,10	50		0,01	0,64
22691	517006-071	39,89	0,06	0,15	0,51		0,00	0,00	0		0,00	n.a.
22692	517006-072	40,88	0,09	0,15	1,59		0,04	0,00	0		0,00	n.a.
22693	517006-073	41,84	0,05	0,45	0,13		0,00	0,00	0		0,00	n.a.
22694	517006-074	42,82	0,16	0,20	0,10		0,00	0,00	0		0,00	n.a.
22695	517006-075	43,81	0,26	0,40	1,04	449	0,08	0,01	4		0,01	0,66
22696	517006-076	44,65	0,29	0,25	0,56		0,00	0,00	0		0,00	n.a.
22697	517006-077	45,66	0,10	1,16	0,50		0,02	0,00	0		0,00	n.a.
22698	517006-078	46,59	0,14	0,50	1,07		0,00	0,00	0		0,00	n.a.
22699	517006-079	47,49	0,07	0,77	0,40		0,01	0,00	0		0,00	n.a.
22700	517006-080	48,51	0,02	0,03	0,02		0,00	0,00	0		0,00	n.a.
22701	517006-081	49,53	0,15	0,19	0,03		0,00	0,00	0		0,00	n.a.
22702	517006-082	56,27	0,14	0,78	0,78		0,00	0,00	0		0,00	n.a.
22703	517006-083	57,04	0,15	0,80	0,82	445	0,02	0,03	20		0,00	0,62
22704	517006-084	58,05	0,10	2,24	0,56		0,00	0,00	0		0,00	n.a.
22705	517006-085	59,03	0,15	1,05	0,74	447	0,02	0,01	7		0,00	0,64
22706	517006-086	59,97	0,23	1,00	0,98	446	0,02	0,03	13		0,00	0,62
22707	517006-087	60,95	0,15	0,83	0,51		0,01	0,00	0		0,00	n.a.
22708	517006-088	61,96	0,20	4,26	0,40		0,00	0,00	0		0,00	n.a.
22709	517006-089	62,80	0,14	0,60	0,22		0,00	0,00	0		0,00	n.a.
22710	517006-090	63,80	0,19	1,10	0,84		0,01	0,00	0		0,00	n.a.
22711	517006-091	64,75	0,21	0,85	1,18	446	0,01	0,02	10		0,00	0,63

Table 5.1a. TC/TOC/TS/Rock-Eval type screening pyrolysis data on samples from the Dunken-2 core. TOC: Total Organic Carbon (wt-%); TC: Total Carbon (wt-%); TS: Total Sulphur (wt-%); Tmax: Rock-Eval Tmax, (°C); S1: Rock-Eval S1 (mg hydrocarbons / g rock); S2: Rock-Eval S2 (mg hydrocarbons / g rock); HI: Hydrogen Index; PI: Production Index; PC: Pyrolyzable Carbon; Ro (%) Calculat.: Vitritine reflectance calculated from Tmax using correlation shown in Fig. 5.1.

Lab.no.	Sample	Depth (m)	TOC (w/w%)	TC (w/w%)	TS (w/w%)	Tmax (°C)	S1 (mg/g)	S2 (mg/g)	HI	PI	PC	Ro (%), calculat.
22712	517006-092	65,54	0,24	0,97	1,09	445	0,02	0,03	13		0,00	0,62
22713	517006-093	66,61	0,23	1,12	1,17	446	0,04	0,05	21		0,01	0,63
22714	517006-094	67,62	0,25	1,02	1,17	447	0,03	0,05	20		0,01	0,63
22715	517006-095	68,33	0,19	2,05	0,83	447	0,03	0,03	15		0,00	0,64
22716	517006-096	69,33	0,37	0,78	0,54	451	0,05	0,05	13		0,01	0,68
22717	517006-097	70,31	0,21	0,99	0,81	448	0,06	0,05	24		0,01	0,64
22718	517006-098	71,24	0,16	1,01	0,79		0,02	0,00	0		0,00	n.a.
22719	517006-099	71,94	0,17	0,91	0,84		0,03	0,00	0		0,00	n.a.
22720	517006-100	72,94	0,16	1,43	0,95		0,02	0,00	0		0,00	n.a.
22721	517006-101	73,88	0,15	1,09	0,79		0,03	0,00	0		0,00	n.a.
22722	517006-102	74,80	0,22	1,01	0,78		0,04	0,00	0		0,00	n.a.
22723	517006-103	75,82	0,11	0,51	0,15		0,04	0,00	0		0,00	n.a.
22724	517006-104	76,83	0,08	0,10	0,04		0,00	0,00	0		0,00	n.a.
22725	517006-105	77,76	0,20	0,67	0,23		0,03	0,00	0		0,00	n.a.
22726	517006-106	78,73	0,11	0,92	0,67		0,00	0,00	0		0,00	n.a.
22727	517006-107	79,71	0,14	1,34	0,66		0,01	0,00	0		0,00	n.a.
22728	517006-108	80,74	0,14	1,21	0,80		0,00	0,00	0		0,00	n.a.
22729	517006-109	81,75	0,18	1,06	0,77		0,00	0,00	0		0,00	n.a.
22730	517006-110	82,72	0,13	1,16	0,70		0,00	0,00	0		0,00	n.a.
22731	517006-111	83,61	0,14	1,05	0,75		0,00	0,00	0		0,00	n.a.
22732	517006-112	84,64	0,11	1,09	0,62		0,00	0,00	0		0,00	n.a.
22733	517006-113	85,71	0,19	1,39	0,65		0,03	0,00	0		0,00	n.a.
22734	517006-114	86,58	0,43	1,25	1,05	449	0,19	0,34	78	0,36	0,04	0,65
22735	517006-115	87,59	0,20	1,20	0,58	448	0,09	0,05	25		0,01	0,65
22736	517006-116	88,59	0,15	0,99	0,42		0,05	0,00	0		0,00	n.a.
22737	517006-117	89,44	0,09	1,23	0,34		0,03	0,00	0		0,00	n.a.
22738	517006-118	90,43	0,10	2,20	0,30		0,02	0,00	0		0,00	n.a.
22739	517006-119	91,41	0,23	0,59	0,72	445	0,07	0,11	47		0,01	0,62
22740	517006-120	92,49	0,14	1,01	0,44		0,06	0,00	0		0,00	n.a.
22741	517006-121	93,50	0,16	1,96	0,33		0,05	0,00	0		0,00	n.a.
22742	517006-122	94,48	0,12	1,52	0,47		0,00	0,00	0		0,00	n.a.
22743	517006-123	95,45	0,24	1,11	0,68		0,00	0,00	0		0,00	n.a.
22744	517006-124	96,47	0,20	0,88	0,77		0,00	0,00	0		0,00	n.a.
22745	517006-125	97,45	0,04	1,65	0,46		0,00	0,00	0		0,00	n.a.
22746	517006-126	98,39	0,12	0,92	0,85		0,00	0,00	0		0,00	n.a.
22747	517006-127	99,24	0,02	4,02	0,08		0,00	0,00	0		0,00	n.a.
22748	517006-128	100,25	0,02	2,21	0,10		0,00	0,00	0		0,00	n.a.
22749	517006-129	101,23	0,06	1,40	0,17		0,00	0,00	0		0,00	n.a.
22750	517006-130	102,13	0,06	3,93	0,09		0,00	0,00	0		0,00	n.a.
22751	517006-131	103,07	0,25	1,80	0,83	450	0,01	0,01	4		0,00	0,66
22752	517006-132	104,09	0,22	1,40	1,19		0,00	0,00	0		0,00	n.a.

Table 5.1b. TC/TOC/TS/Rock-Eval type screening pyrolysis data on samples from the Dunken-2 core. TOC: Total Organic Carbon (wt-%); TC: Total Carbon (wt-%); TS: Total Sulphur (wt-%); Tmax: Rock-Eval Tmax, (°C); S1: Rock-Eval S1 (mg hydrocarbons / g rock); S2: Rock-Eval S2 (mg hydrocarbons / g rock); HI: Hydrogen Index; PI: Production Index; PC: Pyrolyzable Carbon; Ro (%) Calculat.: Vitrinite reflectance calculated from Tmax using correlation shown in Fig. 5.1.

Lab.no.	Sample	Depth (m)	TOC (w/w%)	TC (w/w%)	TS (w/w%)	Tmax (°C)	S1 (mg/g)	S2 (mg/g)	HI	PI	PC	Ro (%), calculat.
22753	517006-133	105,13	0,35	1,96	0,94		0,00	0,00	0		0,00	n.a.
22754	517006-134	106,15	0,08	1,57	0,19		0,00	0,00	0		0,00	n.a.
22755	517006-135	107,13	0,01	4,69	0,04		0,00	0,00	0		0,00	n.a.
22756	517006-136	108,01	0,15	1,24	0,42		0,00	0,00	0		0,00	n.a.
22757	517006-137	109,05	0,07	3,81	0,16		0,00	0,00	0		0,00	n.a.
22758	517006-138	110,05	0,15	1,81	0,24		0,00	0,00	0		0,00	n.a.
22759	517006-139	111,08	0,16	1,99	0,28		0,00	0,00	0		0,00	n.a.
22760	517006-140	112,08	0,17	1,64	0,36		0,00	0,00	0		0,00	n.a.
22761	517006-141	113,06	0,05	5,34	0,55		0,00	0,00	0		0,00	n.a.
22762	517006-142	113,80	0,10	3,60	0,51		0,00	0,00	0		0,00	n.a.
22763	517006-143	114,78	0,16	2,21	0,62		0,00	0,00	0		0,00	n.a.
22764	517006-144	115,75	0,11	3,78	0,50		0,00	0,00	0		0,00	n.a.
22765	517006-145	116,79	0,15	2,13	0,81		0,00	0,00	0		0,00	n.a.
22766	517006-146	117,76	0,20	2,01	0,69		0,00	0,00	0		0,00	n.a.
22767	517006-147	118,74	0,16	2,80	0,67		0,01	0,00	0		0,00	n.a.
22768	517006-148	119,54	0,23	1,78	0,88	448	0,03	0,06	26		0,01	0,64
22769	517006-149	120,51	0,20	2,44	0,69	447	0,03	0,02	10		0,00	0,63
22770	517006-150	121,52	0,25	2,48	1,02	448	0,04	0,07	27		0,01	0,64
22771	517006-151	122,37	0,25	2,93	0,86	449	0,05	0,09	36		0,01	0,65
22772	517006-152	123,33	0,23	2,01	0,84	448	0,04	0,05	22		0,01	0,65
22773	517006-153	124,26	0,27	2,15	0,57	450	0,07	0,10	37		0,01	0,67
22774	517006-154	125,29	0,19	2,45	0,59	449	0,03	0,02	10		0,00	0,65
22775	517006-155	126,04	0,18	3,13	0,55	448	0,03	0,02	11		0,00	0,65
22776	517006-156	127,07	0,15	3,20	0,51	446	0,02	0,01	7		0,00	0,63
22777	517006-157	128,07	0,09	0,58	0,50		0,04	0,00	0		0,00	n.a.
22778	517006-158	128,89	0,10	0,53	0,60		0,02	0,00	0		0,00	n.a.
22779	517006-159	129,92	0,11	1,60	1,15		0,01	0,00	0		0,00	n.a.
22780	517006-160	130,91	0,11	1,68	0,82		0,01	0,00	0		0,00	n.a.
22781	517006-161	131,74	0,13	0,77	0,88		0,03	0,00	0		0,00	n.a.
22782	517006-162	132,71	0,11	0,80	0,73		0,02	0,00	0		0,00	n.a.
22783	517006-163	133,68	0,14	0,75	1,11		0,01	0,00	0		0,00	n.a.
22784	517006-164	134,54	0,12	0,73	0,68		0,01	0,00	0		0,00	n.a.
22785	517006-165	135,52	0,11	0,73	0,69		0,01	0,00	0		0,00	n.a.
22786	517006-166	136,55	0,15	2,42	0,63	449	0,06	0,02	13		0,01	0,66
22787	517006-167	137,53	0,19	0,54	0,80		0,01	0,00	0		0,00	n.a.
22788	517006-168	138,54	0,14	0,56	0,90		0,01	0,00	0		0,00	n.a.
22789	517006-169	139,56	0,19	0,52	0,87	448	0,02	0,03	16		0,00	0,65
22790	517006-170	140,42	0,17	0,51	0,71		0,03	0,00	0		0,00	n.a.
22791	517006-171	141,40	0,22	0,70	0,80	448	0,03	0,06	28		0,01	0,64
22792	517006-172	141,79	0,19	0,46	0,72	447	0,03	0,01	5		0,00	0,64

Table 5.1c. TC/TOC/TS/Rock-Eval type screening pyrolysis data on samples from the Dunken-2 core. TOC: Total Organic Carbon (wt-%); TC: Total Carbon (wt-%); TS: Total Sulphur (wt-%); Tmax: Rock-Eval Tmax, (°C); S1: Rock-Eval S1 (mg hydrocarbons / g rock); S2: Rock-Eval S2 (mg hydrocarbons / g rock); HI: Hydrogen Index; PI: Production Index; PC: Pyrolyzable Carbon; Ro (%) Calculat.: Vitrinite reflectance calculated from Tmax using correlation shown in Fig. 5.1.

### 5.3.2 Biological markers

Biological marker analysis of extracts of four stained samples identified above has been carried out. Extraction and separation data are reported in Table 5.2. Key gas chromatography data are shown in Table 5.3. Data on tricyclic terpanes derived from GC-MS<sub>SIM</sub> analysis monitoring m/z 191 are shown in Table 5.4. Key biological marker facies data are shown in Table 5.5. Key biological marker maturity data are shown in Table 5.6. Gas chromatograms and key ion fragmentograms/parent–daughter transitions are shown in figs. 5.8abcde through 5.11abcde.

Lab.-#	Sample	Depth (m)	Recovery (mg/g)	Asphaltenes %	Saturates %	Aromatics %	NSO %
22684	517006-064	33,19	142,20	17,65	32,43	16,22	51,35
22685	517006-065	34,23	202,19	10,00	33,33	10,42	56,25
22688	517006-068	37,03	178,14	5,71	33,33	8,00	58,67
22734	517006-114	86,58	150,98	5,45	26,83	7,32	65,85

Table 5.2. Solvent extraction and separation data. Recovery in mg extract / g sample. Asphaltenes in wt-% of total extract. Distribution of saturated hydrocarbons, aromatic hydrocarbons and polar compounds in wt-% of asphaltene-free extract (maltenes)

Lab.-#	Sample	Depth (m)	Pristane/Phytane	Pristane/nC17	Phytane/nC18	Carbon Preference Index
22684	517006-064	33,19	1,30	0,73	0,49	1,06
22685	517006-065	34,23	1,21	0,94	0,64	1,03
22688	517006-068	37,03	1,24	0,77	0,58	1,06
22734	517006-114	86,58	1,40	0,91	0,73	1,11

Table 5.3. Key gas chromatography data

Lab.-#	Sample	Depth (m)	Total-T/H30	T23/H30	T26/T25	Extended Tricyclics Ratio
22684	517006-064	33,19	19,10	3,38	0,71	0,77
22685	517006-065	34,23	19,76	3,14	0,72	0,80
22688	517006-068	37,03	19,08	2,93	0,67	0,81
22734	517006-114	86,58	27,70	4,25	0,91	0,78

Table 5.4. Key data on tricyclic terpanes derived from GC-MS<sub>SIM</sub> analysis monitoring m/z 191. Total T/H30: Sum C<sub>19</sub>-C<sub>29</sub> tricyclic terpanes/hopane; T23/H30: C<sub>23</sub> tricyclic terpane / hopane. T26/T25: C<sub>26</sub> tricyclic terpane / C<sub>25</sub> tricyclic terpane; Extended Tricyclic Ratio: (C<sub>28</sub> + C<sub>29</sub> tricyclic terpanes) / (C<sub>28</sub> + C<sub>29</sub> tricyclic terpanes + Ts)

Lab.-#	Sample	Depth (m)	Diahopane index	Gammacerane index	D29/RS29	S27/S29	Total S27 (%)	Total S28 (%)	Total S29 (%)	Total S30 (%)
22684	517006-064	33,19	51,58	13,44	4,08	1,17	34,5	25,2	29,5	10,8
22685	517006-065	34,23	59,12	13,78	5,03	1,09	33,9	24,7	31,0	10,5
22688	517006-068	37,03	61,10	16,57	4,53	0,94	30,2	24,8	32,1	12,9
22734	517006-114	86,58	75,24	20,43	4,46	0,82	28,9	24,2	35,3	11,6

Table 5.5. Key biological marker facies data derived from GC-MSMS data monitoring relevant parent–daughter transitions. Diahopane Index: 100\*diahopane/(diahopane+hopane), Gammacerane Index: 100\*gammacerane/(gammacerane+hopane); D29/RS29: sum C<sub>29</sub>



diasteranes / sum C<sub>29</sub> regular steranes; S27/S29: sum C<sub>27</sub> steranes / sum C<sub>29</sub> steranes. Total S27 (%), Total S28 (%), Total S29 (%), Total S30 (%): normalised distribution of total (regular+dia) C<sub>27</sub>-C<sub>30</sub> steranes.

Lab.-#	Sample	Depth (m)	Ts / (Ts+Tm)	H32 S/S+R	RS27 S/S+R	RS29 S/S+R	RS29 ββ / (ββ+αα)
22684	517006-064	33,19	0,92	0,62	0,57	0,51	0,64
22685	517006-065	34,23	0,94	0,57	0,57	0,52	0,66
22688	517006-068	37,03	0,91	0,61	0,54	0,49	0,64
22734	517006-114	86,58	0,96	0,61	0,55	0,55	0,49

Table 5.6. Key biological marker maturity data derived from GC-MSMS data monitoring relevant parent–daughter transitions. H32 S/S+R: bishomohopane 22S/(22S+22R) isomer ratio; RS27 S/S+R: C<sub>27</sub> regular sterane 20αααS+20αααR: C<sub>29</sub> regular sterane 20αααS / (20αααS + 20αααR) isomer ratio; RS29 ββ / (ββ+αα): C<sub>29</sub> regular sterane 20αββ / (20αββ + 20ααα) isomer ratio.

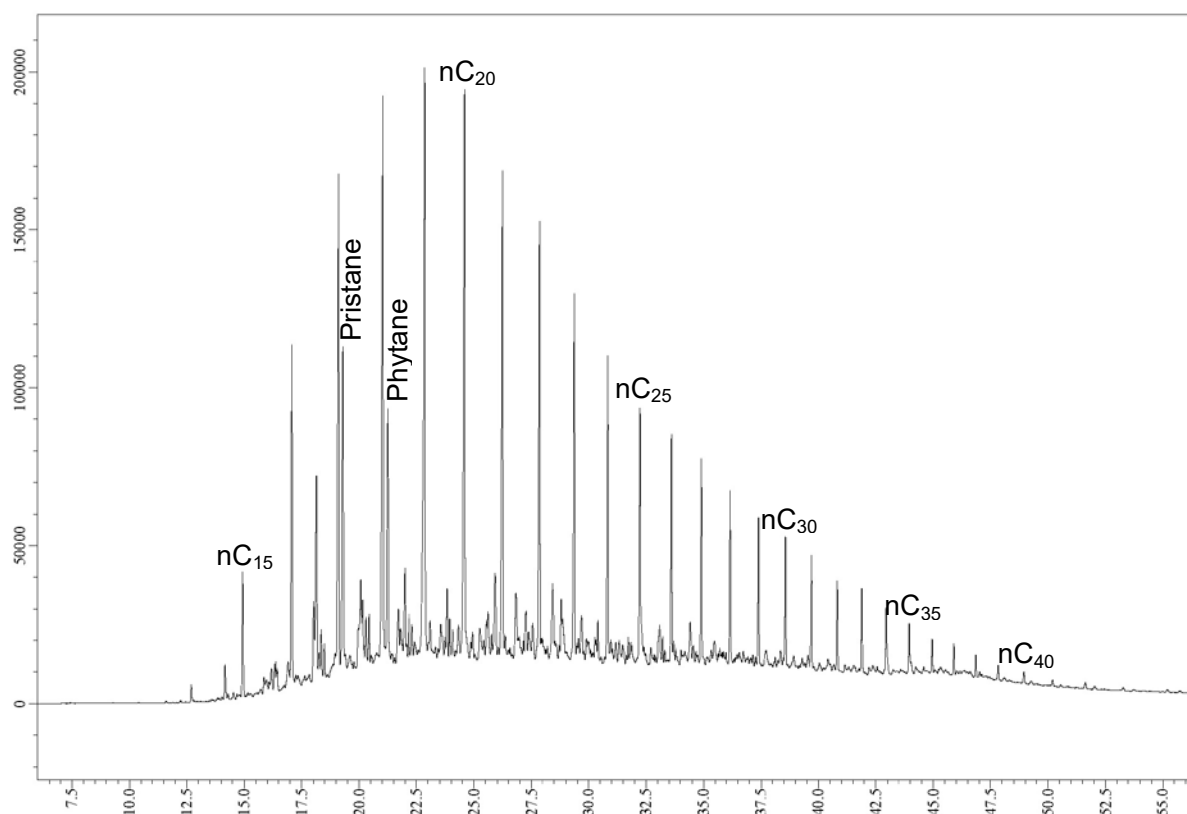


Fig. 5.8a. Gas Chromatogram, saturate-fraction of solvent extract of sample 22684 (517006-064, 33.19m)

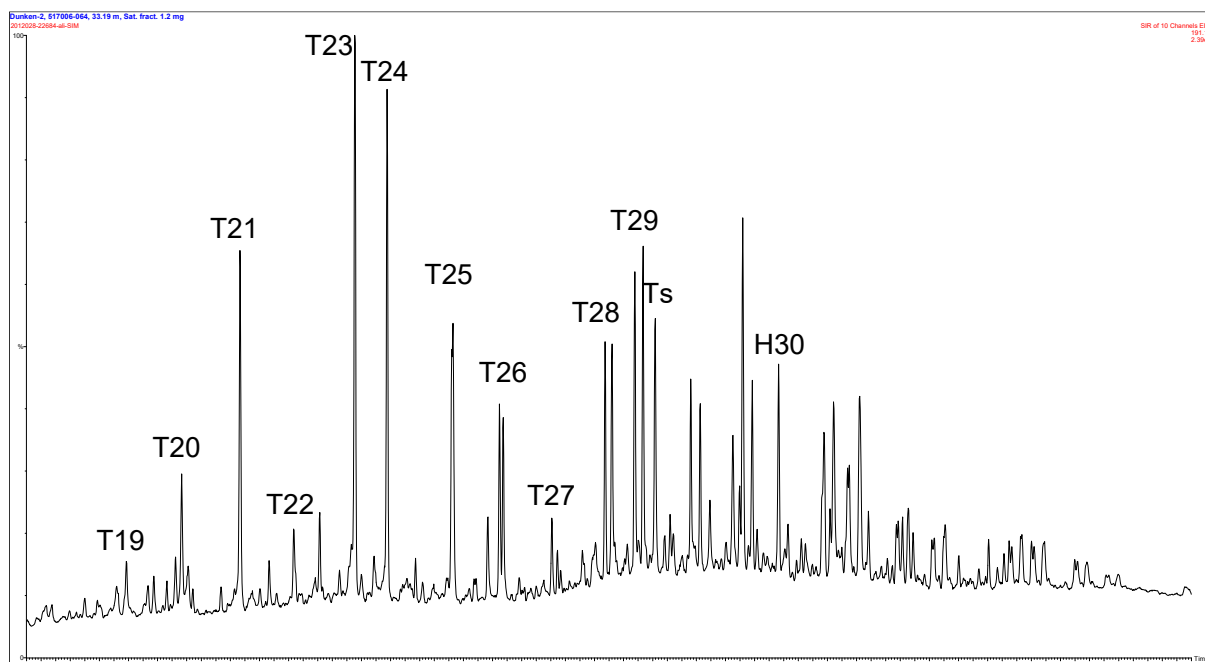


Fig. 5.8b. Sample 22684 (517006-064, 33.19m), GC-MS<sub>SIM</sub> data m/z 191: Tricyclic terpanes, TXX: XX= carbon number; Ts: 18 $\alpha$ -trisnorneohopane; H30: hopane

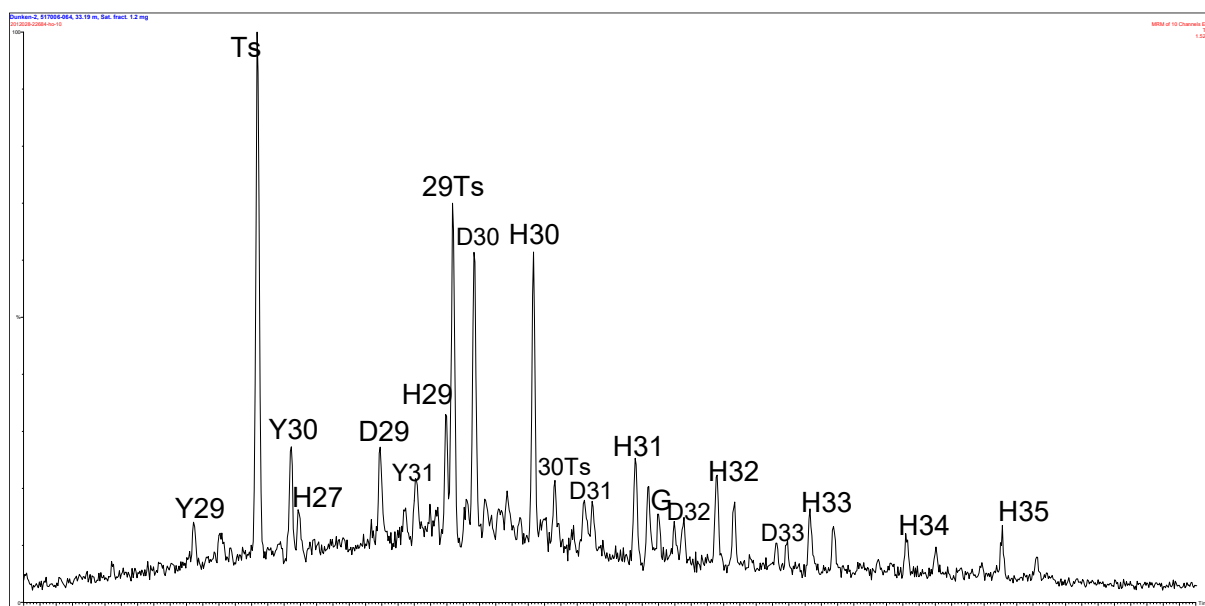


Fig. 5.8c. Sample 22684 (517006-064, 33.19m) GC-MSMS, hopanes/pentacyclics, sum of nine parent-daughter transitions. HXX: Hopanes, XX= carbon number, H31-H35 doublets, 22S and 22R isomers, H27 a.k.a.Tm; DXX: Diahopanes, XX= carbon number, D31-D33 doublets, 22S and 22R isomers; YXX: Early-eluting rearranged hopanes XX= carbon number, H31 doublet, 22S and 22R isomers; Ts, 29Ts, 30Ts: C27, C29 and C30 18 $\alpha$ -neohopanes; G: Gammacerane.

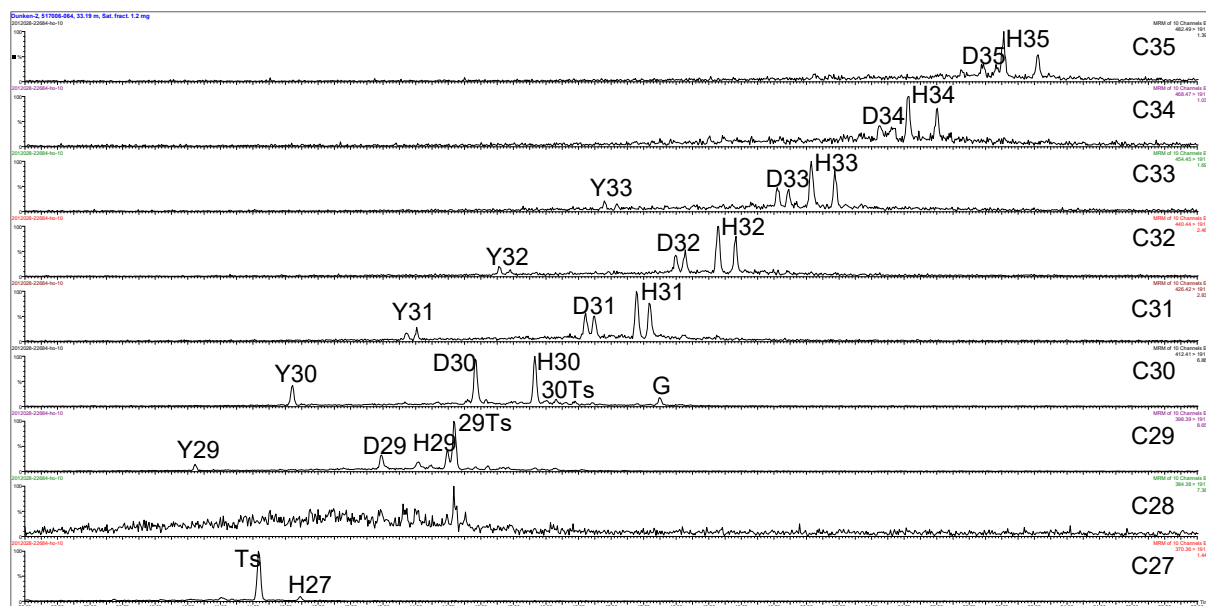


Fig. 5.8d. Sample 22684 (517006-064, 33.19m) GC-MSMS, hopanes/pentacyclics, individual C27-C35 parent-daughter transitions. HXX: Hopanes, XX= carbon number, H31-H35 doublets, 22S and 22R isomers, H27 a.k.a.Tm; DXX: Diahopanes, XX= carbon number, D31-D33 doublets, 22S and 22R isomers; YXX: Early-eluting rearranged hopanes XX= carbon number, H31 doublet, 22S and 22R isomers; Ts, 29Ts, 30Ts: C27, C29 and C30 18 $\alpha$ -neohopanes; G: Gammacerane.

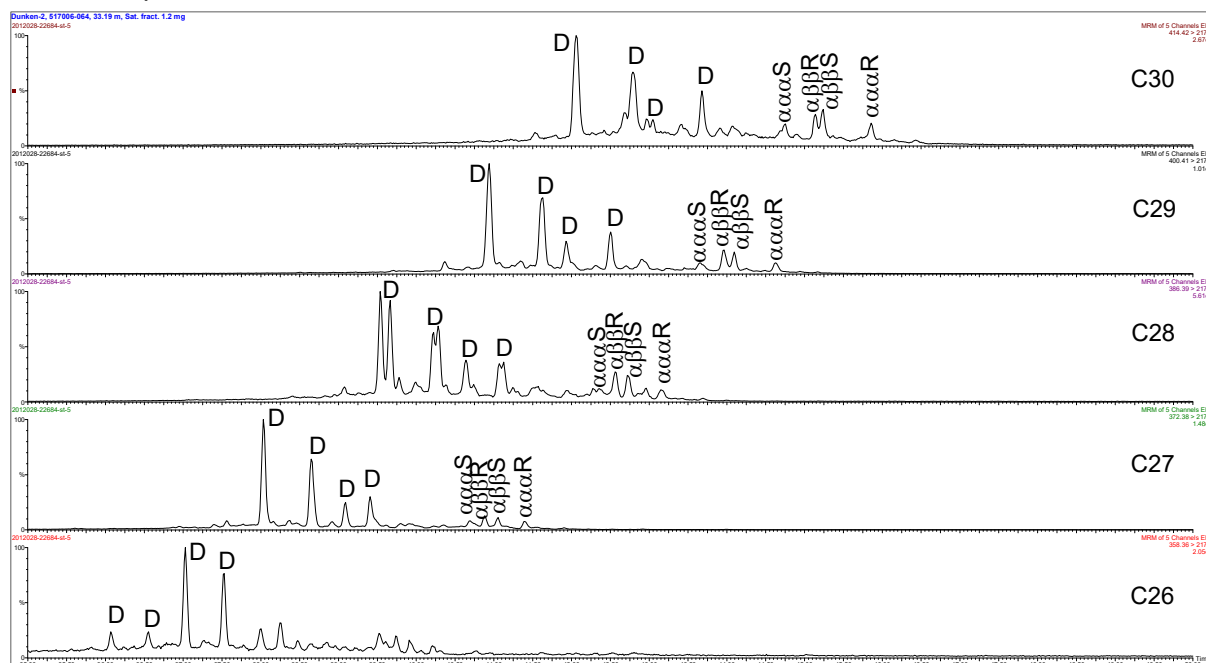


Fig. 5.8e. Sample 22684 (517006-064, 33.19m) GC-MSMS, steranes, individual C26-C30 parent-daughter transitions. D: diastertanes, several isomers;  $\alpha\alpha\alpha$ S: Regular sterane  $\alpha\alpha\alpha$ S isomers;  $\alpha\alpha\alpha$ R: Regular sterane  $\alpha\alpha\alpha$ R isomers;  $\alpha\beta\beta$ S: Regular sterane  $\alpha\beta\beta$ S isomers;  $\alpha\beta\beta$ R: Regular sterane  $\alpha\beta\beta$ R isomers;

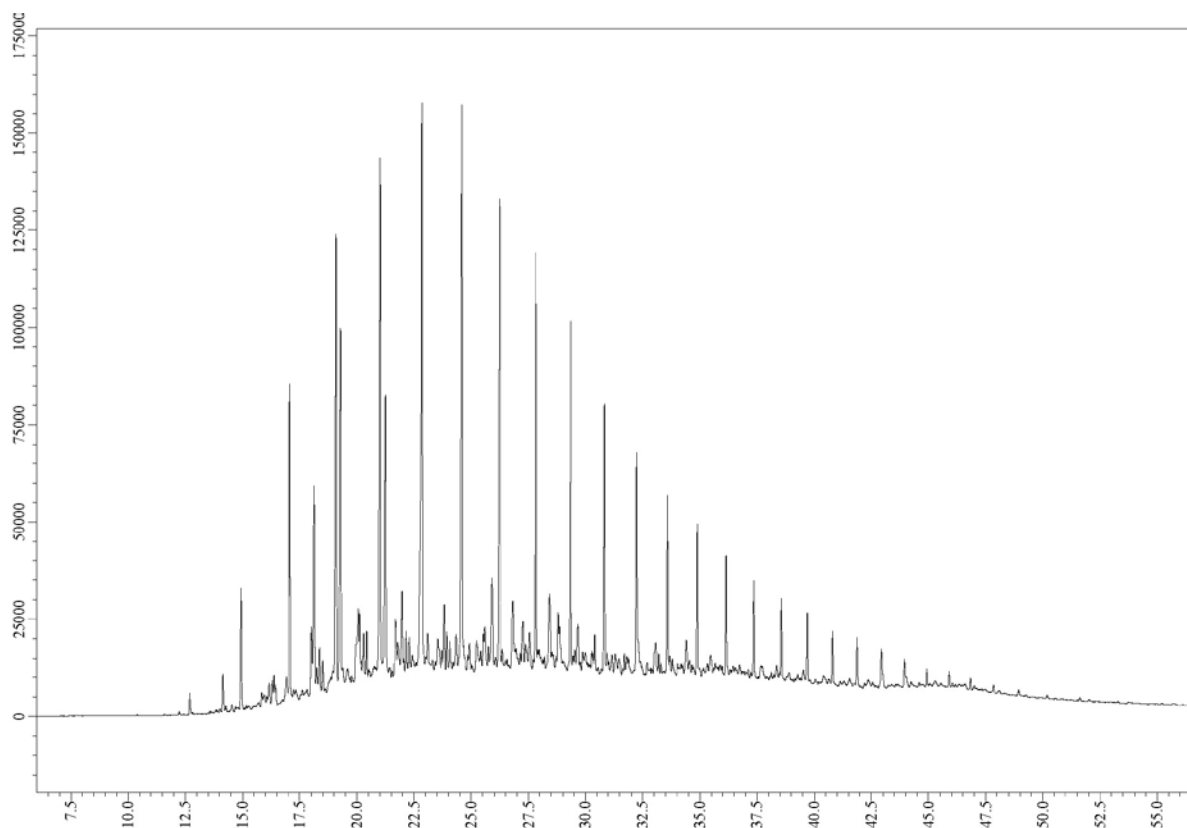


Fig. 5.9a. Gas Chromatogram, saturate-fraction of solvent extract of sample 22685 (517006-065, 34.23m). For compound identification see Fig. 5.8a.

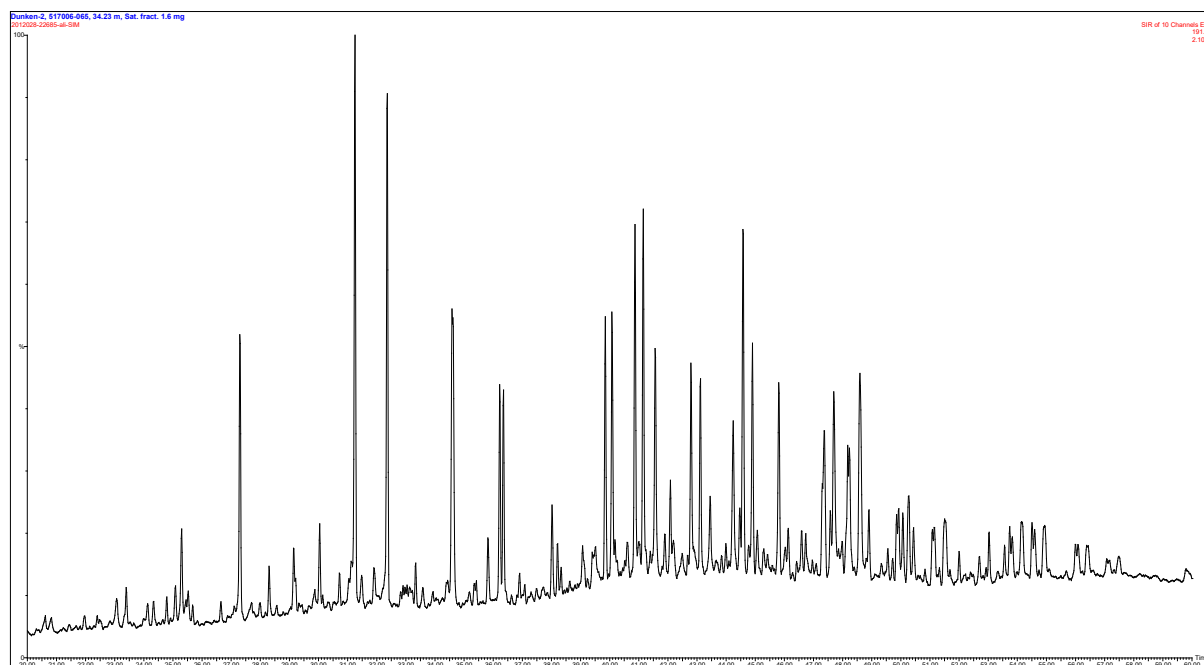


Fig. 5.9b. Sample 22685 (517006-065, 34.23m), GC-MS<sub>SIM</sub> data m/z 191. For compound identification see Fig. 5.8b.

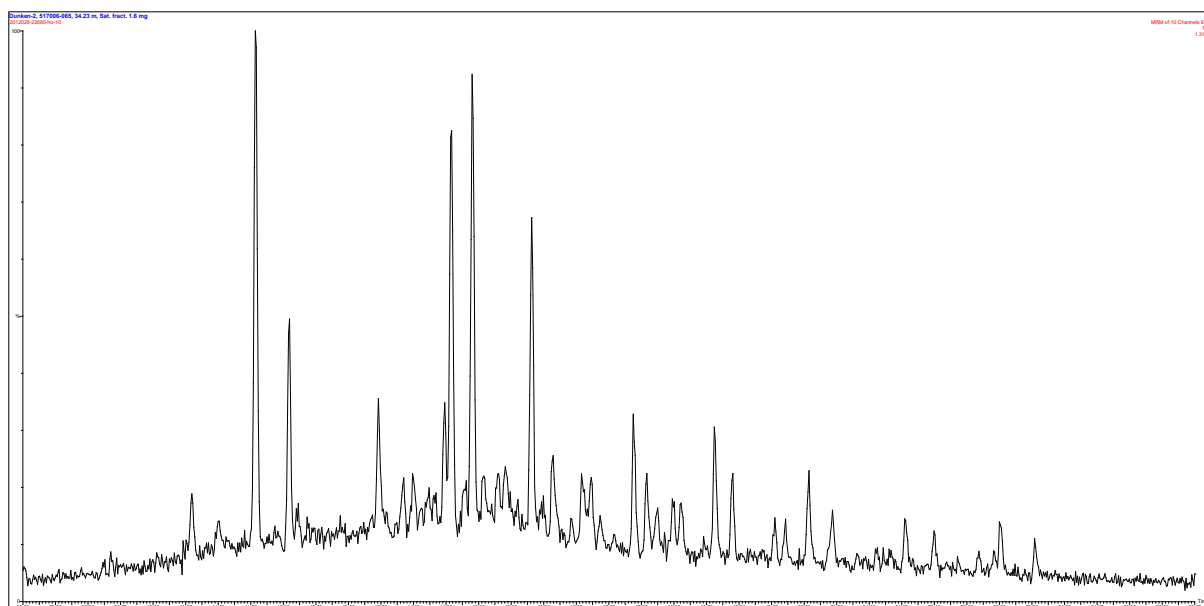


Fig. 5.9c. Sample 22685 (517006-065, 34.23m) GC-MSMS, hopanes/pentacyclics, sum of nine parent–daughter transitions. For compound identification see Fig. 5.8c.

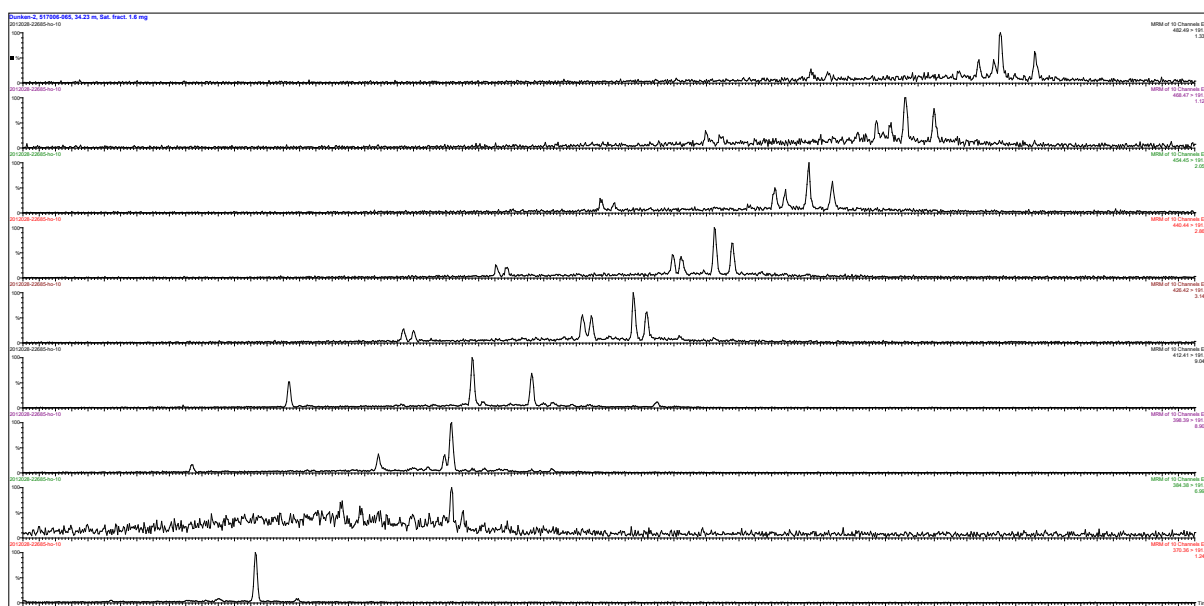


Fig. 5.9d. Sample 22685 (517006-065, 34.23m) GC-MSMS, hopanes/pentacyclics, individual C27-C35 parent–daughter transitions. For compound identification see Fig. 5.8d.

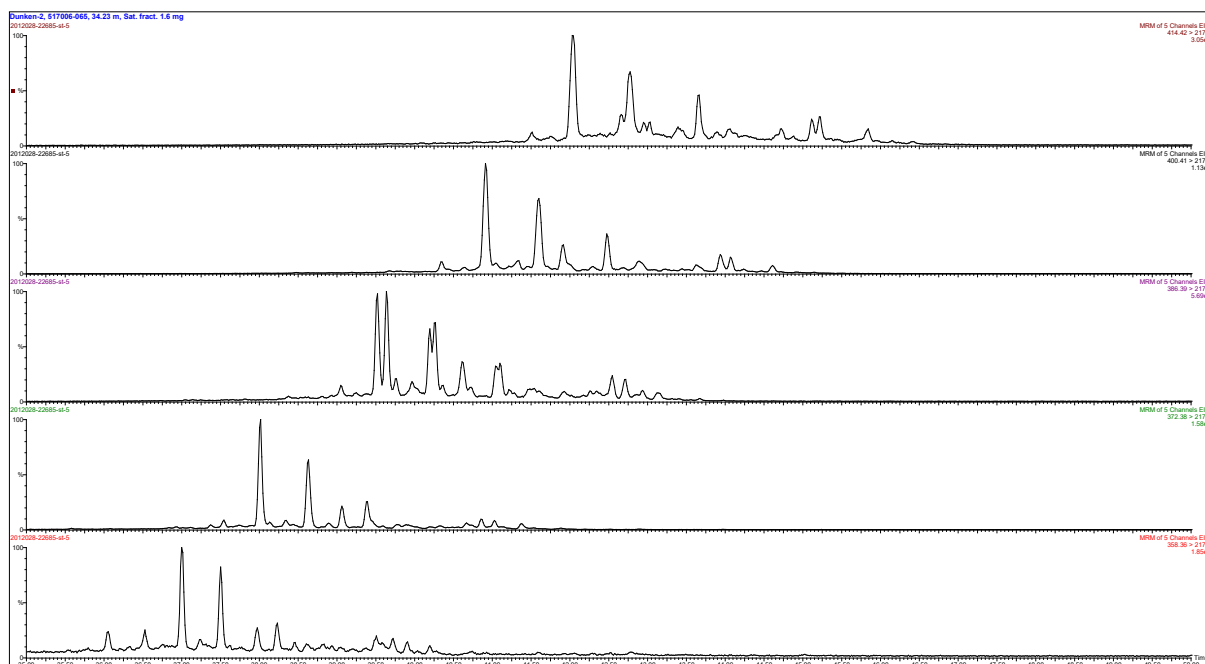


Fig. 5.e. Sample 22685 (517006-065, 34.23m) GC-MSMS, steranes, individual C26-C30 parent–daughter transitions. For compound identification see Fig. 5.8e.

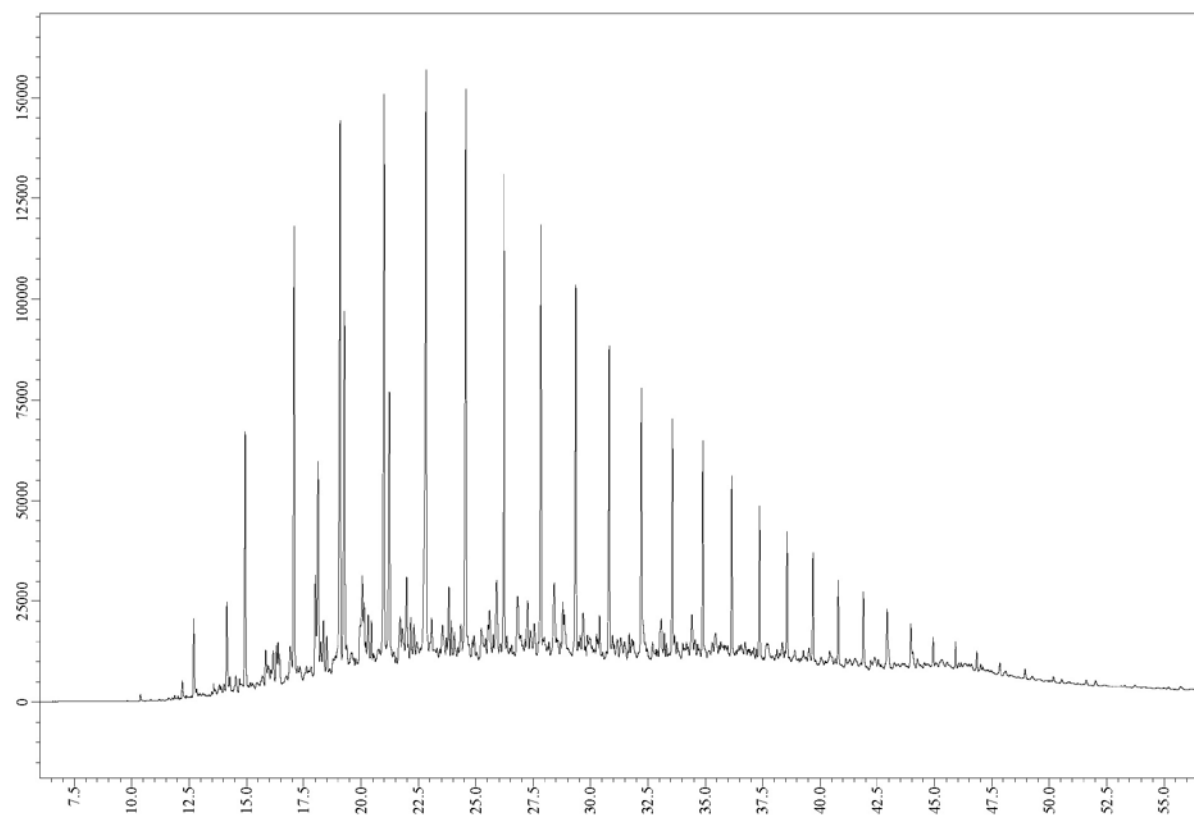


Fig. 5.10a. Gas Chromatogram, saturate-fraction of solvent extract of sample 22688 (517006-068, 37.03m). For compound identification see Fig. 5.8a.

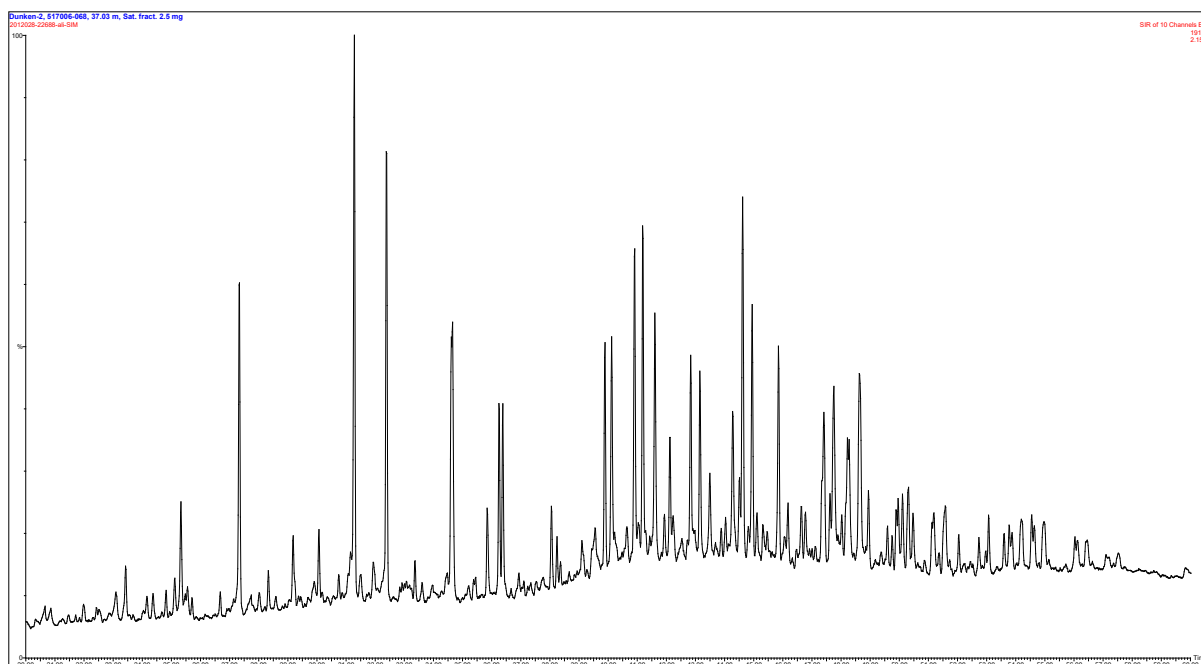


Fig. 5.10b. Sample 22688 (517006-068, 37.03m), GC-MS<sub>SIM</sub> data m/z 191. For compound identification see Fig. 5.8b.

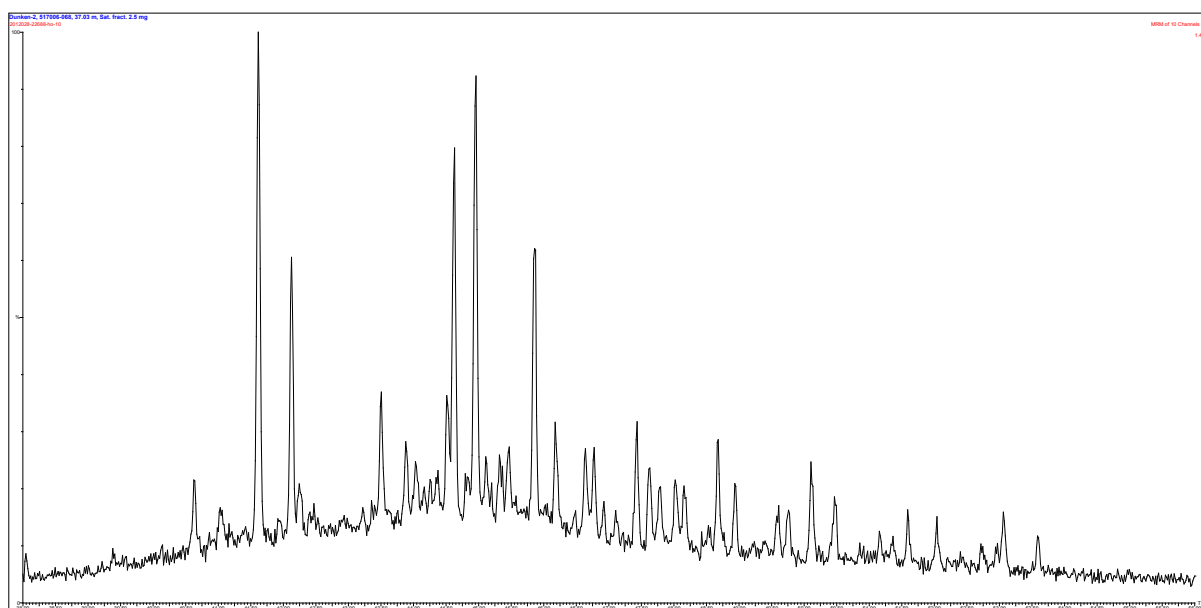


Fig. 5.10c. Sample 22688 (517006-068, 37.03m) GC-MSMS, hopanes/pentacyclics, sum of nine parent-daughter transitions. For compound identification see Fig. 5.8c.

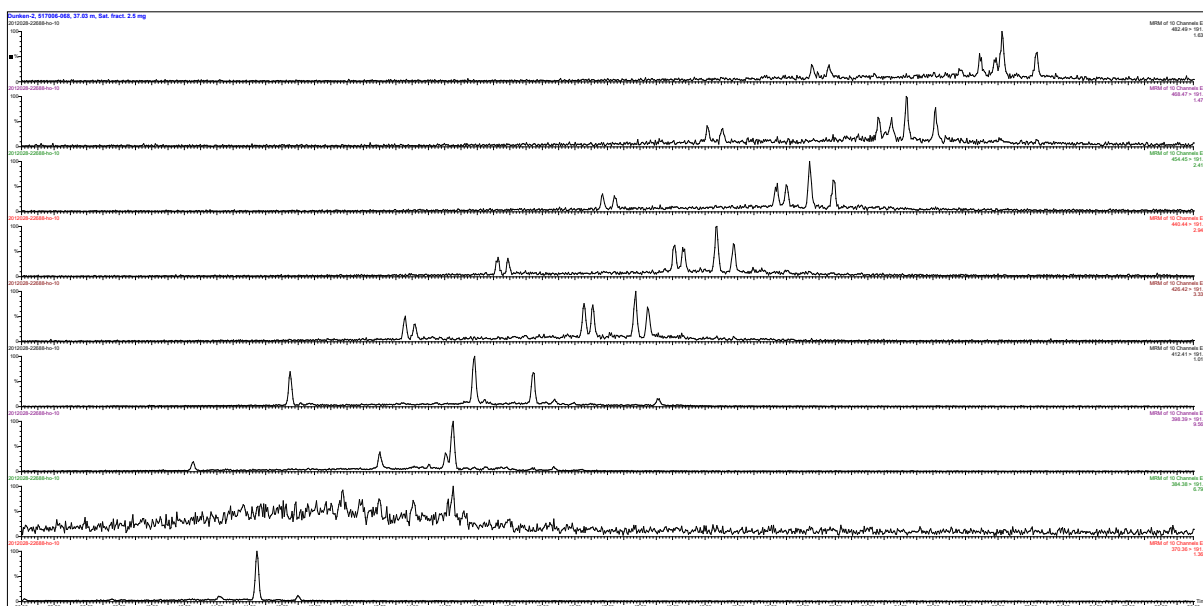


Fig. 5.10d. Sample 22688 (517006-068, 37.03m) GC-MSMS, hopanes/pentacyclics, individual C27-C35 parent-daughter transitions. For compound identification see Fig. 5.8d.

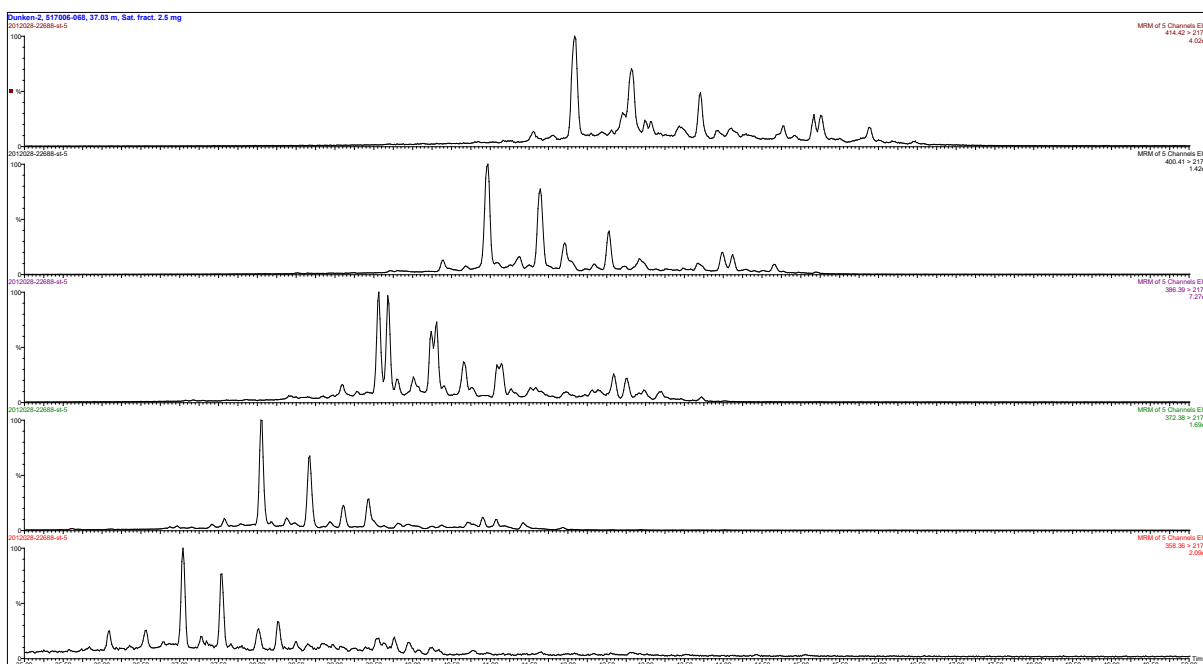


Fig. 5.10e. Sample 22688 (517006-068, 37.03m) GC-MSMS, steranes, individual C26-C30 parent-daughter transitions. For compound identification see Fig. 5.8e.



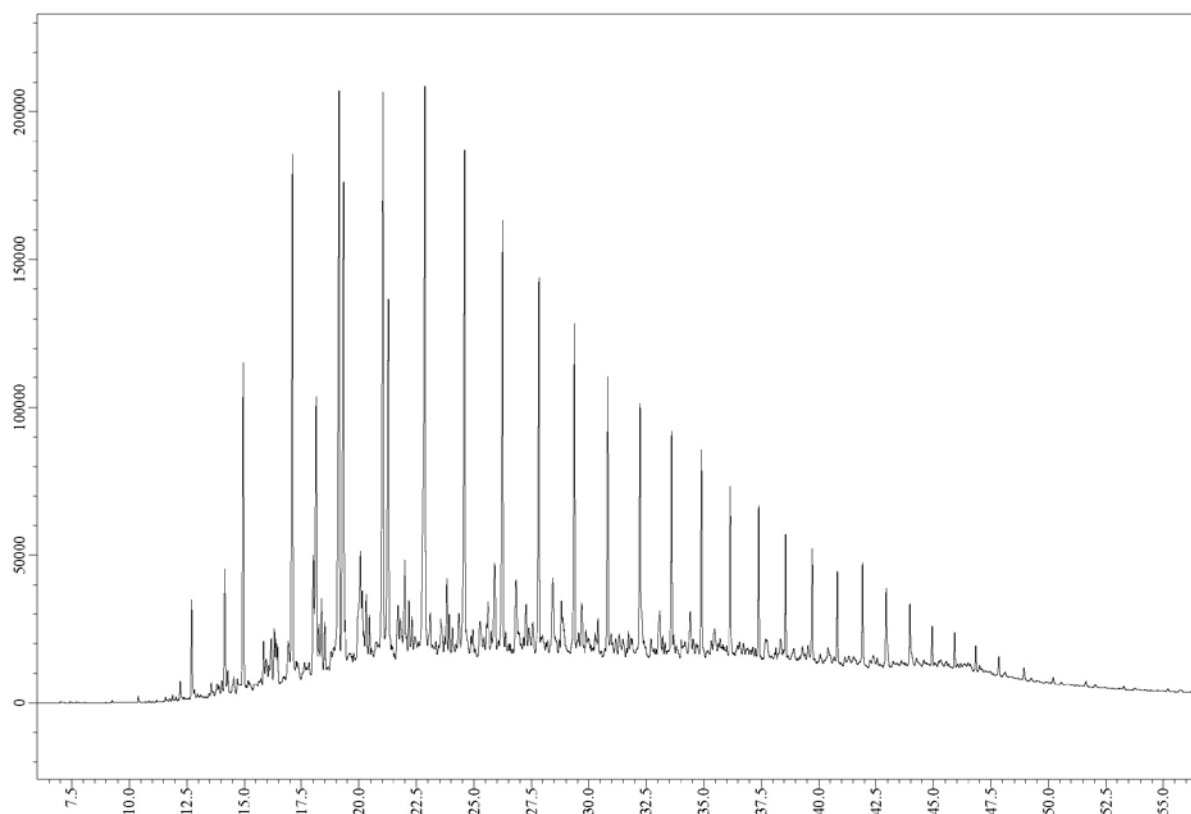


Fig. 5.11a. Gas Chromatogram, saturate-fraction of solvent extract of sample 22734 (517006-114, 86.58m). For compound identification see Fig. 5.8a.

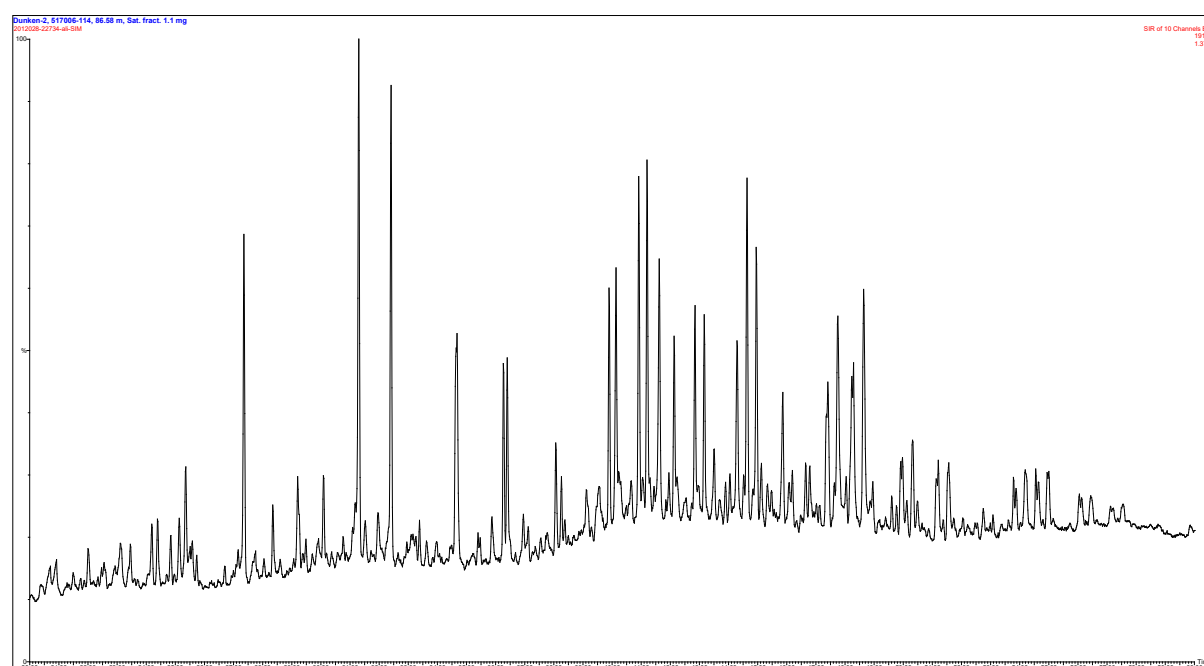


Fig. 5.11b. Sample 22734 (517006-114, 86.58m), GC-MS<sub>SIM</sub> data m/z 191. For compound identification see Fig. 5.8b.

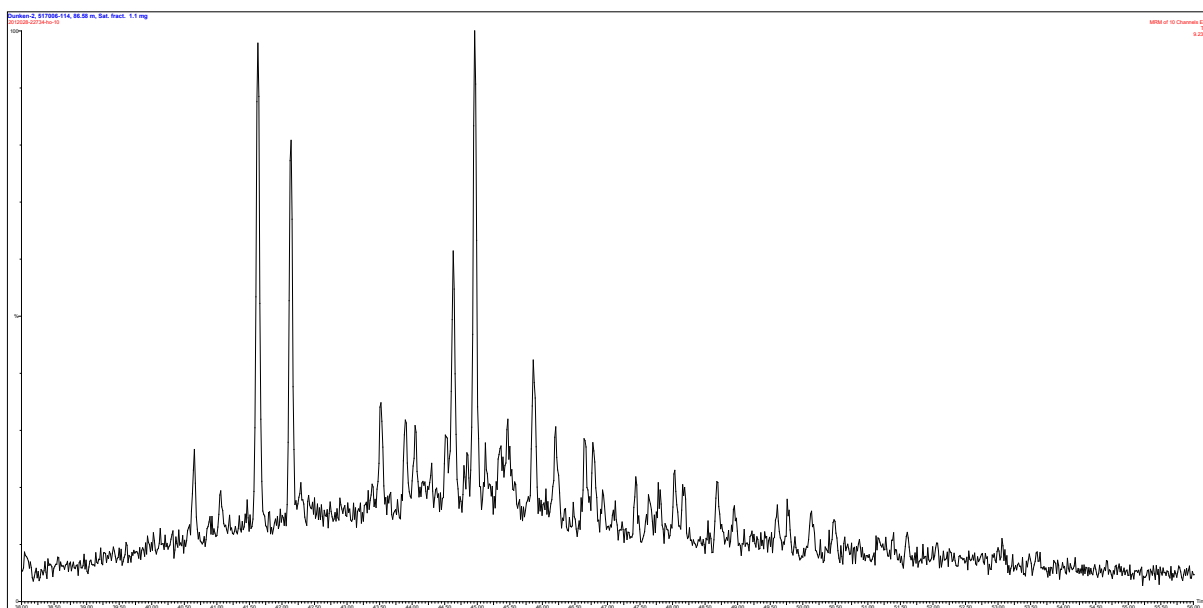


Fig. 5.11c. Sample 22734 (517006-114, 86.58m) GC-MSMS, hopanes/pentacyclics, sum of nine parent–daughter transitions. For compound identification see Fig. 5.8c.

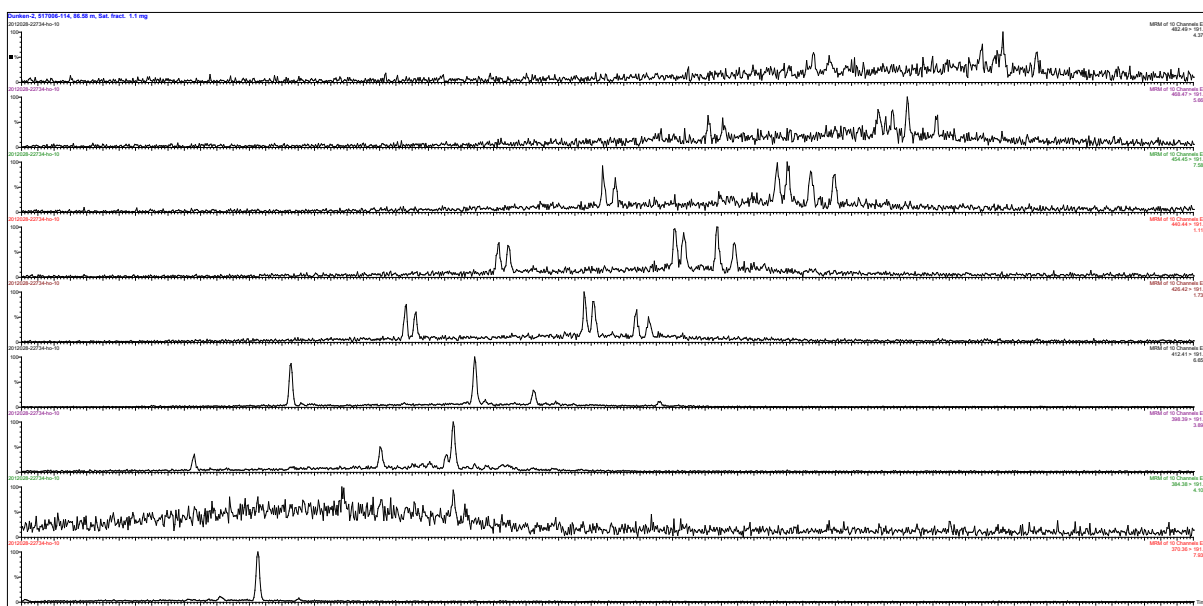


Fig. 5.11d. Sample 22734 (517006-114, 86.58m) GC-MSMS, hopanes/pentacyclics, individual C27-C35 parent–daughter transitions. For compound identification see Fig. 5.8d.

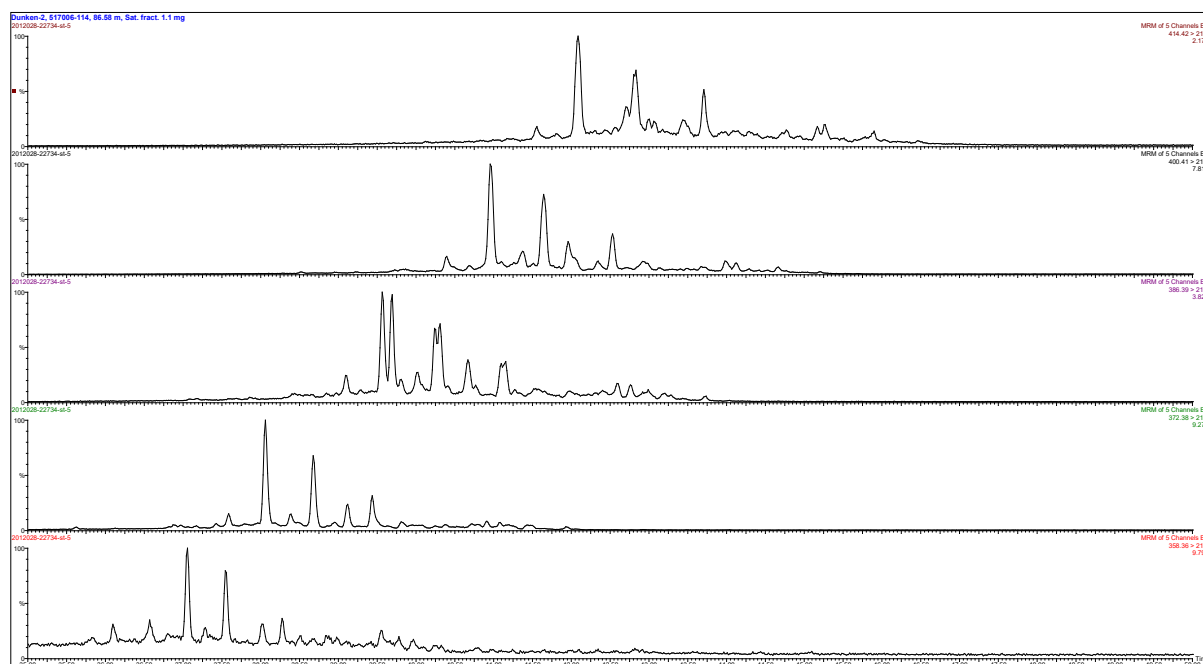


Fig. 5.11e. Sample 22734 (517006-114, 86.58m) GC-MSMS, steranes, individual C26-C30 parent–daughter transitions. For compound identification see Fig. 5.8e.

Extract yields are rather high (Table 5.2) corresponding well to the level of thermal maturity of the succession. Normal alkane distributions show some light-end evaporative losses, but are otherwise asymmetric, light-end skewed with apices close to  $nC_{19}$ , but otherwise extending to include at least  $nC_{40}$  (Figs 5.8a, 5.9a, 5.10a, 5.11a). Pristane/phytane ratios are generally close to 1.3, which together with  $n$ -alkane distributions agrees well with petroleum derived from a mature marine shale source (Table 5.3). The gas chromatograms are all very similar.

Tricyclic terpanes are very abundant, much more abundant than hopanes and steranes (Figs 5.8b, 5.9b, 5.10b, 5.11b, Table 5.4). Both hopanes and steranes are present in rather low concentrations, leading to poor signal to noise ratios (Figs 5.8cde, 5.9cde, 5.10cde, 5.11cde). A notable feature is the prominence of several types of rearranged hopanes: neo-hopanes, diahopanes and the “early eluting series” are all very prominent and present in series of homologs that may extend even to  $C_{35}$ . Another remarkable feature is the presence of notable concentrations of gammacerane. Diasteranes are very prominent compared to regular steranes, but the sterane distributions include a full series of homologs from norcholestanes (S26) to  $n$ -propylcholestanes (S30). A decreasing trend in the S27/S29 sterane ratio with depth seems to be present, but the proportions of both methylcholestanes (S28) and  $n$ -propylcholestanes (S30) seem to remain more or less constant (Table 5.5). High proportions of tricyclic terpanes is a characteristic feature of Triassic oils (Holba *et al.* 2001, Peters *et al.*, 2005 and references therein), which in combination with source age indications provided by the distribution of regular steranes (Grantham & Wakefield 1988) has been used to discriminate Triassic, Palaeozoic, Jurassic and post-Jurassic oils. The Dunken-2 core oil stains fall well within the Triassic field (fig. 5.12). Apart from being a feature of Triassic oils, high levels of tricyclic terpane relative to hopanes and steranes is also a product of elevated maturity. This agrees with the very high relative abundances of rearranged hopanes as well as steranes, which also testify to a high level of

thermal maturity as well as to a clay-rich (shale) source. Steranes otherwise clearly testify to the marine nature of the source, principally by the high relative abundance of n-propylcholestanes, which are strong marine indicators. A remarkable feature is the prominence of gammacerane, which is generally associated with strongly stratified water-columns. However, gammacerane is commonly present in small proportions in marine oils, and the enhancement observed may be an effect of its relative thermal stability.

Biological marker maturity indicators all consistently indicate a level of maturity well within the oil window although in particular sterane parameters show some scatter caused by poor signal-to-noise ratio. Hence, the bishomohopane 22S/(22S+22R) isomer ratio has reached equilibrium, suggesting a level of maturity corresponding to the onset of petroleum generation or higher; the sterane 20S/(20S+20R) isomer ratio is likewise at equilibrium, suggesting a level of thermal maturity well within the oil generative window or higher; sterane  $\alpha\beta\beta/(\alpha\beta\beta+\alpha\alpha\alpha)$  ratios are high but below equilibrium, suggesting a level of thermal maturity close to peak oil generation, and the Ts/(Ts+Tm) ratio, which is also facies dependent, is very high too (Table 5.6). With respect to assessment of the level of thermal maturity, all available parameters, *i.e.* biomarker ratios and Tmax, are subject to some uncertainty. Biomarker ratios due to poor signal-to-noise ratio, hampering clear peak definition; Tmax due to poor pyrolysis yields resulting in small and sometimes rather ill-defined S2-peaks, although nonsense data have been weeded out. However, all parameters indicate a level of thermal maturity well within the oil-generative window.

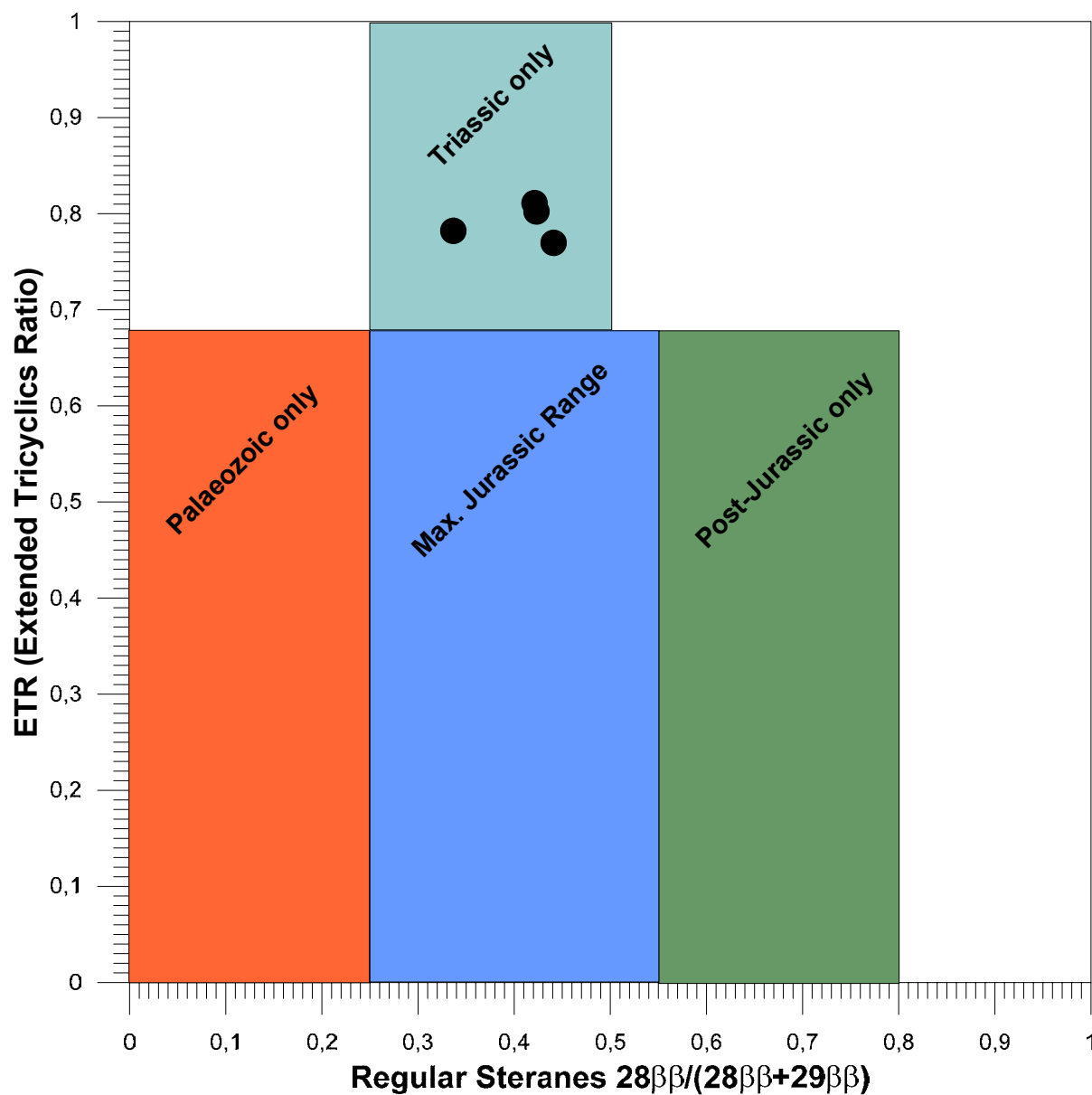


Fig. 5.12. Source-age indication using  $\alpha\beta\beta$ -isomers of  $C_{28}$  and  $C_{29}$  regular steranes after Grantham and Wakefield (1988) versus Extended Tricyclic Ratio ("ETR"  $(T_{28}+T_{29}) / (T_{28}+T_{29}+T_s)$ , Holba et al., 2001). The oil stains from the Dunken-2 core fall within the "Triassic" field as expected.

## 5.4 Summary

- The Dunken-2 fully cored borehole was drilled to test the presence of petroleum source rocks in the Spathian to Norian interval of the Triassic succession of the Wandel sea Basin
- The drilled succession is dated to the early to late Spathian and may thus be slightly older than the oldest target interval.
- Except for the upper 20 metres, which are predominantly sandy, the succession was sampled for every meter, resulting in analysis of 122 samples for petroleum potential
- The succession is generally poor in organic carbon (0 – 0.55%) shows low pyrolysis yields (0 – 0.79), and does not include petroleum source rocks.
- The succession is oil-window mature.
- Two narrow intervals show slightly enhanced organic matter contents and petroleum potentials.
- These intervals are stained by small quantities of oil, probably generated *in situ*
- The presence of intervals with slightly enhanced petroleum potential and oil staining may hint at the presence of petroleum source rocks within the succession elsewhere, presumably in more palaeo-basinwards settings.
- The upper interval may stratigraphically correspond to the Steinkobbe Formation of the Svalis Dome (Barents Sea) where petroleum source rocks occur.
- The biological marker compositions of the oil stains include high proportions of tricyclic terpanes relative to pentacyclics, and high proportions of rearranged hopanes and steranes relative to regular hopanes and steranes.
- In general, the molecular composition complies with generation from a marine shale source rock of Triassic age, at a level of maturity well within the oil generative window.

## 5.5 References

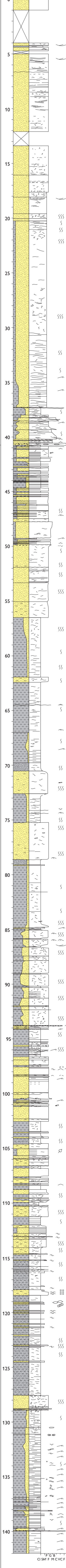
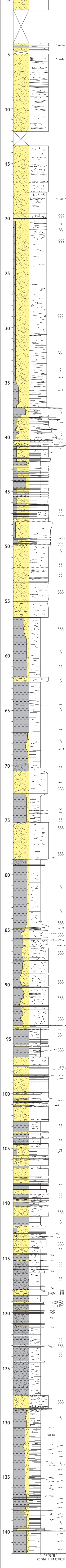
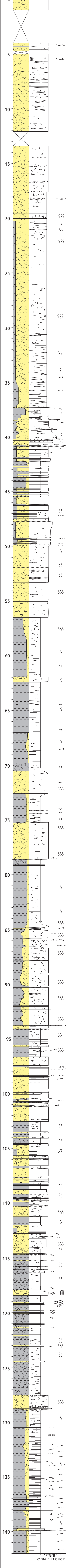
- Grantham, P.J. & Wakefield, L.L. 1988: Variations in the sterane carbon number distributions of marine source rock derived crude oils through geological time. *Organic Geochemistry* 12, 61-73
- Holba, A.G., Ellis, L. Dzou, I.L., Hallam, A., Masterson, W.D., Francu, J., 6 Fincannon, A.L., 2001: Extended tricyclic terpanes as age discriminators between Triassic, early Jurassic and middle-late Jurassic oils. 20<sup>th</sup> International Meeting on Organic Geochemistry (IMOG, Nancy 2001), book of abstracts p. 464, and poster shown at meeting.
- Leith, T.L., Weiss, H.M., Mørk, A., Århus, N., Elvebakk, G., Embry, A.F., Brooks, P.W., Stewart, K.R., Pchelina, T.M., Bro, E.G., Verba, M.L., Danyushevskaya, A., & Borisov, A.V. 1992: Mesozoic hydrocarbon source-rocks of the Arctic region. In: Voren, T.O., Bergsager, E., Dahl-Stamnes, Ø.A., Holter, E., Johansen, B., Lie, E. & Lund, T.B. (eds.) *Arctic Geology and Petroleum Potential*, NPF Special Publication 2, 1-25
- Lundschien, B.A., Høy, T. & Mørk, A., 2014: Triassic hydrocarbon potentiel in the Northern Barents Sea; integrating Svalbard and stratigraphic core data. In: Mørk, A., Lundschien, B.A. & Høy, T. (eds.) *NPD Bulletin* 11, 3-20
- Peters, K. E., Magoon, L- B., Bird, K. J., Valin, Z. C. & Keller, M. A. 2006: North Slope, Alaska: Source rock distribution, richness, thermal maturity, and petroleum charge. *AAPG Bulletin* 90, 261–292
- Peters, K.E., Walters, C.C. & Moldowan J.M. 2005: *The Biomarker Guide*. Cambridge University Press, 1155pp (2 volumes)

## Appendix

1. Sedimentological log in scale 1:50
2. Core photographs natural light, dry (A) and wet (B) conditions
3. Core Photographs UV light
4. Detailed core photographs
5. Petrography and Diagenesis Data Sheets
6. Thin sections, overview photographs (digital version only)
7. Cap-rock data (digital version only)
8. Gamma log scanning (digital version only)



## **Appendix 1   Sedimentological log in scale 1:50**

Chrono-stratigraphy		Litho-stratigraphy	Fossils, traces etc.	Facies	Interpretation	Sequence-stratigraphy	Ammonite stratigraphy	Dinoflagellate cyst stratigraphy
Anisian								
Upper Spathian		Dunken Fm		Sandstone, biomottled, units with low-angle cross bedding	Lower – upper shoreface	SB		
Lower Spathian		Ugleungernes Dal Fm		Heteroliths, sandstone dominated, biomottled	Lower shoreface	HST		
Smithian				Wavy bedding and ripple laminations	Offshore transition	HST		
				Heteroliths		HST		
				Sandstones, with wavy-and cross-bedding, common mudrapes Pebble conglomerate	Shallow marine	TST		
				Heteroliths, sandstone or mudstone dominated	Offshore transition	SB		
						HST		
						TST		
				Sandstones, massive or biomottled	Gravity flows debrites	SB		
				Sandstones, biomottled	Lower shoreface	LHST		
						HST		
				Mudstones, biomottled	Offshore transition	MFS		
				Sandstones, biomottled	Lower shoreface	SB		
						HST		
				Mudstones, biomottled	Offshore transition	TS		
						TST		
				Sandstones, biomottled	Lower shoreface	SB		
						HST		
				Heteroliths, biomottled	Lower shoreface	TS		
						TSE		
				Pebble conglomerate	Lag deposit	SB		
						HST		
				Mudstones, biomottled, thin sandstones	Offshore transition	TS		
						SB		
				Sandstones, massive and planar bedded	Lower shoreface	HST		
				Alternating units of: Sandstones, biomottled or massive. Mudstones and heteroliths	Lower shoreface – Offshore transition	SB		
						TS		
						SB		
				Mudstone, sandy, biomottled	Offshore transition	TS		
						LTS (SB)		
						HTS		
				Mudstones, laminated with thin planar and ripple laminated sandstones	Offshore	MFS		
						TSE		
				Pebble conglomerate	Lag deposit			
					Offshore			

Legend

Lithology

- Mudstone
- Sandy mudstone
- Muddy sandstone
- Sandstone
- Heterolithic mudstone/sandstone
- Conglomerate
- Breccia
- Extraformational clast
- Mudstone drapes and clast
- Coal clast

Depositional environment

- Fluvial
- Flood plaine
- Submarine channel
- Upper shoreface
- Lower shoreface
- Offshore – Offshore transition
- Basinal-offshore
- Marine carbonate

Sedimentary structures

- Low angle cross-stratification
- Trough cross-stratification
- Planar cross-bedding
- Planar lamination/bedding
- Hummocky cross-stratification
- Asymmetric ripple cross-stratification
- Wave-ripple cross-lamination
- Climbing ripple cross-stratification
- Heterolithic bedding (mud dominated)
- Heterolithic bedding (sand dominated)
- Erosive contact
- Contorted bedding
- Loading
- Water escape structure
- Structureless
- Slump fold
- Imbrication
- Cross lamination

Fossils

- Fragment
- Plant fragments
- Ammonite
- Gastropod
- Logs
- Brachiopods
- Bivalve

Trace Fossils

- Chondrites
- Diplocraterion isp.
- Helminthopsis
- Macaronichnus isp.
- Nereites
- Ophiomorpha isp.
- Planolites
- Rhizocorallium isp.
- Skolithos isp.
- Thalassinoides isp.
- Vertical shaft

Miscellaneous

- Fracture
- Palaeocurrent direction
- Current lineation
- Wave ripple crest orientation
- Bedding dip
- TS Transgressive surface
- TSE Transgressive surface of erosion
- SB Sequence boundary
- MFS Maximum flooding surface
- TST Transgressive systems tract
- HST Highstand systems tract
- LHST Late highstand systems tract
- Trend of the coarsests grain size fraction
- Degree of bioturbation
  - Intense
  - Moderate
  - Weak

## **Appendix 2A Core photographs, natural light, dry condition**

BOX  
1



GEUS DUNKEN-2 0,00 - 11,20 m



BOX  
2



GEUS DUNKEN-2 11,34 - 19,44 m



BOX  
3



GEUS DUNKEN-2 19,34 - 26,04 m



BOX  
4



GEUS DUNKEN-2

26,04 - 33,16 m



BOX  
5



GEUS DUNKEN-2

33,11 - 39,85 m



BOX  
6



GEUS DUNKEN-2 39,88 - 46,55 m



BOX  
7



GEUS DUNKEN-2

46,52 - 53,44 m



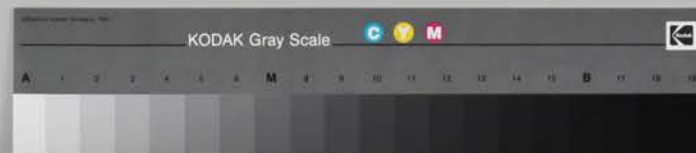
BOX  
8



GEUS DUNKEN-2 53,25 - 59,94 m



BOX  
9



GEUS DUNKEN-2 59,91 - 66,56 m



BOX  
10



GEUS DUNKEN-2

66,40 - 72,89 m



BOX  
11



GEUS DUNKEN-2

72,91 - 79,68 m



BOX  
12



GEUS DUNKEN-2

79,74 - 86,56 m



BOX  
13



GEUS DUNKEN-2 86,48 - 93,49 m



BOX  
14



GEUS DUNKEN-2 93,46 - 100,19 m

BOX  
15



GEUS DUNKEN-2 100,24 - 107,10 m



BOX  
16



GEUS DUNKEN-2

107,03 - 113,77 m

BOX  
17



GEUS DUNKEN-2 113,90 - 120,44 m



BOX  
18



GEUS DUNKEN-2

120,45 - 127,02 m



BOX  
19



GEUS DUNKEN-2

126,93 - 133,71 m



BOX  
20



GEUS DUNKEN-2

133,58 - 140,34 m



BOX  
21



21/7 - 27/7 - 2012

John Bozemp

San Vancie

Anda Clara



GEUS DUNKEN-2

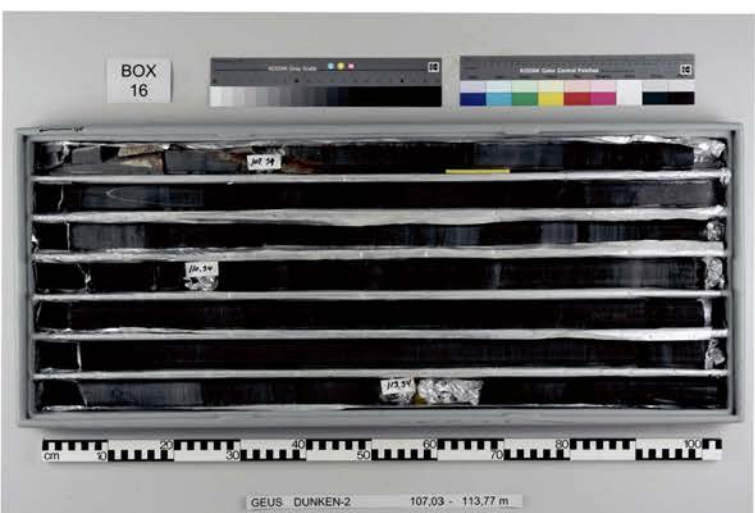
140,39 - 141,84 m

## **Appendix 2B Core photographs, natural light, wet condition**





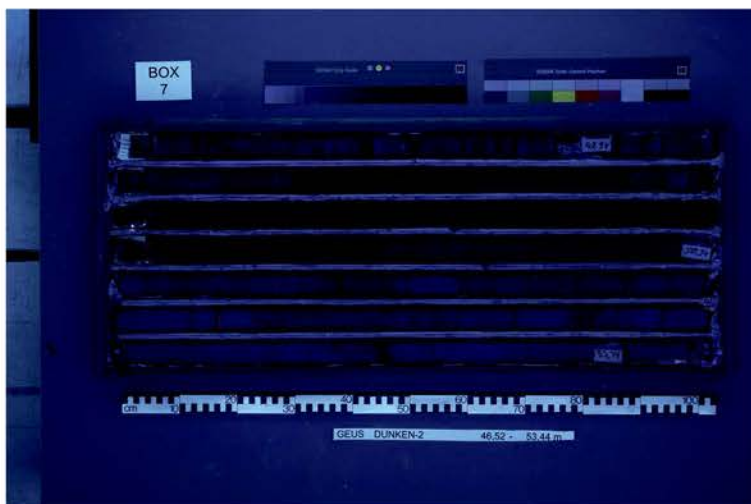
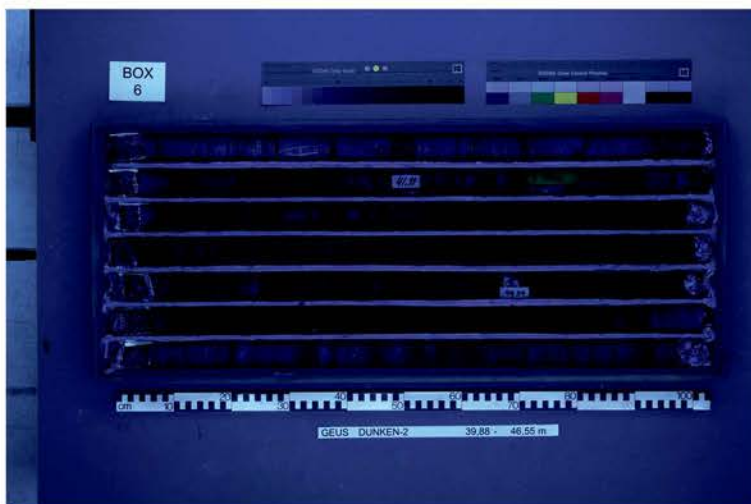
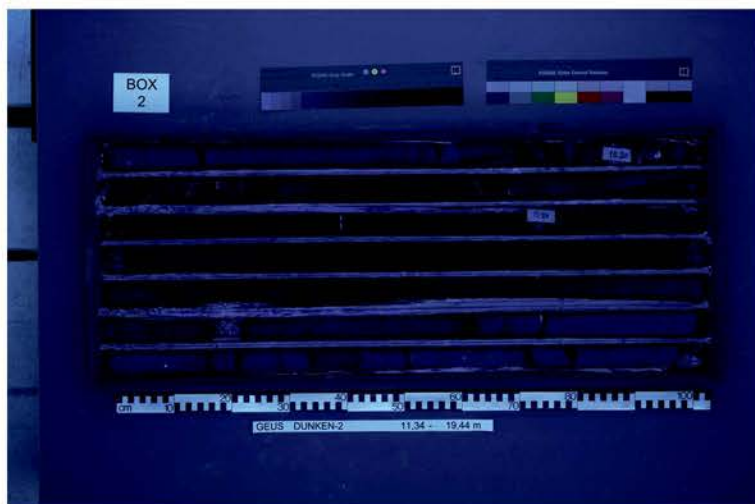
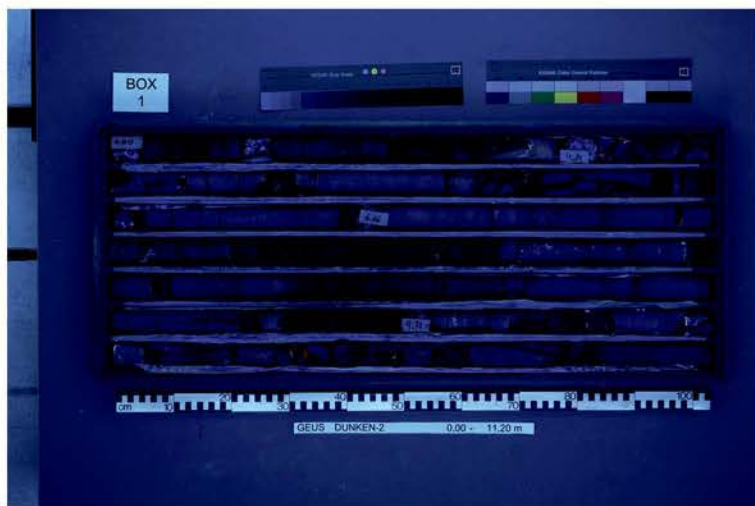




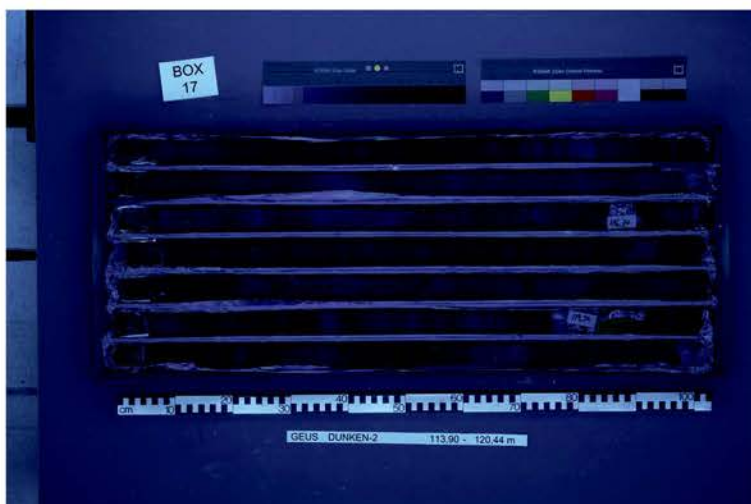
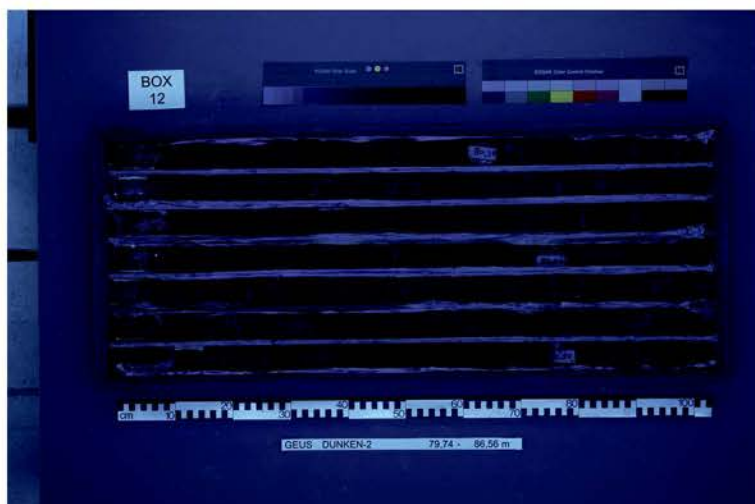
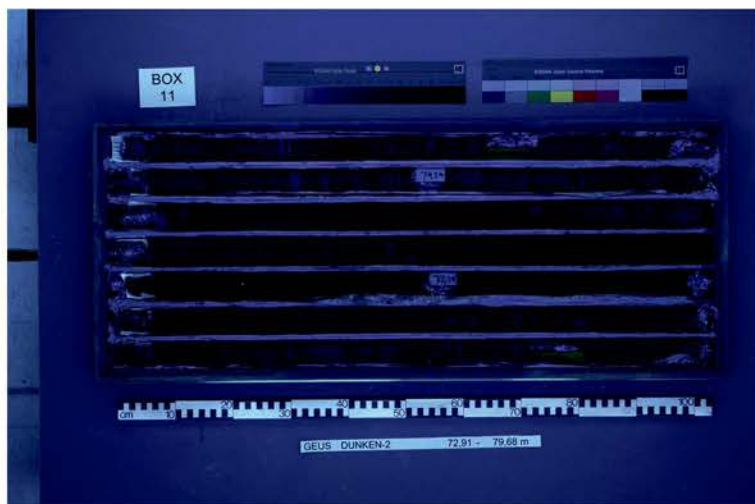
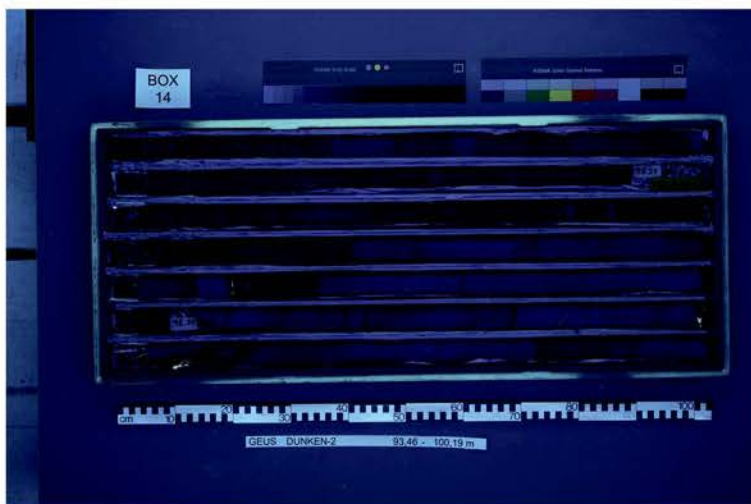
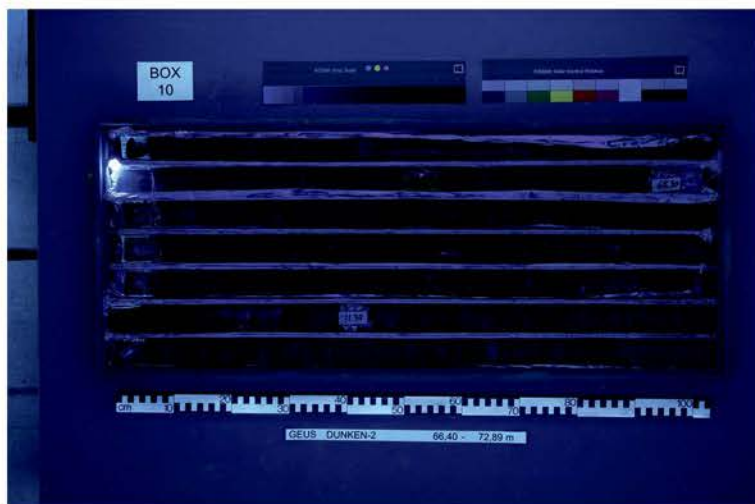
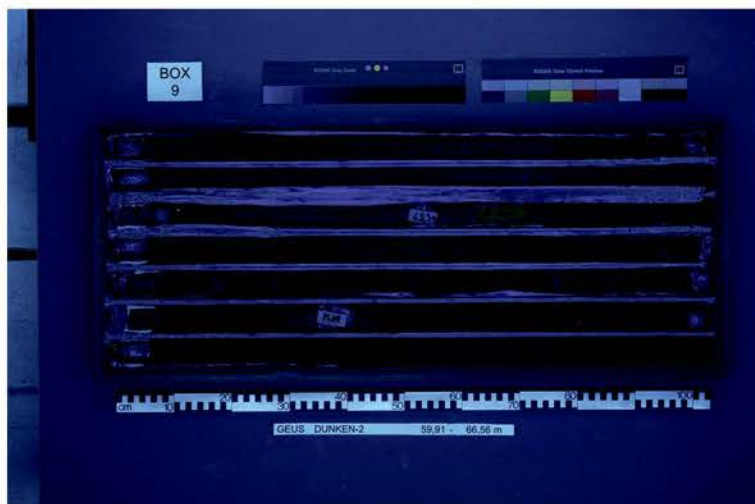




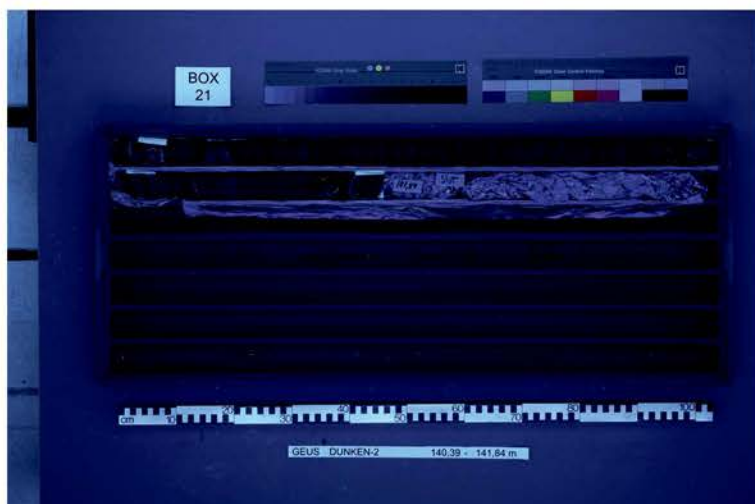
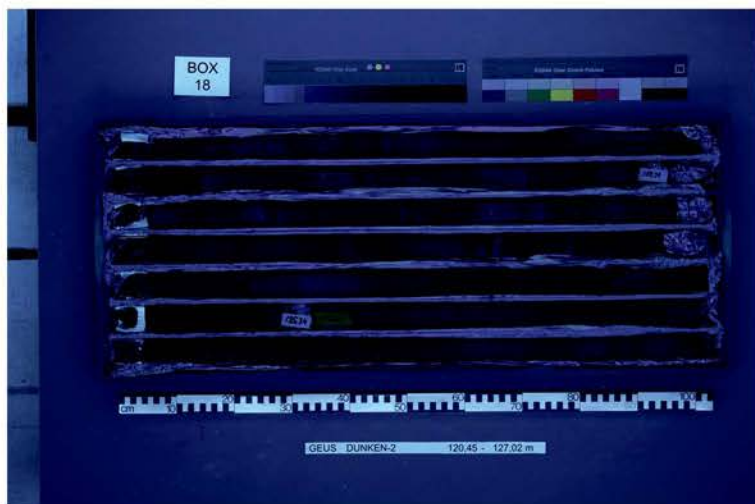
## **Appendix 3 Core photographs, UV light**



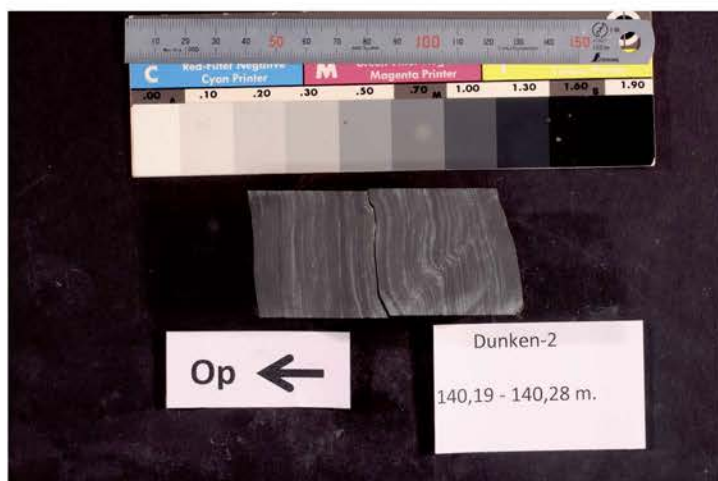
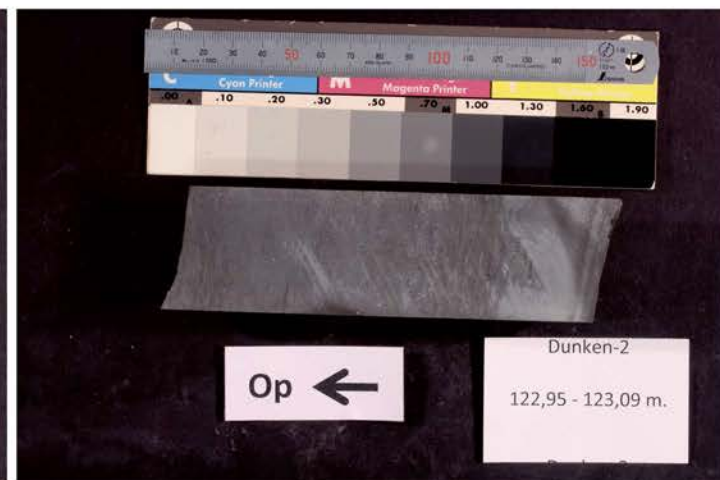




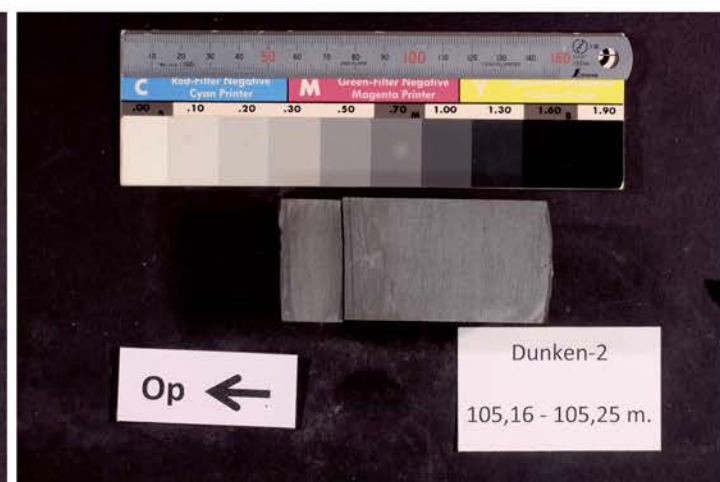
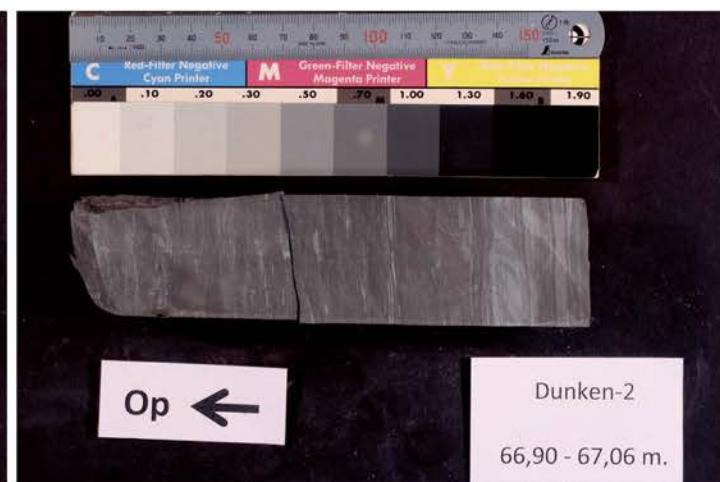
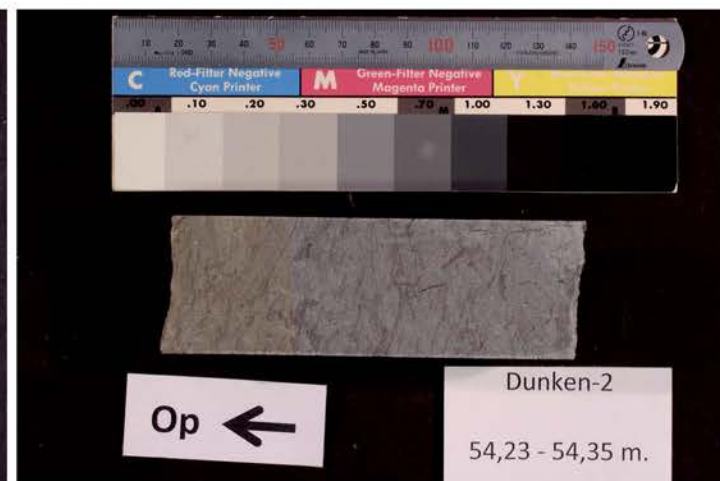




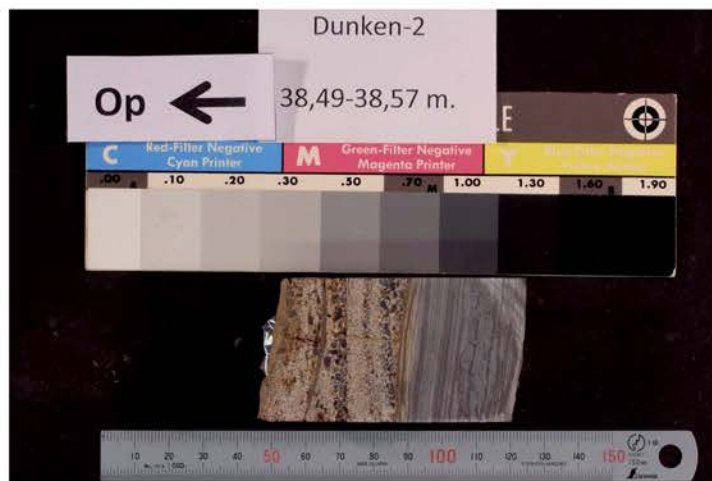
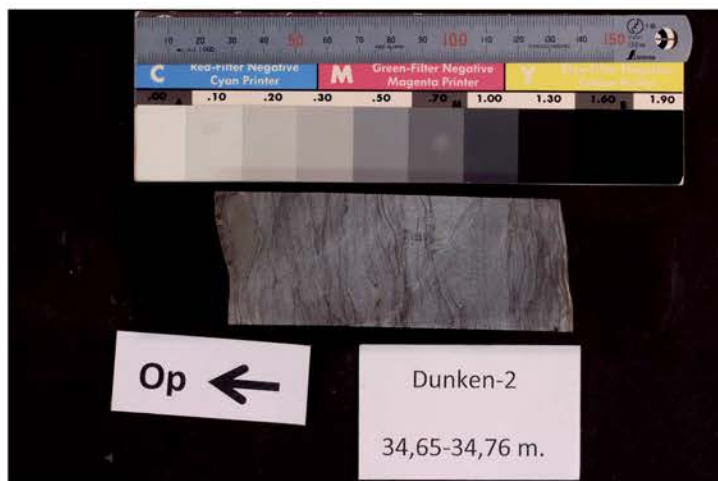
## **Appendix 4 Detailed core photographs**



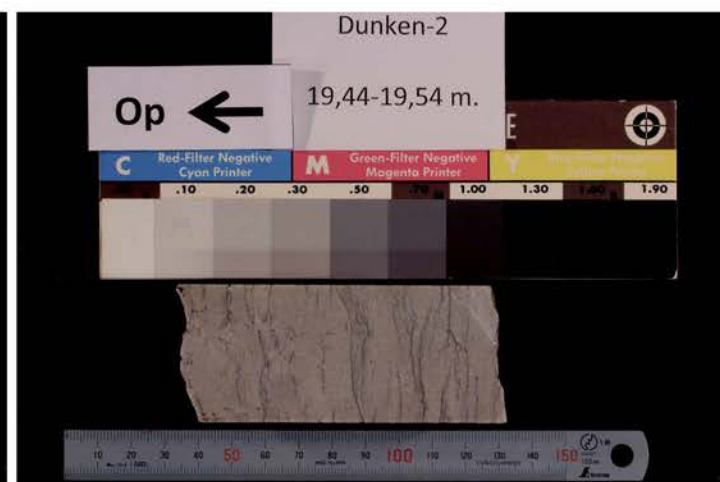
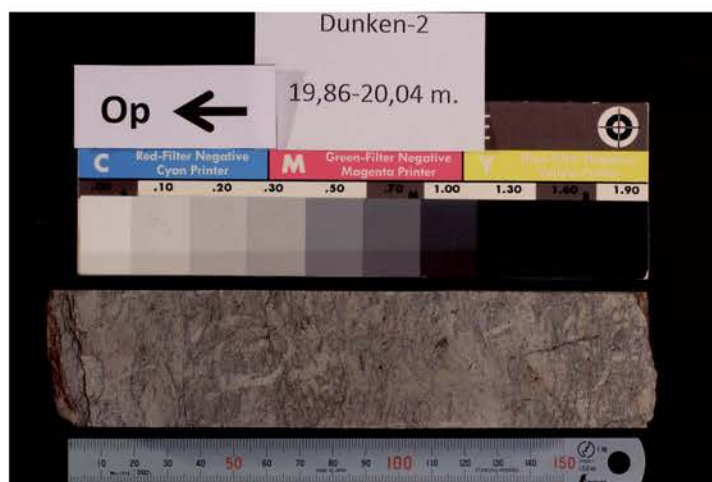
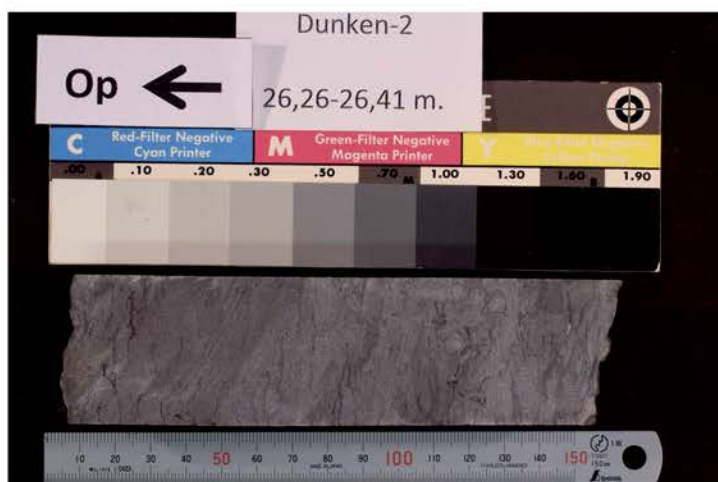
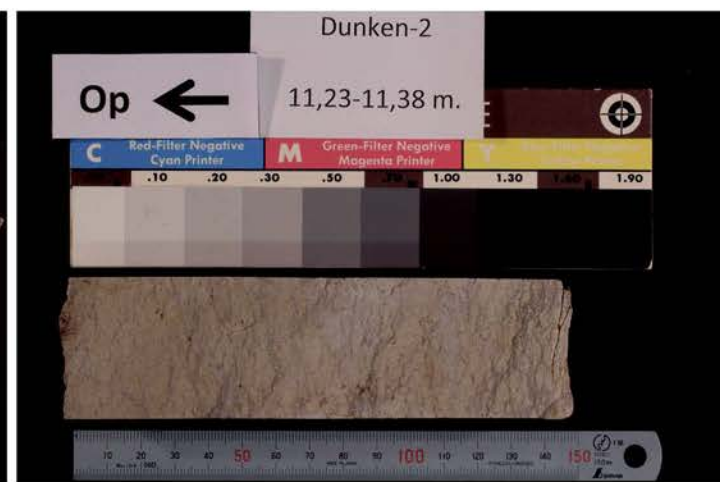
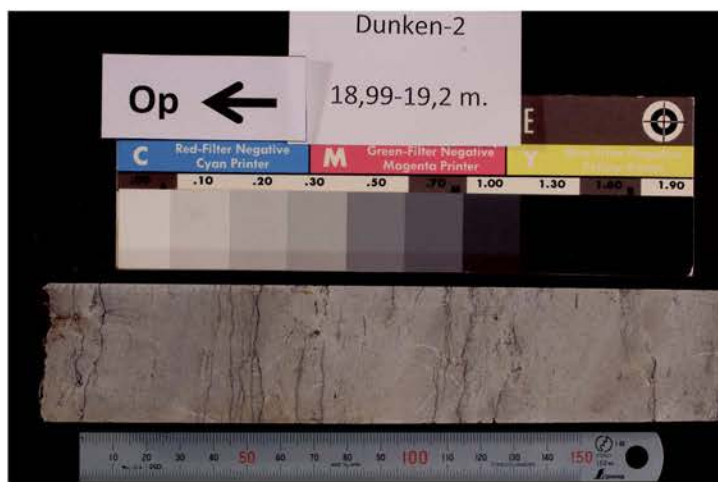
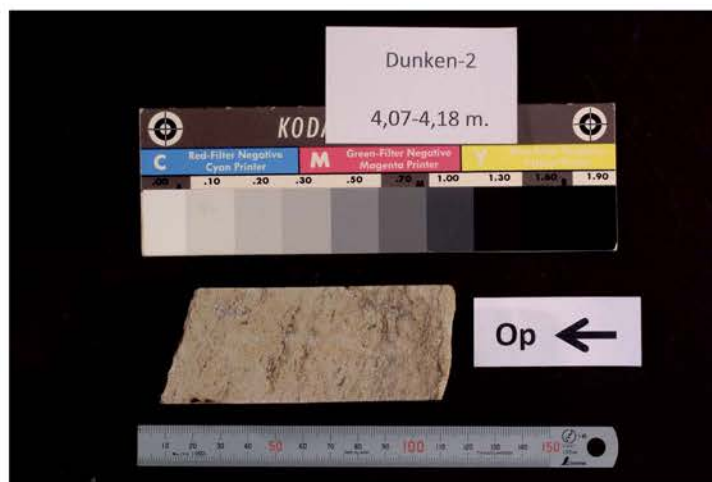
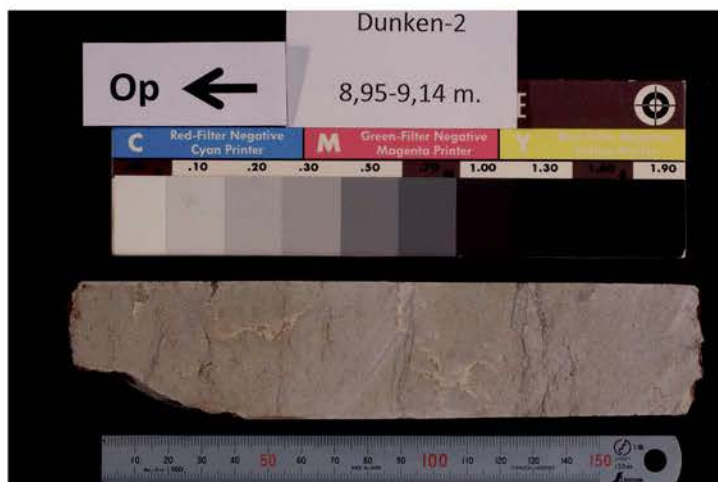












## **Appendix 5 Petrography and Diagenesis Data Sheets**



## **Appendix 5:** Datasheets from the examined thin sections.

The abundance of different framework grains and authigenic phases given on data sheets is roughly visually estimated:

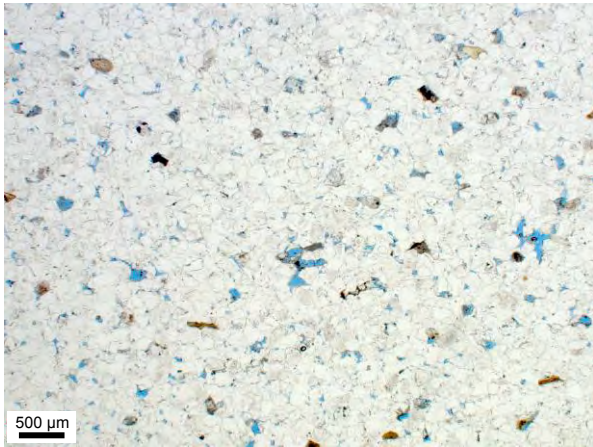
Dominating: > 50 %

Abundant: 15 – 50 %

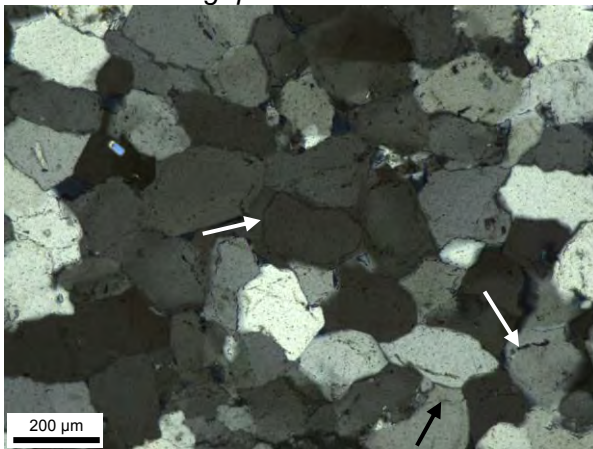
Common: 5 – 15 %

Minor: 1 – 5 %

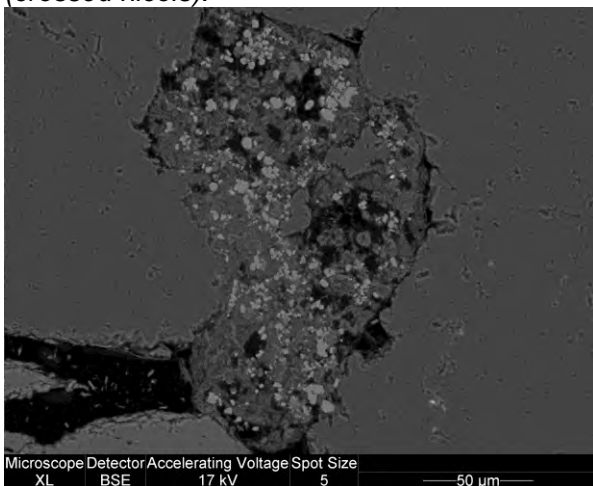
Rare: < 1 %



Overview. Strong quartz cementation.



Dominating authigenic phase: pore-occluding quartz cement. Some detrital quartz grains show dust-rims (examples indicated by arrows) (crossed nicols).



Mud-clast containing illitic clay, mica, quartz grains and apatite crystals (whitish crystals) (BSE image).

**Well / locality:** Dunken-2

**Depth / m in log:** 5.46 m

**Formation:** Dunken Fm

**Facies association:** Lower–upper shoreface (biomottled)

**Sample preparation:** Blue epoxy, polished

**Grain size (range):** 200 μm (100 – 350 μm)

**Sorting:** Very well

**Plug porosity and permeability at thin sec.:**  
5% and 0.07 mD

#### **Framework grains:**

Quartz dominates, feldspar is rare (often partially or completely dissolved), chert occur in minor amount and metamorphic rock fragments and mud-clasts (some apatitic) are rare, apatitic shell fragments are rare, detrital clay and heavy minerals are rare.

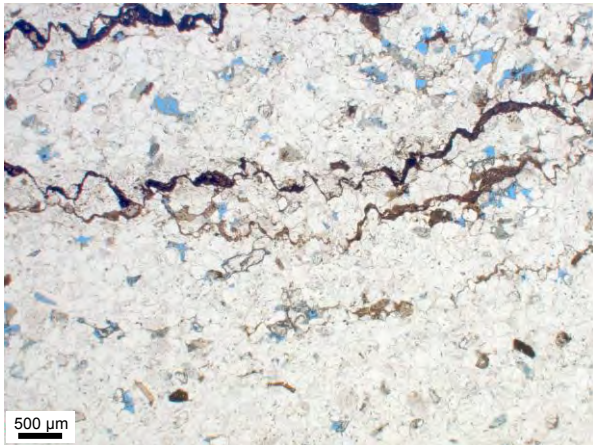
#### **Diagenetic changes in paragenetic order:**

Abundant euhedral and pore-occluding quartz cement.

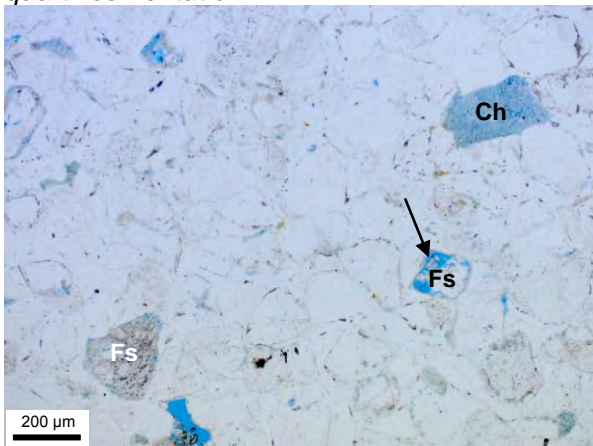
Rare to minor dissolution of feldspars and chert, which creates secondary porosity.

#### **Conclusion:**

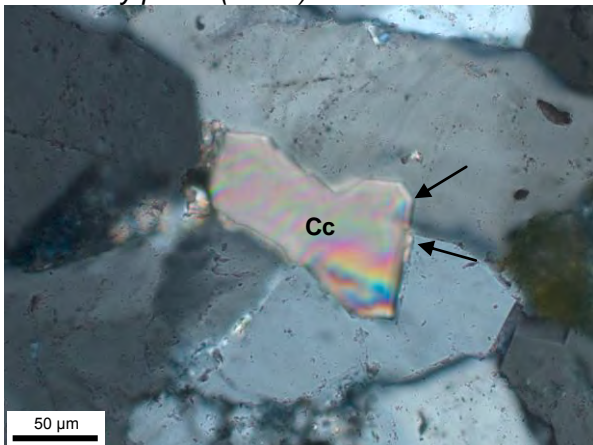
Fine-grained sandstone with abundant euhedral and pore-occluding quartz cement, which results in low porosity and permeability.



Overview. Well-developed stylolites and strong quartz cementation.



Dominating authigenic phase: pore-occluding quartz cement. Note partial dissolved chert (Ch) and feldspar (Fs). Calcite cement occurs in secondary pores (arrow).



Pore-filling calcite cement (Cc), which is pre-dating quartz overgrowths (arrows) (crossed nicols).

**Well / locality:** Dunken-2  
**Depth / m in log:** 8.17 m  
**Formation:** Dunken Fm  
**Facies association:** Lower–upper shoreface (biomottled)  
**Sample preparation:** Blue epoxy, polished  
**Grain size (range):** 225 μm (125 – 325 μm)  
**Sorting:** Very well to well  
**Plug porosity and permeability at thin sec.:** 5% and 0.06 mD

**Framework grains:**

Quartz dominates, feldspar is rare to minor, chert occur in rare to minor amount, mica are rare, metamorphic rock fragments and mud clasts are rare to minor, apatitic shell fragments are rare. Detrital clay is rare to minor. Heavy minerals are rare.

**Diagenetic changes in paragenetic order:**

Pyrite (octahedral crystals and framboids) are rare.

Traces of sparry and equant calcite cement (appears to pre-date feldspar dissolution and quartz cement).

Well-developed stylolites (chemical compaction).

Abundant pore-occluding quartz cement.

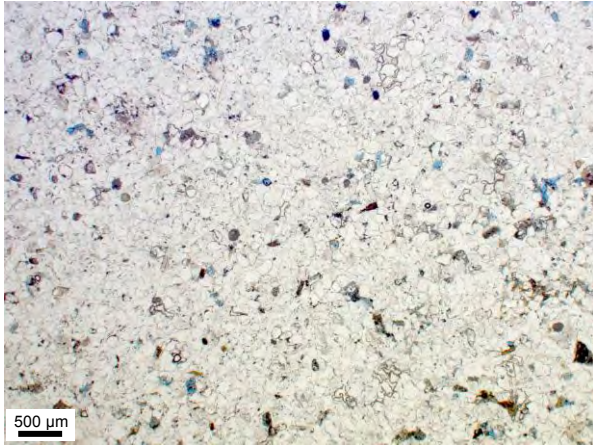
Minor grain dissolution (feldspars and chert).

Rare sparry and equant calcite cement. The calcite may replace feldspars or chert.

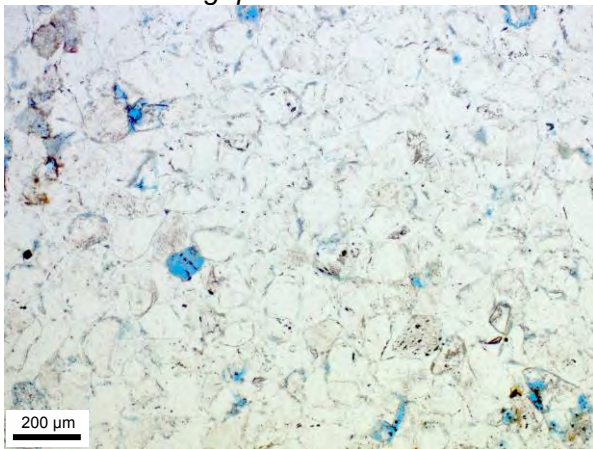
**Conclusion:**

Fine-grained sandstone with abundant pore-occluding quartz cement, which results in low porosity and permeability.

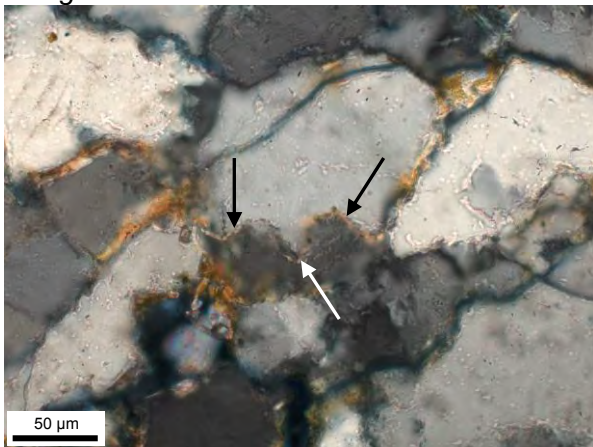




Overview. Strong quartz cementation.



Dominating authigenic phase: pore-occluding quartz cement. Note scattered secondary porosity after feldspar dissolution (blue) and dust-rims between detrital quartz grains and their overgrowths.



Sutured dissolution contacts (arrows) wherein illitic clay is present (crossed nicols).

**Well / locality:** Dunken-2

**Depth / m in log:** 18.55 m

**Formation:** Dunken Fm

**Facies association:** Lower–upper shoreface (biomottled)

**Sample preparation:** Blue epoxy, polished

**Grain size (range):** 150 μm (100 – 400 μm)

**Sorting:** Very well to well

**Plug porosity and permeability at thin sec.:**  
4% and 0.04 mD

**Framework grains:**

Quartz dominates, feldspar is rare to minor, chert occurs in rare to minor amount, metamorphic rock fragments and mud-clasts/detrital clay are rare to minor, apatitic shell fragments are rare. Heavy minerals and mica are rare.

**Diagenetic changes in paragenetic order:**

Pyrite (octahedral and cubic crystals) are rare.

Traces of sparry and equant calcite cement (appears to pre-date quartz cement).

Few incipient stylolites and few sutured grain contacts (chemical compaction).

Abundant pore-occluding quartz cement.

Minor grain dissolution (feldspars and chert).

Rare sparry and equant calcite cement. The calcite may replace feldspars or chert.

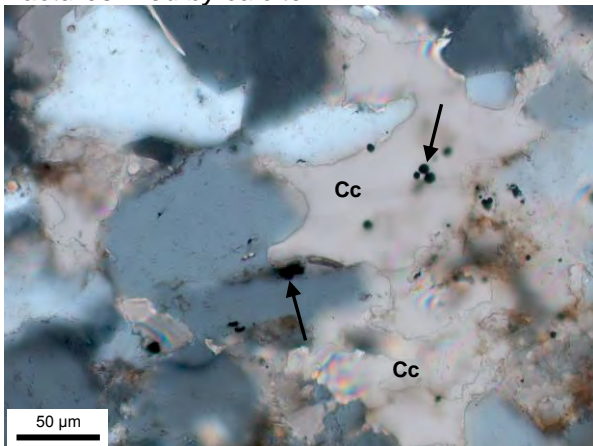
**Conclusion:**

Fine-grained sandstone with abundant pore-occluding quartz cement, which results in low porosity and permeability.

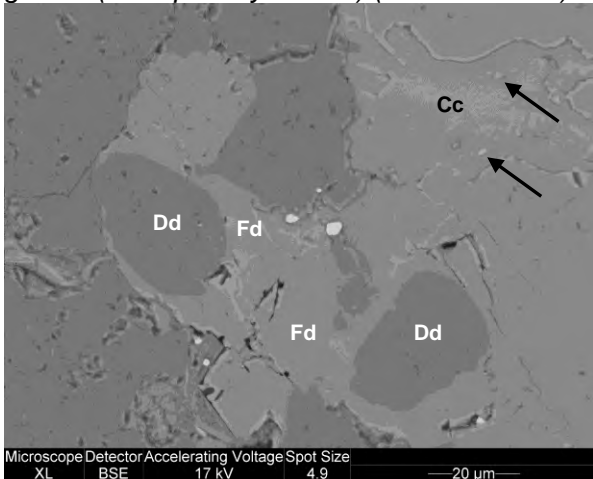




Overview. Note horizontal stylolites and vertical fractures filled by calcite.



Dominating authigenic phase: pore-occluding calcite cement (Cc). Note scattered pyrite in the calcite cement and engulfed in quartz overgrowth (exemplified by arrows) (crossed nicols).



Rounded detrital dolomite (Dd) engulfed in ferroan dolomite cement (Fd). Calcite cement (Cc) is post-dating the latter. In the calcite cement remnants of K-feldspar are displayed (arrows). Whitish crystals in centre are pyrite (BSE image).

**Well / locality:** Dunken-2

**Depth / m in log:** 32.75 m

**Formation:** Dunken Fm

**Facies association:** Lower shoreface (bio-mottled)

**Sample preparation:** Blue epoxy, polished

**Grain size (range):** 125 μm (75 – 175 μm)

**Sorting:** Very well to well

**Plug porosity and permeability at thin sec.:**  
2% and <0.04 mD

#### **Framework grains:**

Quartz dominates, feldspar is minor, chert and metamorphic rock fragments occur in minor amount, mica and apatitic shell fragments are rare. Rare dolomite clasts. Detrital clay is minor. Heavy minerals are rare.

#### **Diagenetic changes in paragenetic order:**

Pyrite (octahedral and cubic crystals) are rare to minor.

Minor to common quartz cement, probably related to stylolites.

Rare to minor rhombohedral ferroan dolomite.

Common patchy poikilotopic and sparry calcite cement, which is pore-occluding. Calcite seems to replace detrital feldspar and chert.

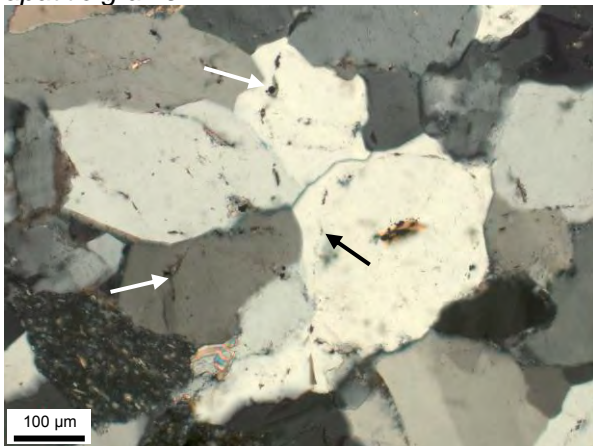
Late fracture-filling calcite.

#### **Conclusion:**

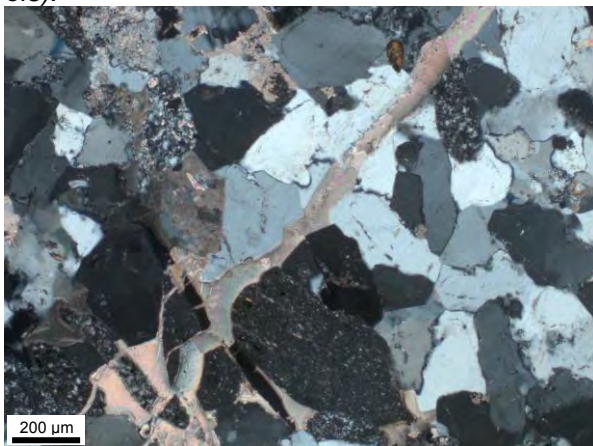
Very fine to fine-grained sandstone with pore-occluding common quartz and calcite cement, which results in low porosity and permeability.



Overview. Note brownish-grey detrital chert and apatitic grains.



Dominating authigenic phase: pore-occluding quartz cement. Dust-rims between detrital quartz grains and overgrowths are common (examples indicated by arrows) (crossed nicols).



Late stage fracture (post-dating quartz cementation) filled by calcite cement (crossed nicols).

**Well / locality:** Dunken-2

**Depth / m in log:** 40.27 m

**Formation:** Ugleungernes Dal Fm

**Facies association:** Shallow marine (biomottled)

**Sample preparation:** Blue epoxy, polished

**Grain size (range):** 250 µm (125 – 975 µm)

**Sorting:** Well to moderately well

**Plug porosity and permeability at thin sec.:**  
2% and 0.04 mD

**Framework grains:**

Quartz dominates, feldspar is rare, chert is common. Metamorphic and sedimentary (apatitic) rock fragments, mud-clasts and apatitic shell fragments are rare. Heavy minerals occur as traces.

**Diagenetic changes in paragenetic order:**

Pyrite (octahedral and cubic crystals) are rare.

Abundant quartz cement which is pore-occluding.

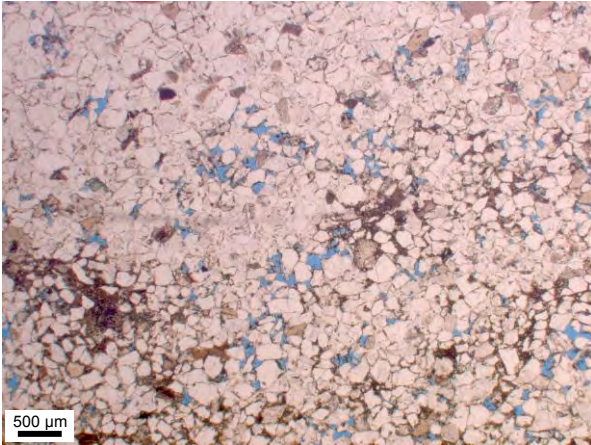
Minor pore-occluding poikilotopic calcite, which seems to precipitate in or replace detrital grains. This may be related to fracture-filling calcite.

Feldspars may occur replaced by calcite.

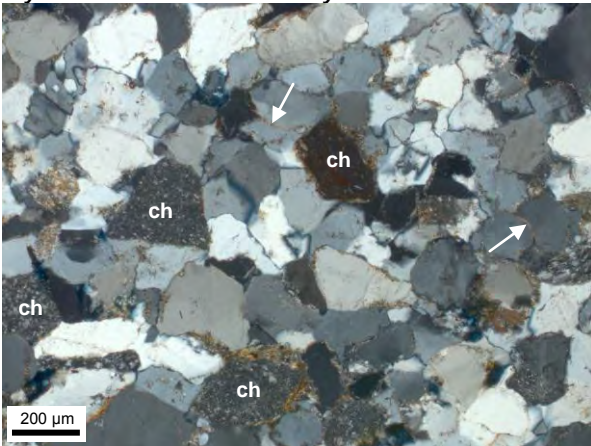
**Conclusion:**

Fine- to medium-grained sandstone with abundant pore-occluding quartz cement and minor pore-filling calcite, which result in low porosity and permeability.

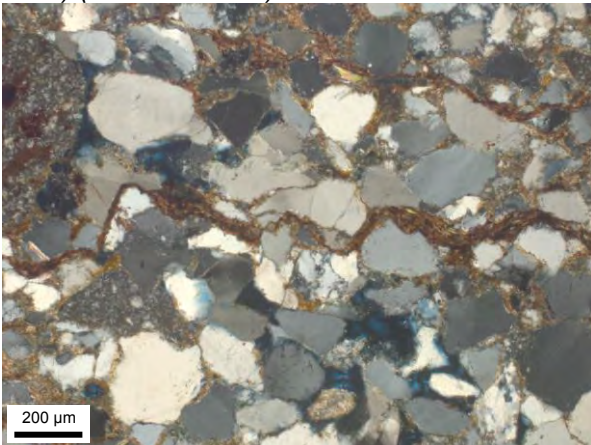




Overview. Note patches with clay, which probably has been introduced by bioturbation.



Dominating authigenic phase: pore-occluding quartz cement. Note scattered chert grains (ch) and clay rims in grain contact interfaces (arrows) (crossed nicols).



Stylolites consisting of illitic clay, mica and pyrite. Note the common clay rims in grain contact interfaces (crossed nicols).

**Well / locality:** Dunken-2

**Depth / m in log:** 48.17 m

**Formation:** Ugleungernes Dal Fm

**Facies association:** Offshore transition (biomottled)

**Sample preparation:** Blue epoxy, polished

**Grain size (range):** 225 μm (100 – 300 μm)

**Sorting:** Well to moderately well

**Plug porosity and permeability at thin sec.:**  
8% and 3.44 mD

**Framework grains:**

Quartz dominates, feldspar is rare, chert is common, metamorphic rock fragments and detrital clay are rare to minor, mica, mud-clasts and apatitic shell fragments are rare. Heavy minerals are rare.

**Diagenetic changes in paragenetic order:**

Pyrite and goethite (former pyrite?) are rare.

Rare early patchy poikilotopic calcite.

Abundant pore-occluding quartz cement, probably related to stylolitization and saturation contacts between quartz grains.

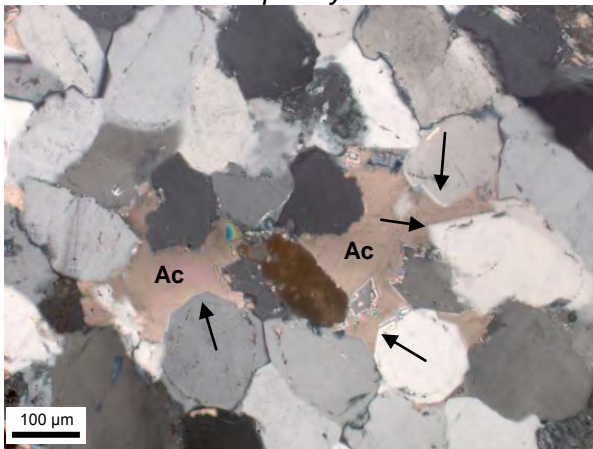
Minor dissolution of detrital grains (feldspars, chert, mud clast, metamorphic rock fragments).

**Conclusion:**

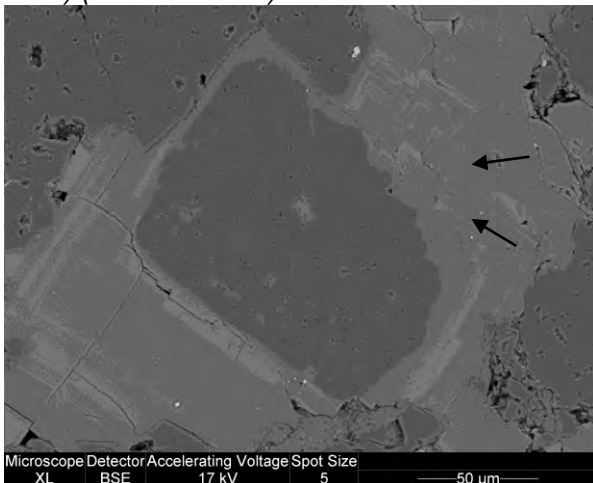
Bioturbated fine-grained sandstone with abundant pore-occluding quartz cement and consequently of relatively low porosity and permeability.



Overview. Note multiple stylolites.



Dominating authigenic phase: pore-occluding quartz cement. In the centre is pore-filling ankeritic cement (Ac) present, which is post-dating quartz overgrowths (examples marked by arrows) (crossed nicols).



Reworked and rounded dolomite-clast engulfed in ankeritic cement. Note that to the right of the dolomite grain a partially dissolved K-feldspar (marked by arrows) has been replaced by ankerite (BSE image).

**Well / locality:** Dunken-2

**Depth / m in log:** 50.38 m

**Formation:** Ugleungernes Dal Fm

**Facies association:** Gravity flow (slightly biotmottled)

**Sample preparation:** Blue epoxy, polished

**Grain size (range):** 175 µm (75 – 325 µm)

**Sorting:** Very well to well

**Plug porosity and permeability at thin sec.:**  
3% and 0.07 mD

#### **Framework grains:**

Quartz dominates, feldspar is minor, chert and metamorphic rock fragments occur in minor amount, mica, mud-clasts and apatitic shell fragments are rare. Rare dolomitic clasts. Heavy minerals and detrital (concentrated in stylolites) are rare.

#### **Diagenetic changes in paragenetic order:**

Pyrite (octahedral and cubic crystals) are rare.

Rare poikilotopic calcite cement, which is pore-occluding.

Abundant pore-occluding quartz cement related to stylolitization and sutured contacts between detrital quartz grains.

Rare to minor ankeritic sparry cement, which often replaces detrital grains.

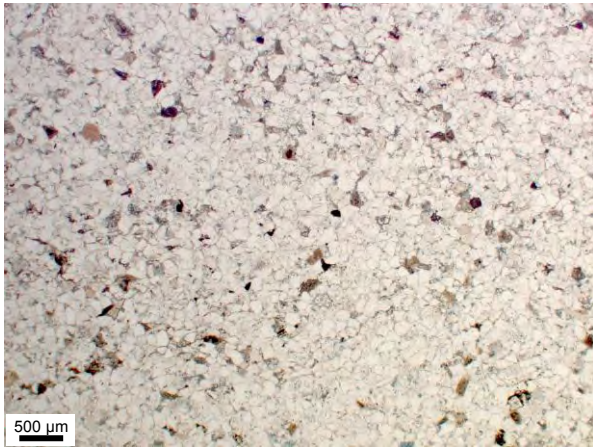
Rare calcite cement filling the gap in stylolite interfaces (decompaction related?).

Detrital grains (feldspars, chert, metamorphic rock fragments) may occur partially dissolved.

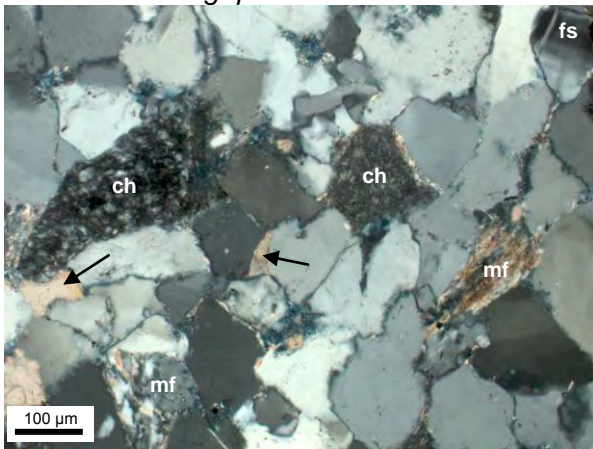
#### **Conclusion:**

Fine-grained sandstone with abundant pore-occluding quartz cement and minor carbonate cement, which result in low porosity and permeability.

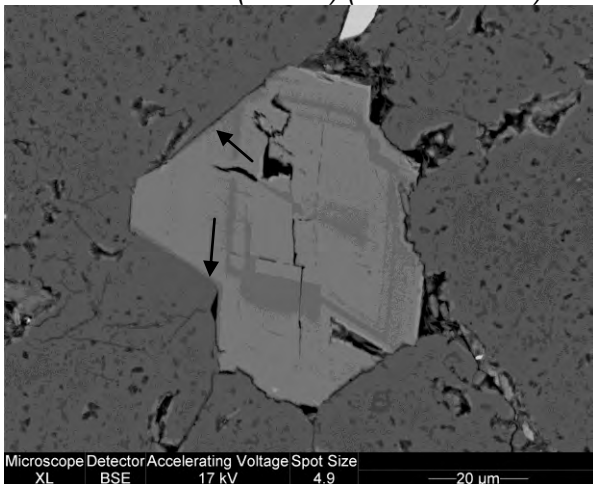




Overview. Strong quartz cementation.



Dominating authigenic phase: pore-occluding quartz cement. Note scattered chert (ch), feldspar (fs), metamorphic rock fragments (mf) and carbonate cement (arrows) (crossed nicols).



Ankeritic cement (post-dating quartz cement, exemplified by arrows) is filling pore space (BSE image).

**Well / locality:** Dunken-2

**Depth / m in log:** 52.65 m

**Formation:** Ugleungernes Dal Fm

**Facies association:** Gravity flow (slightly biotmottled)

**Sample preparation:** Blue epoxy, polished

**Grain size (range):** 175 µm (100 – 275 µm)

**Sorting:** Very well to well

**Plug porosity and permeability at thin sec.:**  
4% and 0.04 mD

**Framework grains:**

Quartz dominates, feldspar, chert and metamorphic rock fragments are rare to minor. Detrital dolomite clasts are rare. Heavy minerals, detrital clay and mica are rare.

**Diagenetic changes in paragenetic order:**

Pyrite (octahedral crystals) are rare.

Rare apatite crystals.

Abundant quartz cement which is pore-occluding. Sutured dissolution contacts are common.

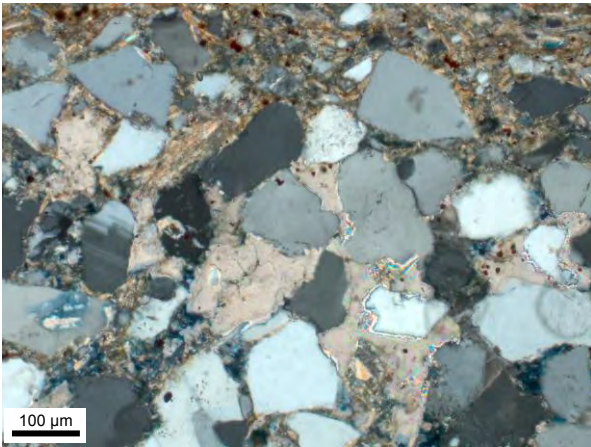
Minor ankeritic cement post-dates quartz overgrowths and seems to grow in secondary pores or replace feldspars.

**Conclusion:**

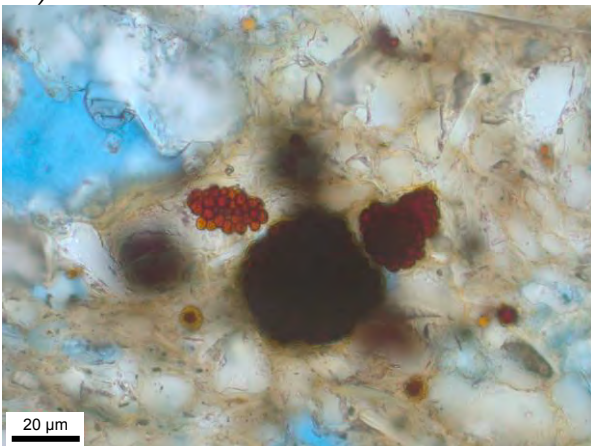
Fine-grained sandstone with abundant pore-occluding quartz cement and minor ankerite cement filling secondary pores/replacing grains, resulting in low porosity and permeability.



Overview.



*Dominating authigenic phase: early patchy poikilotopic pore-occluding calcite cement in sand-dominated part of the thin section (crossed nicols).*



*Framboidal goethite, which probably are pseudomorphs after pyrite. The goethite is often occurring engulfed in calcite cement.*

**Well / locality:** Dunken-2  
**Depth / m in log:** 77.93 m  
**Formation:** Ugleungernes Dal Fm  
**Facies association:** Offshore transition (biomottled)  
**Sample preparation:** Blue epoxy, polished  
**Grain size (range):** 175  $\mu\text{m}$  (75 – 350  $\mu\text{m}$ )  
**Sorting:** Bioturbated sandy mudstone

**Plug porosity and permeability at thin sec.:**  
9% and 0.08 mD

**Framework grains:**

Quartz dominates, feldspar is common, chert and mica are minor, metamorphic rock fragments are rare to minor and apatitic shell fragments are rare. Detrital clay is abundant. Heavy minerals are rare.

**Diagenetic changes in paragenetic order:**

Pyrite and goethite (octahedral and cubic crystals) are rare.

Rare to minor sparry calcite cement, which often is pore-occluding. Feldspars may occur replaced by calcite.

Rare grain dissolution.

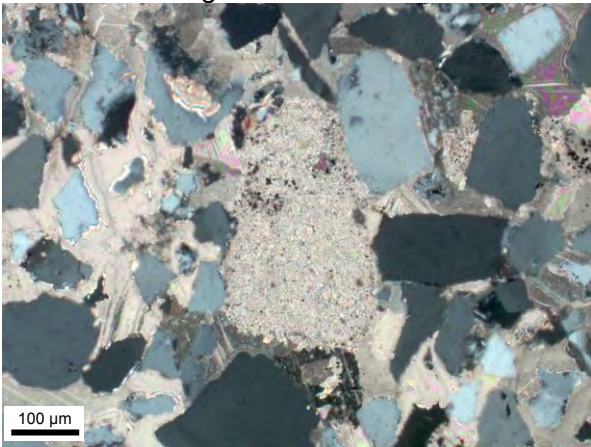
**Conclusion:**

Bioturbated sandy (fine-grained) mudstone with abundant detrital clay resulting in low porosity and permeability.

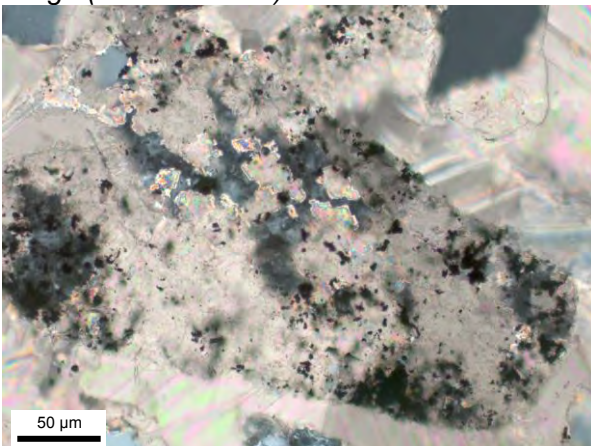




Overview. Strong calcite cementation.



Dominating authigenic phase: early concretionary pore-occluding calcite cement, which is surrounding detrital carbonate clast in centre of image (crossed nicols).



Detrital chert grain, which is almost completely replaced by carbonate. Black spots are pyritic impurities. The grain is surrounded by patchy calcite cement (crossed nicols).

**Well / locality:** Dunken-2  
**Depth / m in log:** 98.25 m  
**Formation:** Ugleungernes Dal Fm  
**Facies association:** Lower shoreface - off-shore transition  
**Sample preparation:** Blue epoxy, polished  
**Grain size (range):** 150 μm (50 – 300 μm)  
**Sorting:** Moderately well

**Plug porosity and permeability at thin sec.:**  
0.34% and <0.04 mD

**Framework grains:**

Abundant to dominating quartz, feldspar and mica are rare to minor, chert is common, metamorphic rock fragments are minor to common, carbonate clasts are rare to minor and mud-clasts are rare. Heavy minerals and detrital clay are rare.

**Diagenetic changes in paragenetic order:**

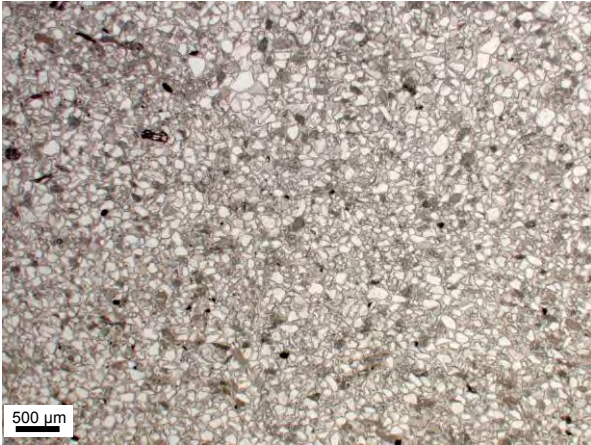
Pyrite (octahedral and cubic crystals) are rare.

Rare incipient carbonate overgrowths on detrital dolomitic? clasts.

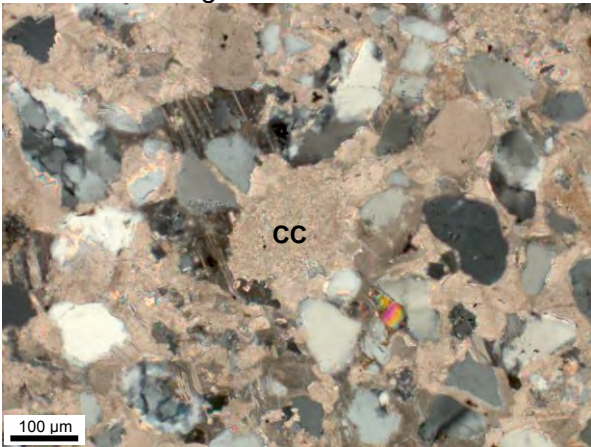
Abundant concretionary calcite cement, which is pore-occluding. Feldspars and chert may occur replaced by calcite.

**Conclusion:**

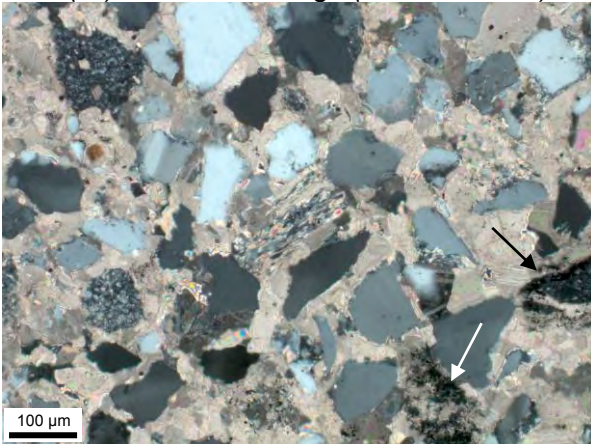
Fine-grained sandstone with abundant concretionary and pore-occluding calcite cement, resulting in very low porosity and permeability.



Overview. Strong calcite cementation.



Dominating authigenic phase: early concretionary pore-occluding calcite cement. Carbonate clast (cc) in centre of image (crossed nicols).



Scattered metamorphic rock fragments (in centre) and chert grains. Note blackish impure chert grains (arrows) which are partially replaced by calcite cement (crossed nicols).

**Well / locality:** Dunken-2  
**Depth / m in log:** 110.98 m  
**Formation:** Ugleungernes Dal Fm  
**Facies association:** Lower shoreface - off-shore transition  
**Sample preparation:** Blue epoxy, polished  
**Grain size (range):** 150 µm (75 – 325 µm)  
**Sorting:** Very well to well

**Plug porosity and permeability at thin sec.:**  
0.21% and <0.04 mD

**Framework grains:**

Abundant quartz, feldspar and mica are minor, chert is common, metamorphic rock fragments are minor to common, carbonate clasts are minor and mud-clasts are rare. Heavy minerals, detrital clay and woody tissue are rare.

**Diagenetic changes in paragenetic order:**

Pyrite (octahedral and cubic crystals) are rare.

Rare incipient carbonate overgrowths on detrital dolomitic? clasts.

Abundant concretionary calcite cement, which is pore-occluding. Feldspars and chert may occur replaced by calcite.

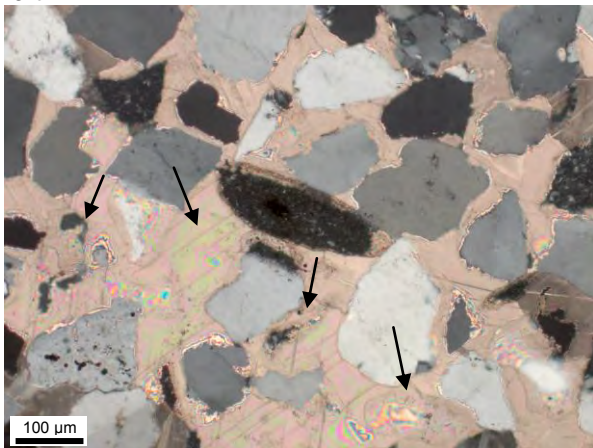
**Conclusion:**

Fine-grained sandstone with abundant early concretionary and pore-occluding calcite cement, resulting in very low porosity and permeability.

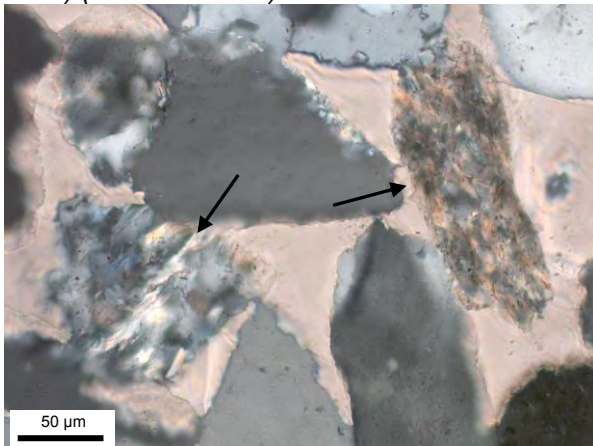




Overview. Note fracture filled by calcite in upper left.



Dominating authigenic phase: early concretionary pore-occluding calcite cement. Note that the calcite has partially and totally replaced detrital grains, probably feldspars (exemplified by arrows) (crossed nicols).



Two metamorphic rock fragments (arrows) engulfed in concretionary calcite (crossed nicols).

**Well / locality:** Dunken-2

**Depth / m in log:** 127.96 m

**Formation:** Ugleungernes Dal Fm

**Facies association:** Lower shoreface (bio-mottled)

**Sample preparation:** Blue epoxy, polished

**Grain size (range):** 200 µm (125 – 375 µm)

**Sorting:** Well to moderately well

**Plug porosity and permeability at thin sec.:**  
0.2% and <0.04 mD

**Framework grains:**

Quartz dominates, feldspar is rare, chert occur in abundant amount and mica, metamorphic rock fragments and apatitic shell fragments are rare. Heavy minerals occur as traces.

**Diagenetic changes in paragenetic order:**

Pyrite (octahedral and cubic crystals) are rare.

Abundant concretionary calcite cement, which is pore-occluding. Feldspars may occur replaced by calcite.

Fracture-filling calcite post-dates concretionary calcite.

**Conclusion:**

Fine-grained sandstone with abundant concretionary and pore-occluding calcite cement, resulting in very low porosity and permeability.

## **Appendix 6**

**Thin sections, overview photographs (digital version only)**

## **Appendix 7 Cap rock data (digital version only)**

## **Appendix 8 Gamma log scanning (digital version only)**